Measuring, Evaluating, and Describing Pile-Up and Sink-In During Nanoindentation of Thin Films on Substrates

by

MariAnne Sullivan

A dissertation submitted to the Graduate Faculty of
Auburn University
in partial fulfillment of the
requirements for the Degree of
Doctor of Philosophy

Auburn, AL
December 12, 2015

Keywords: nanoindentation, thin films,
nanoscale mechanics, pile-up

Approved by

Barton C. Prorok, Chair, Professor of Materials Engineering
Dong-Joo Kim, Professor of Materials Engineering
Ruel A. Overfelt, Professor of Materials Engineering
Jeffrey Suhling, Professor of Mechanical Engineering

Abstract

Nanoindentation is a valuable tool for extracting material properties such as elastic modulus and hardness at the nanoscale. Knowing material properties at this scale enhances the use of thin films as protective coatings and various electronic applications. It is essential that material behavior is well-known before manufacture to ensure material selection will prevent catastrophic failures. The research presented here has led to the creation of a model that extracts elastic modulus from the film or substrate, termed the Zhou-Prorok model, and has been tested on a wide variety of film/substrate combinations. Other researchers have been concerned with a change in area when the film and substrate have different elastic moduli; phenomena such as sink-in or pile-up can occur, leading to a difference in contact area, the crucial term used to calculate the material properties. The model, however, is not affected elastically, and it is hypothesized that the plastic properties are the only effect on the pile-up and sink-in. Within this work, new methods are outlined to characterize and measure projected pile-up and sink-in. Additionally, yield stress was controlled prior to indentation, and pile-up was then examined across a variety of plastically deforming substrates with metallic films. Overall, this research contributes a number of new findings of pile-up and sink-in related to plasticity, and improves the field of nanoindentation as this new information can be utilized for the most accurate extraction of material properties from simple small-scale nanoindentation tests.

Acknowledgements

I would like to thank first, most wholeheartedly, my advisor Dr. Bart Prorok. I am lucky to have found such a personable advisor, and have learned much from his thought processes and will utilize them in my own ways in the future. Next, I would like to thank my committee members Dr. Kim, for his support and accommodations, Dr. Overfelt for his sound advice on all fronts, Dr. Suhling, for his helpfulness outside the department both with research and recognitions, and my outside reader, Dr. Auad, for both committee help and general support with my Spanish abroad. Additionally, I would like to thank Steve Moore for his availability and insight on all things in our department, and I've been happy to share our materials enthusiasm over the years.

Next, I would like to thank my labmates: Naved Siddiqui, who without all the chats, support, and life advice, I could not have survived graduate school, Yan Chen, for his extensive knowledge and camaraderie, Anqi Zhang, Jiahui Xu, Daniel Slater, and Zhan Xu for continuously listening to my research through group meetings. Also previous group members, Kevin Schweiker, Brandon Frye with which my research all started. Additionally, my REU mentee, Andrew Kirk, who made initial headway on this project.

My time in graduate school could not have been successful without the unwavering support from my friends and family, including Rob and JD Yantz, Carlos Gonzalez, and most importantly my devoted boyfriend, Richard Davis, with whom I am excited to share the title of an Auburn doctorate. To my parents, Charles and Virginia Sullivan, I have appreciated countless phone calls and support from 1000 miles away, and I absolutely cannot thank them enough for all their love that gives me the motivation to be the best that I can be.

Table of Contents

List of Tables

List of Figures

1. Introduction

Many tools are available to study the mechanical properties of materials. When materials' applications evolve, the tools must adapt, as well. For example, thin films are readily used today for a range of applications from protective coatings to electronic packaging. It is gravely important that these films have correct known material properties to prevent failure before use. In an application as a microchip in a cell phone, it is pertinent to understand the materials being utilized, and as they are continuously becoming smaller and smaller, it is necessary to test at reduced scales, even the nanoscale. To examine these films, bulk testing methods do not suffice. Other small scale testing devices may call for samples to be prepared in a certain manner, which will alter the way the material is being tested, as well. Nanoindentation is crucial for these types of materials that have delicate structures or multiple layered components. This work was completed to improve nanoindentation as a tool for film/substrate material property extraction, and improvements for this particular system. It has been a challenge to remove substrate effects in order to solely examine the film properties. Equations to account for these changes have been studied and improved.

Additionally, another challenge in nanoindentation is the separation of elastic and plastic properties. This is a topic that has not been completely uncovered in the realm of nanoindentation. Elastic properties can be examined because nanoindentation tools utilize solely unloading information, which is entirely elastic. When plastic deformation plays a role, there has been much controversy over what is necessary to extract the data in order to obtain the same film properties as garnered without the problems of plasticity. Here, novel techniques are used to control the plasticity of the substrate in order to dissect the film behavior in this work. The overall goal is to predict film material properties before they are implemented in real world applications and confirm that they have the actual expected mechanical properties, regardless of elastic or plastic phenomena.

2. Motivation and Objectives

2.1 Measuring Pile-Up and Sink-In

Pile-up has been considered a major problem during calculations of material properties such as elastic modulus. In order to discover the contributions of pile-up, it is necessary to

measure correctly and in a repeatable manner. This has been difficult in the past because most nanoindenters only have low magnification microscopes, and it is not possible to view the indentation *in situ*. It takes an additional step of transferring the sample to a scanning electron microscope, SEM, in order to visualize the pile-up, or using an atomic force microscope, AFM, to scan the profile of the indent. Both of these are tedious and time consuming, and impossible to complete for every single indent. However, in this research, SEM images are coupled with a novel measurement technique, with which leads to the next goal of predicting pile-up in the film solely based on material properties, removing the step of nanoscale area measurements. This must be confirmed visually at first, and by making the preliminary measurements here, this step can be removed in the future.

2.2 Accounting for Pile-Up and Sink-In

Another goal of this research was to determine what criteria are affected by pile-up and sink-in, if any. Other researchers have tried certain techniques to measure and account for pile-up, but in this work there may be certain material and film/substrate systems where it is possible to disregard pile-up area changes when addressing elastic issues. The Zhou-Prorok model was predominantly used because of its adeptness in calculating the elastic modulus regardless of pile-up or sink-in. In this research, the first goal was to outline what criteria the area of the indent with pile-up or sink-in may or may not be necessary to account for when regarding elastic modulus. Additionally, multiple systems of film and substrate are studied, and if the inherent material properties are controlling the sink-in and pile-up, it may be possible to predict in the future, even without testing methods.

2.3 Plastic Properties from Pile-Up and Sink-In

Nanoindentation has been mostly used for elastic properties, extracting values from the unloading curve to calculate stiffness, which leads to elastic modulus. Hardness can also be calculated, but the extent of nanoindentation possibilities has ended there. There are different mechanisms to indentation than there are to tensile tests, therefore, it is difficult to extract all of the same information. Plastic properties are particularly elusive because they have been difficult to separate from elastic, and often work in conjunction with elastic-plastic mechanisms. However, it has been shown that pile-up is a plastic property, where

the material is deformed enough to result in the residual indent with extra material piled up. In this research, the pile-up is scrutinized in a variety of different film/substrate combinations. Sink-in is done in this same manner, but more challenges with plasticity to consider to a greater extent. Additionally, yield stress alterations of film or substrate were employed to see the effects of the substrate yield stress on pile-up and sink-in. Ultimately, it is valuable to measure plastic properties from typical indentation, and this is one of the final end goals of this research.

3. Literature Review

3.1 Nanoindentation

Nanoindentation is used for extracting material properties at the nanoscale. Original hardness testers such as Knoop or Vickers are used for bulk samples, and require imaging of residual indents in order to calculate the resistance to plastic deformation of these indented materials [1-4]. Original indent machines include others such as Rockwell, Shore, or Brinell. The principle behind these are to test metals experimentally and compare to an empirically derived scale to obtain a hardness value. The type of indenter plays a role, and the hardness is a measure of the plastic deformation that occurs [5]. This testing method is destructive, however, as it is necessary to employ a weight on the sample in order to make an indent impression and then view it to measure crack formation. Nanoindentation, however, is an automated process with capabilities of nano-newton loads and sub-angstrom displacements. Additionally, imaging is not necessary because the machine calculates values of elastic modulus and hardness based on the area of contact. This is important when some phenomena such as sink-in or pile-up occur, which could introduce error into the area of contact. Therefore, these phenomena have been examined for relationships with mechanical property determination. The purpose of this study is to understand pile-up and sink-in mechanisms and what is controlling their development. Before this work can be outlined further, it is essential to understand the previous technologies.

Nanoindentation arose in the 1970s with a number of improvements over the traditional hardness testing methods. The testing methods and their analyses are constantly improving. Mostly, besides hardness testers, nanoindentation can also garner elastic

properties, such as elastic modulus [5]. Previously, this could only be done with a tensile test machine, and some delicate samples do not allow for this type of testing for elastic properties. One additional component of the nanoindentation tests seen in this work is the use of a continuous stiffness method.

3.1.1 Continuous Stiffness Measurement

As previously mentioned, with nanoindentation, imaging the indent is unnecessary. The information is extracted from a load-displacement curve, seen in Figure 1. In these studies, we use continuous stiffness measurement (CSM), which is depicted in Figure 1a. Maximum load or displacement can be controlled, but there is an oscillation of 2 nm to the applied load that allows for stiffness readings. In a single normal indent, a load-displacement curve uses the slope of the unload curve for stiffness values, seen in Figure 1b as *S*. This method has eliminated the necessity of imaging the indent, as was done in traditional tests such as Knoop hardness.

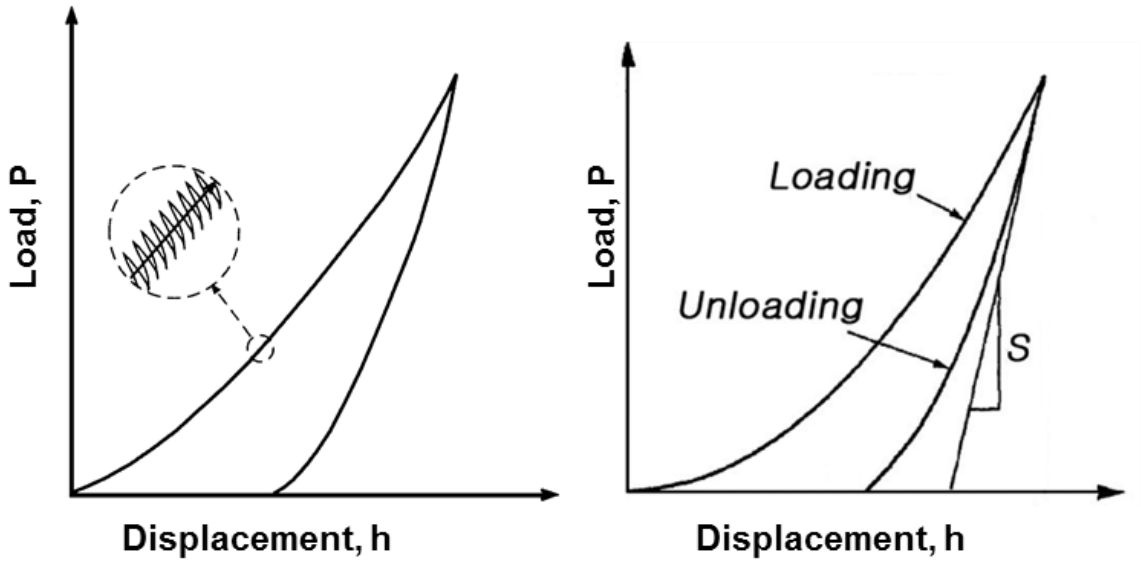

Figure 1. Typical load-displacement curve with a) continuous stiffness measurements and b) listed parameters [6].

The stiffness, *S*, is defined by parameters seen in Equation 1:

$$S = \frac{dP}{dh} = \frac{2}{\sqrt{\pi}} E_r \sqrt{A} \tag{1}$$

Where P is the load, h is displacement, E_r is reduced modulus, and A is the contact area. The reduced modulus E_r is defined based on parameters from the indenter tip, seen in Equation 2:

$$\frac{1}{E_r} = \frac{(1-\nu^2)}{E} + \frac{(1-\nu_i^2)}{E_i} \tag{2}$$

where v and E are respectively Poisson's ratio and elastic modulus related to the sample, and v_i and E_i are the same properties for the indenter tip material, which in this case is diamond; E_i=1140GPa and v_i=0.07. Because of these high values, it can be assumed that this term for the diamond tip is negligible. These findings are the original equations defined by Oliver and Pharr, and are used even to this day, with some variations [7]. Problems arise because of the area term, as the indent impression does not follow the exact geometry of the indenter tip. At times, pile-up or sink-in can occur, which is discussed in depth later.

3.1.2 Berkovich Tip

In this work, all testing was completed with a Berkovich indenter tip. This is a three-sided pyramid typically made of diamond. It is important that the material for the tip is hard and non-compliant, as is diamond, because when nanoindenting, if the properties can be assumed negligible, there are fewer assumptions on the interactions of the tip and sample surface. The modulus of diamond is high and its Poisson's ratio is low, so this very hard, strong material is a great choice for nanoindentation tips.

Other types of indenter tips are spherical, conical, and cube corner. Berkovich is easiest to fabricate, as three sides will always come to a single point. With four sides, it is possible they may not be aligned. Spherical and conical also behave differently and exhibit a round projected image. The three-sided pyramid results in a three-sided projected image, a triangle that is easy to image from an aerial view. The geometry of the Berkovich tip is seen in Figure 2. Also, this shape is self-similar, meaning that as the indent is pushed deeper into the tested material, it is done so in the same predictable rate, based on the geometry. This area is dictated as $24.5h^2$, where h is the indent depth. In order to possess the ideal equilateral triangle, the angles are not all identical. The projected image may be

the triangle, but seen in Figure 2, the cross-section of the Berkovich tip results in two separate angles, 65.3 and 77.05 degrees. Knowing these angles is useful for some separate calculations, but essentially, the projected area is well-known, and is solely dependent on the indent depth, *h*. The geometry speaks for itself to calculate the projected area of the indent.

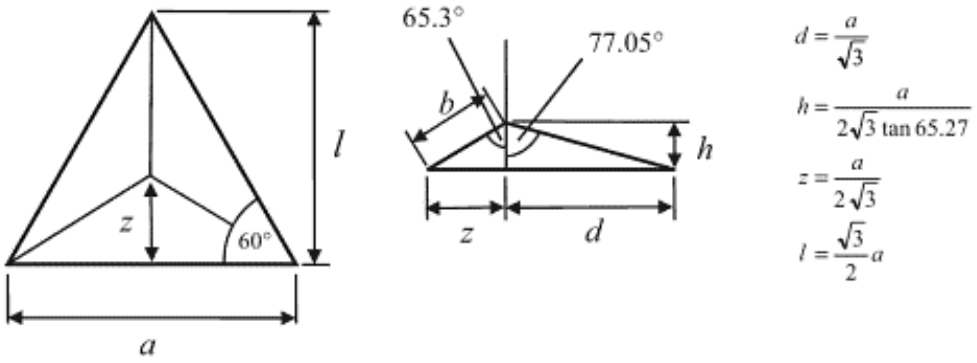

Figure 2. Berkovich tip geometry from Fischer-Scripps [8].

3.1.3 Film-Substrate Models

To go a step further, there have been a variety of equations to explain not just a monolithic material, but film and substrate behavior when there is a layered combination. In many cases, it is important to know solely film properties, so equations that describe the composite can be back-calculated for the film properties alone. The first researchers to do this were Doerner and Nix [9], with a basic idea to apply a weighting factor for the substrate. This improves the calculations, but is not a perfect fit, even with modifications [10]. Gao [11] modeled mathematically the film properties using many variables, again improving, but not perfecting, the fit. Hay et al. believe the film and substrate can be modelled by springs in series [12]. Others have defined new terms, such as work of indentation [13], or attributed other phenomena such as creep and viscoelasticity to the pile-up [8, 14-16]. A limitation of testing only 10% into the film has also been described by some [17-20], but without much justification.

The area of contact is dependent on the indenter tip when utilizing nanoindentation. Some studies have been done with spherical indenter tips [21-23], but most research has utilized

Berkovich indenter tips. The Prorok research group has previously created a model that is a great improvement compared to similar equations such as Doerner and Nix to extract film properties from a film/substrate composite under nanoindentation. For example, in their work, the researchers Doerner and Nix applied a weighting factor to account for the change in the contribution of the substrate as a function of the indenter depth. The model is seen here in Equation 3:

$$\frac{1}{E'} = \frac{1}{E'_f} + \left(\frac{1}{E'_s} - \frac{1}{E'_f}\right)\Phi_{D-N} \tag{3}$$

$$\text{where } \Phi_{D-N} = \mathrm{e}^{-\alpha\left(\frac{\mathrm{t}}{\mathrm{h_{eff}}}\right)}$$

Where *E'* is reduced elastic modulus of the composite material, film (E'_f), or substrate (E'_s). The Φ term is a single weighting factor to adjust for the change when penetrating deeper into the film. The *h* in this equation is the effective indent depth, and α is empirically determined, but Doerner and Nix suggested 0.25 for most materials. Because there was no physical explanation of the α term, the Prorok research group dissected this equation and accounted for more than just the change in the film contribution, but also the substrate's.

This model now considers a discontinuous elastic interface, where the film and substrate contribute in separate terms [24]. The Zhou-Prorok model, which improves the Doerner and Nix equation is seen in Equation 4:

$$\frac{1}{E'} = \frac{1}{E'_f}(1 - \Phi_s) + \frac{1}{E'_s}\Phi_f \tag{4}$$

$$\text{where } \Phi_f = e^{-\alpha_f\left(\frac{t}{h}\right)}, \text{ and } \Phi_s = e^{-\alpha_s\left(\frac{t}{h}\right)}$$

Where *E'* is reduced elastic modulus of the composite material, film (E'_f), or substrate (E'_s). The term *t* is thickness of the film, and *h* is displacement into the film. The α_s and α_f were thought to be individual constants, but surprisingly, it was discovered that the correct values fit as the Poisson's ratio for the substrate, α_s, and Poisson's ratio for the film, α_f. Comparing this equation to the Doerner and Nix model, we are now accounting for both the film and substrate contribution in each of the terms separately. This can be

visualized in Figure 3, which separates the strain fields that are imparted on both the film and substrate. Before, it was assumed the indenter tip was engaging the substrate in the same amount as it was the film, but by utilizing the weighting factors, it is clearer how the mechanisms are acting together and in the manner shown in the figure.

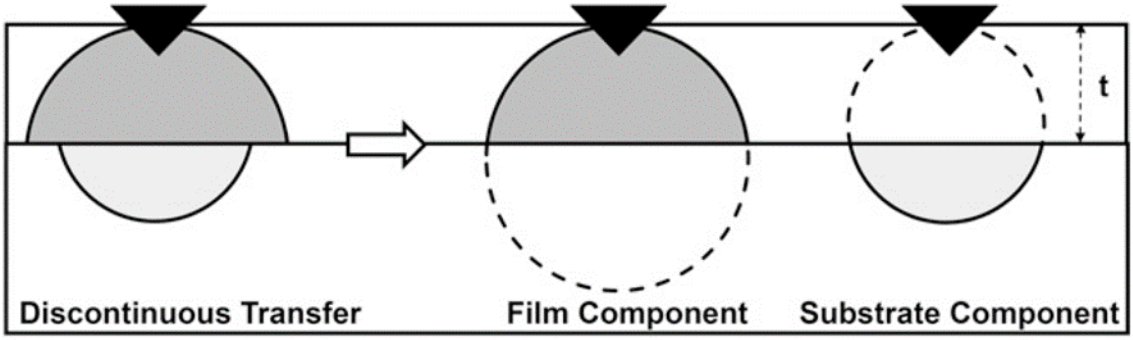

Figure 3. Schematic of film and substrate components for the discontinuous elastic interface model [25].

This model was then verified with a variety of samples, including all combinations of five different films on five different substrates. After further investigation, the data seemed to fit better with an additional term, titled E_{flat}, because as soon as the indenter hits the composite, it is not solely the film properties predicting the behavior; substrate plays a role from the initial indentation. Because of this finding, empirical data was used to include an extra term for E_{flat}, seen shaded in Equation 5:

$$\frac{1}{E'} = \frac{1}{E'_f}(1-\Phi_s)\cdot\left(\frac{E'_f}{E'_s}\right)^{0.1} + \frac{1}{E'_s}\Phi_f \tag{5}$$

Where E' is reduced elastic modulus of the composite material, film (E'_f), or substrate (E'_s). The other Φ terms are defined as: $\Phi_f = e^{-\alpha_f\left(\frac{t}{h}\right)}$, and $\Phi_s = e^{-\alpha_s\left(\frac{t}{h}\right)}$, where α_s and α_f are substrate and film Poisson's ratios respectively, t is thickness of the film, and h is displacement into the film. This additional term has only one unexplained unit, the 0.1 power, which is still under consideration. Otherwise, all of the terms in the Zhou-Prorok equation are constant material properties that readily predict the composite elastic modulus of the film/substrate system as a function of indent depth. It can also be rearranged to

extract the film properties, especially E_f, the elastic modulus of the film. The model and its use in this work will be explained further in the results section.

3.2 Pile-Up and Sink-In

Seen in Figure 4, indent impression can vary based on the materials of the film and substrate, and additionally in bulk which will be explained later. These micrographs are all platinum films on various substrates. When the substrate is more compliant than the film, sink-in can occur (Figure 4a), which in this image is platinum on a tin substrate. A normal indent impression in tests with a Berkovich indenter tip is seen in Figure 4b. The combination is platinum on platinum, and may not always show zero pile-up or sink-in. Even though the materials are the same, the film properties will be dependent on the deposition technique, and could vary with grain size different from the bulk substrate. Finally, pile-up is in Figure 4c, where there is excess material outside of the triangle than is expected. This system is platinum on silica, a ceramic-like substrate that is negligibly plastically deforming. Many researchers have tried to determine how these different geometries affect the calculations of the elastic modulus and hardness [26-29]. The initial focus in this work was solely on pile-up and its effects on elastic modulus [30]. Then, adding plasticity changes in the substrate was utilized to further examine plastic properties that drive pile-up and sink-in.

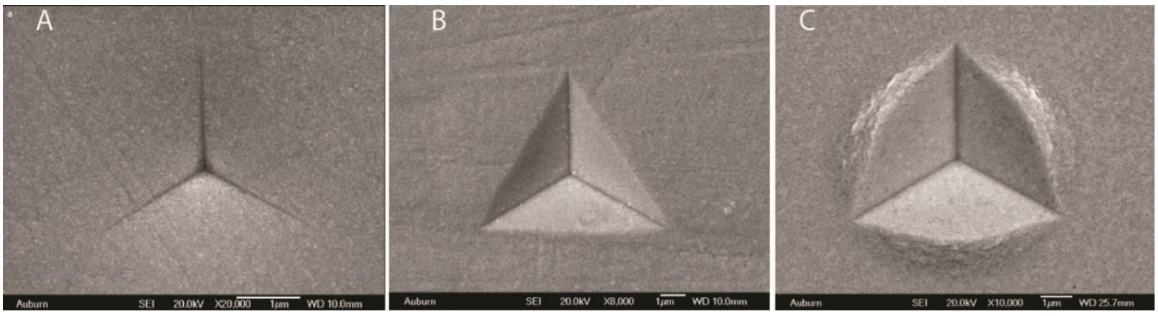

Figure 4. SEM micrographs showing a) sink-in, b) normal projected area, c) pile-up.

3.2.1 Previous Research into Measuring Pile-Up

To correct for pile-up, the trend of other researchers has been to correct for extra area that may be pushing back against the indenter tip. For example, Kese et al. [31-33] explained

a “semi-ellipse” method, where a geometrical shape was fit to the outer edge of pile-up. This, however, is not exactly the shape that is present in the residual indent, and is difficult to measure consistently. Figure 5 shows a schematic of this assumption, with a_i being the extra contact area.

Also, others have used tedious atomic force microscopy (AFM) measurements to find the pile-up area, seen in Figure 6. It is difficult to find these small indents, and very time consuming to measure them individually when it is typical to utilize an array of 25 to obtain the necessary elastic data. Even more researchers have used modelling to predict the pile-up and make corrections [34]. Some have looked at the work hardening of materials to understand the pile-up, as well [35]. Oliver and Pharr have defined a material property ratio that affects pile-up, being E_{eff}/σ_y. This has only been done with finite element analysis, seen in Figure 7. The yield stress, however, is not able to be measured via nanoindentation, and deposition of films may produce a variety of yield stresses that cannot be predicted easily in order to apply empirically to these formulas.

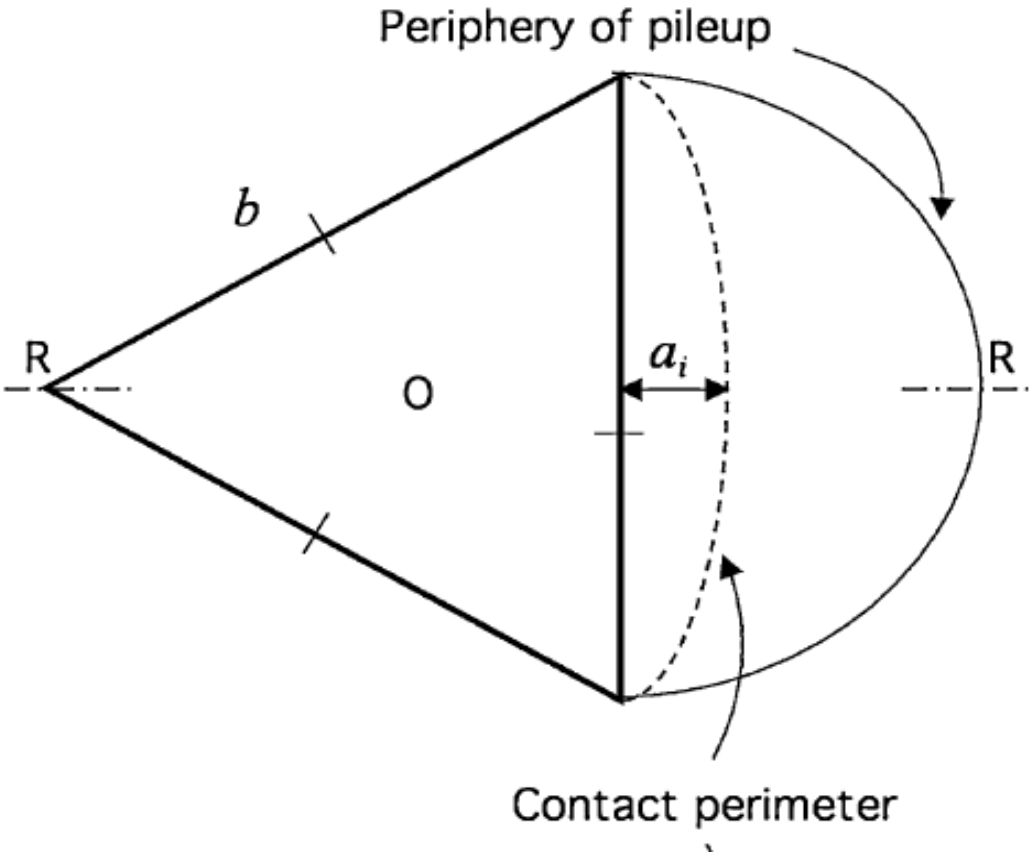

Figure 5. Kese's semi-ellipse method for pile-up [31].

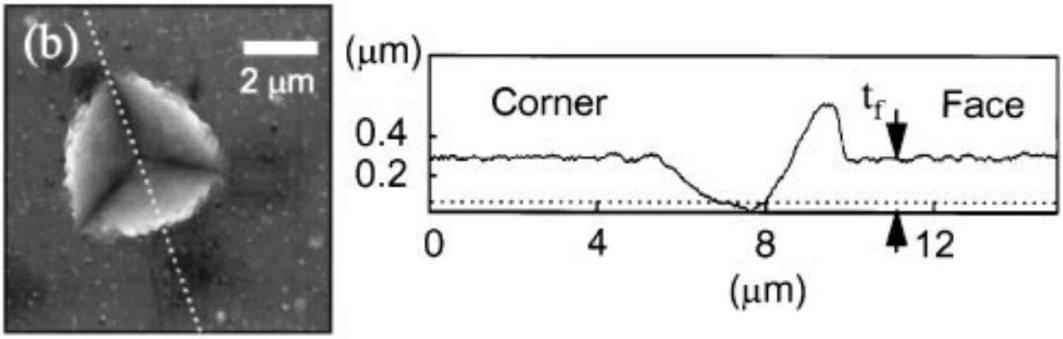

Figure 6. AFM measurements of an indent exhibiting pile-up [36].

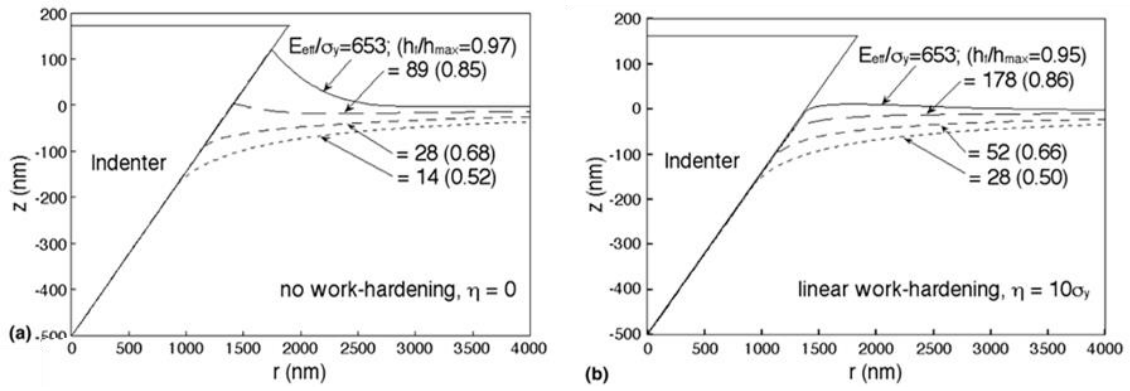

Figure 7. Finite element simulations of sink-in and pile-up using assumptions for E_{eff} and σ_y for a) pile-up and b) sink-in [37].

Others have cited that orientation of the materials may affect pile-up, as well [38]. This would correlate with anisotropy of materials, if the plastic and elastic properties are different based on the directions. For example, any single crystal orientations tested may vary in a material like aluminum. Comparing the pile-up across these samples could lead to information on the variation in plastic properties of each direction. Also, studies into how the material may or may not spring back during this indentation have been analyzed. Oliver and Pharr show this in a schematic seen in Figure 8, as there is a problem separating elastic and plastic properties [39] and there are countless ways to define the indentation depth, *h*. Some of these criteria may change, but overall, every researcher that has studied nanoindentation has encountered the phenomena of pile-up and sink-in, and have combatted in from many angles.

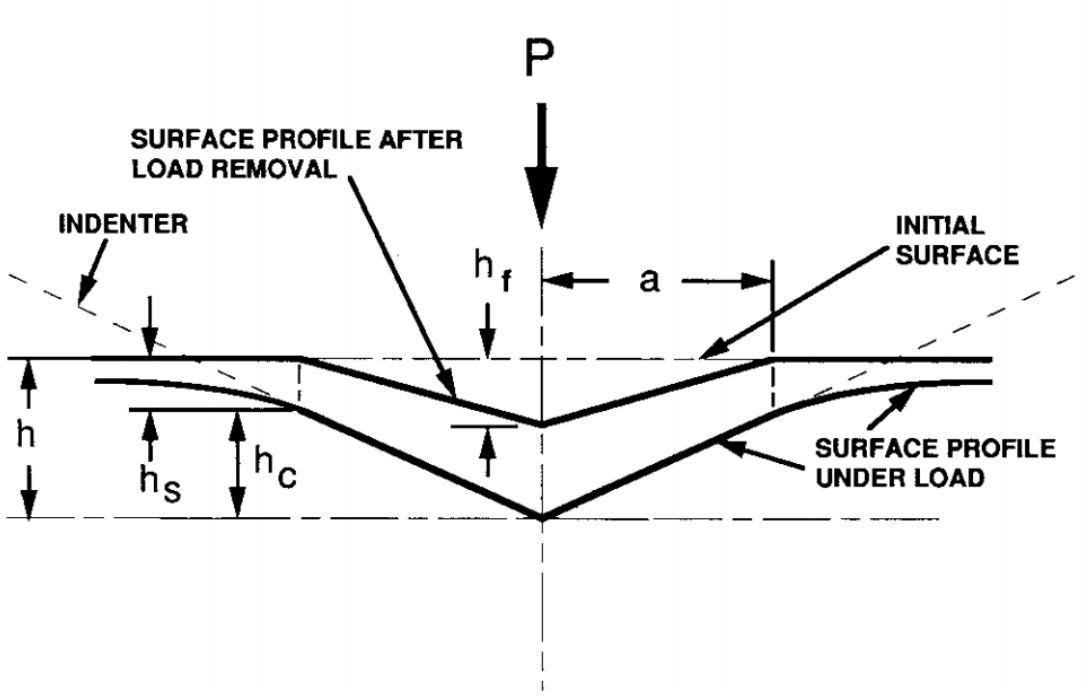

Figure 8. Schematic of cross-sectional indentation process from Oliver and Pharr [40].

3.3 Plastic Properties from Nanoindentation

Plasticity from nanoindentation has only been examined in recent years. Elastic properties were solely studied as they could be easily extracted from the relationships utilized in nanoindentation. Current studies are delving into the smallest range, within about 100nm indent depth to discover the onset of plasticity [41, 42]. This idea has been termed "pop-in" by fellow researchers [43-46]. A visualization of this is seen in Figure 9. As the load is increased, the onset of plasticity can be seen by the jump, where force is constant but displacement is still increasing, shown shaded in the image. This is at such a small load and indentation depth, it would be difficult to image or visualize *in situ*. This may, however, correlate with the onset of pile-up, but in this research, the pile-up was not considered until 200nm indent depth, where it could be seen using SEM techniques.

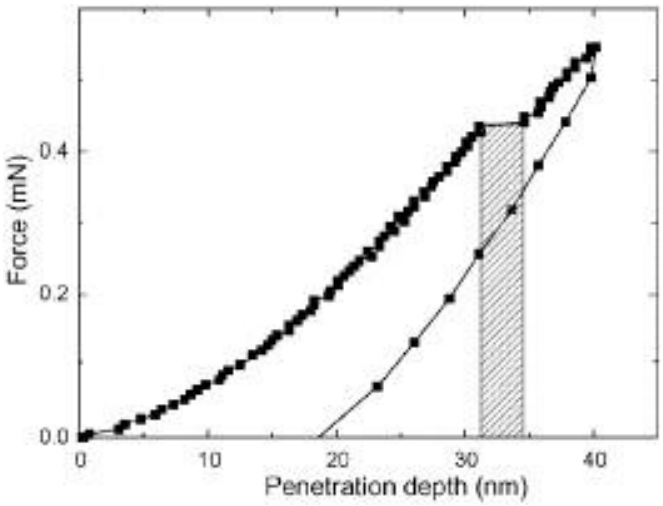

Figure 9. Pop-in from load-displacement curve at small indent depths [46].

Studies in this small-scale plasticity have explained some slip between grain boundaries, and what constitutes incipient plasticity both with experiments and atomic simulations [47-50]. Also, previous work has been done on freestanding films in order to extract material properties [51]. However, this is a complicated procedure that involves many steps to remove the substrate and obtain beams that can be tested easily. The yield stress of gold thin films was garnered from these shapes in previous work [51-55], and compared to the findings here.

4. Experimental Procedure

4.1 Materials Selection

From previous experiments, there was a base knowledge of sputtering and indentation that worked well for the setup. For example, gold was found to be easy to sputter, and silicon was a standard for substrate. Other ceramic substrates were chosen based on their elastic moduli differences and their ability to non-plastically deform. These are seen in Table 1 listed with their tested elastic modulus, if available, and citations indicate literature values, mostly for the Poisson's ratios.

For metallic substrates, the samples were chosen based on their availability from the company, Pasco (Roseville, CA). These ranged from annealed steel, cold rolled steel, aluminum, and brass. The base material properties are seen in Table 2. Because they were

made from the company, the samples were expected to have uniform quality and the manufacturing of the coupon shape was already completed upon arrival.

Table 1. Material Properties of Chosen Films and Substrates.

		Elastic Modulus, E (GPa)	Poisson's Ratio, ν
Films	**Au**	**79 [56]**	**0.42 [56]**
	Pt	**168 [56]**	**0.38 [56]**
Ceramic Substrates	Si	179 ± 3	0.28 [56]
	AlN	302 ± 14	0.26 [57]
	Al_2O_3	300 ± 8	0.22 [56]
	MgO	318 ± 7	0.23 [58]

Table 2. Material Properties of Metallic Coupons from Pasco.

	Tensile Strength (MPa)	Tensile Elongation	Elastic Modulus (GPa)
Cold-rolled steel	620	None	200
Annealed steel	300	42-45%	200
Aluminum	145	6%	69
Brass	430	25%	117

4.2 Film Deposition

Films were created with a Denton DC Magnetron (Moorestown, NJ) sputtering system with a rotating sample holder, seen in Figure 10. Gold and platinum films were utilized in this work. Parameters were chosen based on previous experiments [24, 25], and can be seen in Table 3 and Table 4 for gold and platinum, respectively. Before coating with these metallic films, a titanium adhesion layer with an aim of 10nm film thickness was deposited initially.

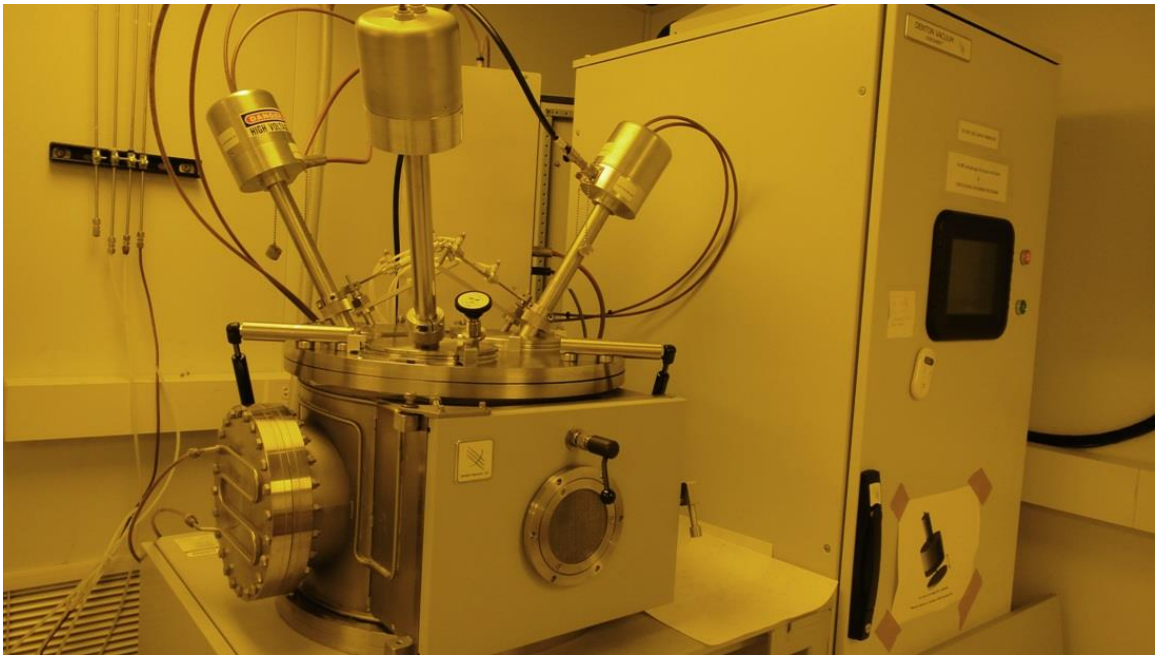

Figure 10. Denton Sputter Coating system in Wilmore Laboratories, 2015.

Table 3. Sputter conditions for gold film.

Presputter Power	100 W
Presputter Time	60 sec
Sputter Power	100 W
Gas (Ar) flow	25 sccm

Table 4. Sputter conditions for platinum film.

Presputter Power	100W
Presputter Time	60 sec
Sputter Power	100 W
Gas (Ar) flow	25 sccm

4.3 Thickness Measurements

It was found that thickness is a crucial property in modelling the behavior of thin films on substrates during nanoindentation. The metallic film samples were prepared in a way that an edge was masked by Kapton tape (Torrance, CA). When the tape was removed, there was a clear step between film and substrate. The Bruker/Veeco Dektak 150 Profilmeter shown in Figure 11 was utilized at Auburn University, Mechanical Engineering Department. An average of four locations were taken from each edge, and the thickness of the films were compared across materials, as well. It was believed that the edges may not be the best representation of the local indent, however, which is typically done to avoid the edges. Instead, it was confirmed with focused ion beam (FIB) utilizing a TESCAN LYRA FIB-SEM from University of Alabama, Department of Materials Science and Engineering, seen in Figure 12. This equipment was also used to image cross-section area of the indents, which is shown in later work.

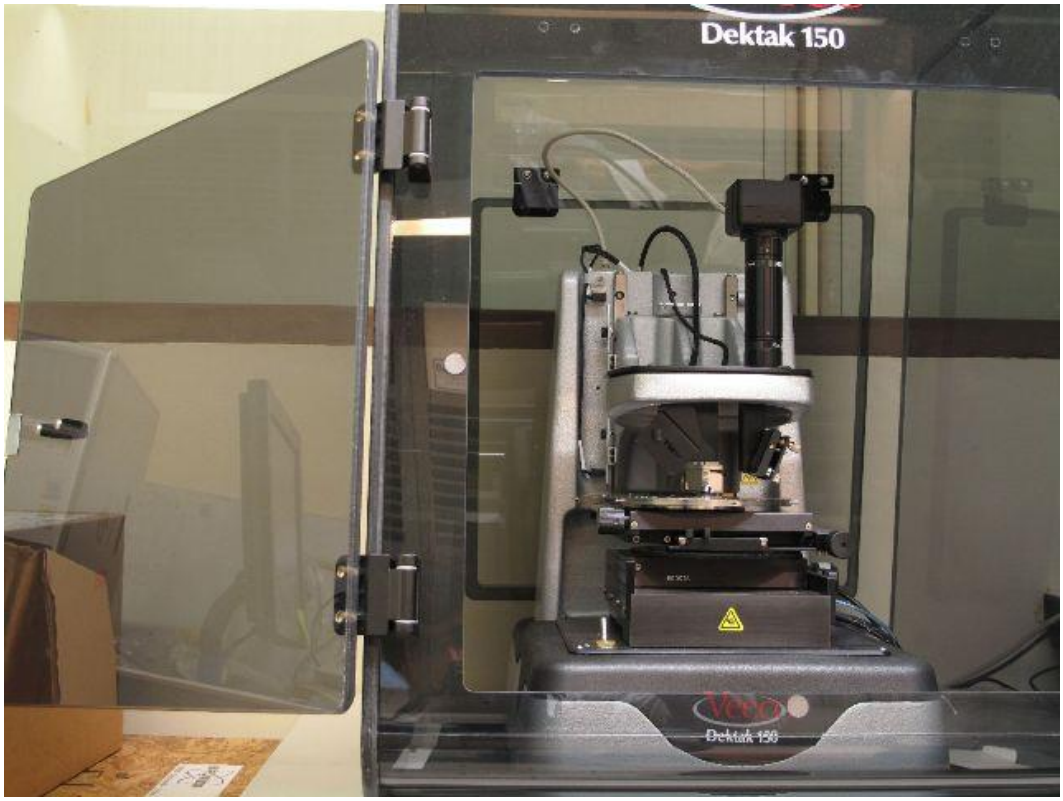

Figure 11. Bruker/Veeco Dektak 150 Profilometer from Dr. Robert Jackson's laboratory, Wiggins Hall, Auburn University, 2015.

Figure 12. FIB TESCAN LYRA FIB-FESEM from Central Analytical Facility, University of Alabama, 2015.

4.4 Tensile Testing

A normal tensile test setup could not be utilized in this work because of the miniaturization of the samples. The force required would be much too low for a standard setup of metallic dogbone samples. Instead, a handheld tester was found via Pasco (Roseville, CA), titled Materials Stress Strain Experiment, PASPORT. This machine allows for a manual displacement change measured by a force sensor to 50 N. The force is multiple based on the lever arm used, seen to the left in Figure 13, so the maximum force is increased to 500 N. The piece seen labeled as stress/strain apparatus is the component that has a wheel that moves to convert rotational displacement into lateral displacement. With a turn of the wheel, the machine is calibrated in order to move the sample a certain amount. The sample is secured with a series of washers and nuts, with a spring closest to the sample, in order to prevent slippage during testing or torsion during tightening.

The data from the force sensor and rotational displacement are input into a USB port, and are compiled with software package from Pasco, titled PASCO Capstone, that is coupled with an 850 Universal Interface. Multiple samples can be tested, and are all calibrated before the initial run. Additionally, the variables can be changed to express stress,

calculated form the load over cross-sectional area, and strain, taken from the displacement data, change in length over original length.

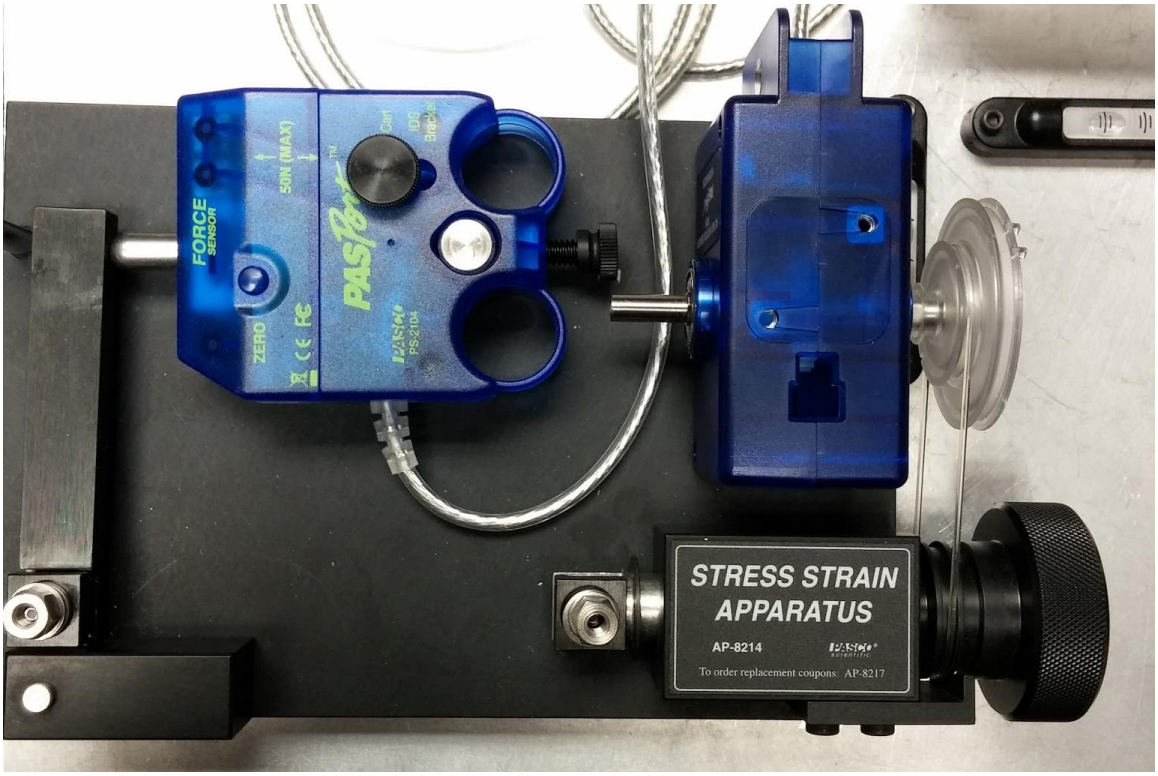

Figure 13. Pasco handheld tensile test setup.

4.5 Metals Preparation

The ceramic sample substrates were purchased from the company, MTI Corp (Richmond, CA) pre-polished, as the ceramic substrates can be difficult to polish to a smooth surface. The other metallic coupons, however, were cut from the samples that were pulled by tensile testing. Their surface was not completely smooth to start, as the samples were previously processed to be made into the coupon dogbone shape. Post tensile testing, coupon pieces were cut from tested samples and carefully mounted on aluminum pucks using a melt polymer, Crystalbond (West Chester, PA). Using typical metallographic preparation techniques, the coupons pieces were polished to a mirror finish. Grinding was skipped because first, the samples were relatively smooth, and second, the initial cross-section was very small at 0.003 inches. Polishing was completed with 0.1 alumina suspension on a Struers RotoPol-11 Surface Polisher (Cleveland, OH), followed by colloidal silica

polishing; the equipment is pictured in Figure 14. The end result was a smooth surface ready for indentation or sputter coating.

Figure 14. A Struers RotoPol-11 Surface Polisher located at Auburn University, Materials Engineering Department 2015.

4.6 Nanoindentation

Indents were created with an MTS Nanoindenter XP, seen in Figure 15. The tip was a Berkovich diamond indenter tip with a tip radius <10nm. Continuous stiffness measurement was used in order to gather material property information as a function of displacement. This gives maximum information from the indent, compared to a singular indentation test, there is only one data point taken from the top of the unloading curve. However, in CSM, the complete data set from every indent depth can be visualized and is crucial in this work as the Zhou-Prorok model utilizes the information throughout the indent, and also, it is prudent to measure the properties as a function of displacement when there are thickness variations, as well.

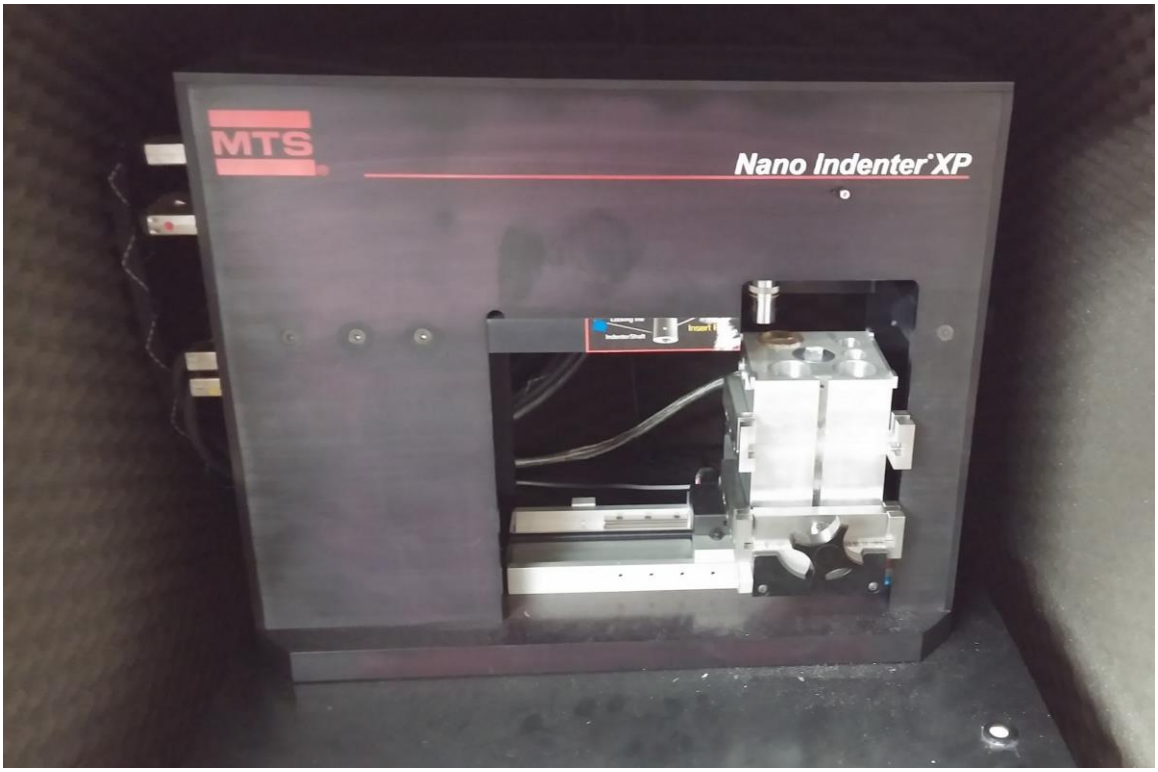

Figure 15. MTS Nanoindenter XP at Auburn University, Materials Engineering Department, 2015.

4.7 Imaging

Images of the sample after nanoindentation were completed with a JEOL 7000F (Peabody, MA) scanning electron microscope (Figure 16). Samples were imaged with secondary electrons at 20kV and a working distance of 10mm. The images were taken at uniform magnifications for easy comparison. Some analysis utilized electron dispersive x-ray spectroscopy, an attachment of the SEM machine. X-rays from the sample surface are analyzed and compared to a database of elemental properties. It is possible to examine the samples in this manner especially when mapping the indent in order to see the indenter punching past the film into the substrate.

Figure 16. JEOL 7000F Scanning Electron Microscope in Wilmore Laboratories, Auburn University 2015.

4.8 X-Ray Diffraction

X-ray diffraction (XRD) was an additional testing method utilized for a substrate comparison between steels that had been cold rolled or annealed. It is possible to analyze the peak broadening that is due to the lattice strain in order to compare the samples. The equipment utilized was a Bruker Discover D8 (Billerica, MA) in Wilmore Laboratories at Auburn University. Chosen 2θ angles ranged from 5 – 90 degrees in order to obtain any peaks that were present. The information was analyzed through EVA software to obtain the overall peak information, along with calculations of the full width half maximum of the individual peaks.

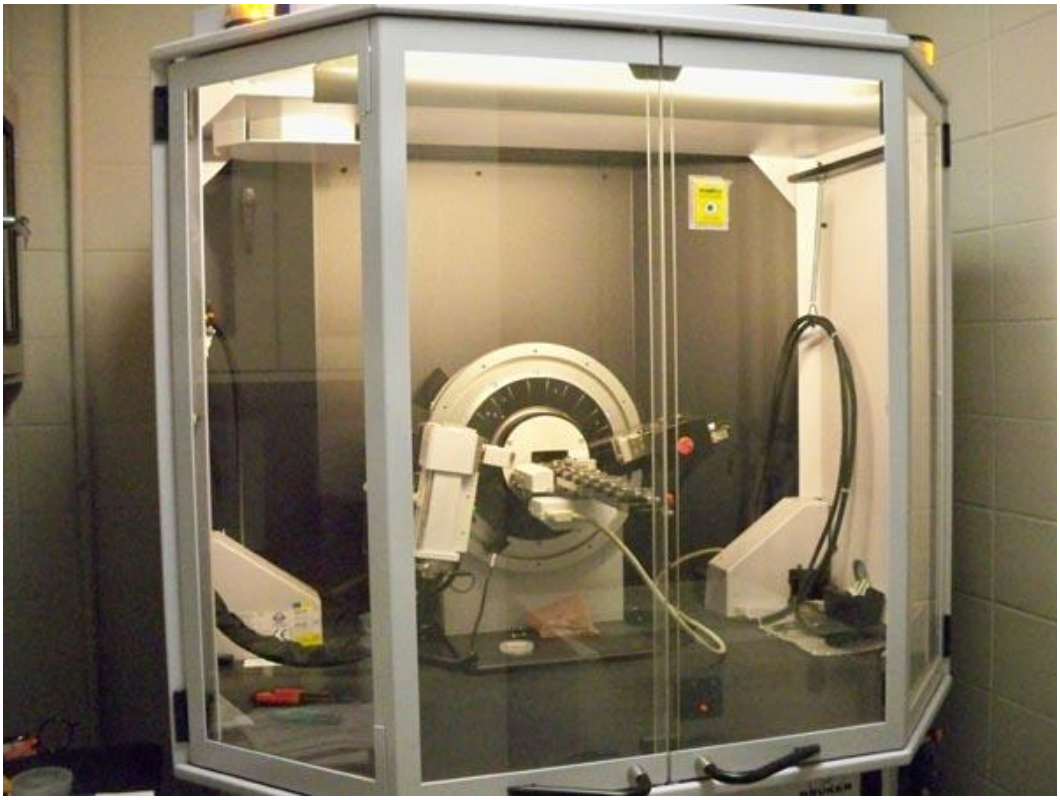

Figure 17. Bruker D8 Discover located in Wilmore Laboratories, Auburn University 2015.

4.9 Measurements

Measurements were completed with ImageJ software [59]. The novel method is further explained in the results section. The basic protocol for ImageJ includes a standard for measuring the scale bar included on an SEM image to correlate the number of pixels to microns. Then, it is possible to draw lines and areas that outline the necessary projected areas seen. This program has been utilized by others, but never for measuring indentation areas from the projected indent images.

5. Results and Discussion

5.1 Fitting the Zhou-Prorok Model

The first task was to confirm the model from Equation 5 operated in the first chosen system of materials, which was gold on ceramic-like substrates. Most simply, gold on silicon has been a common combination that has been studied in this lab and others [30]. Gold is easy

to sputter, and its inertness is an advantage as no oxide layer is formed on the surface, which has seen to skew initial results in other metals. Silicon is inexpensive and is very readily available as a substrate. As seen Figure 18, the Zhou-Prorok model was applied to a gold film 625 nm thick on a silicon substrate. The black solid line denotes the film modulus (gold, 79 GPa) and the red solid line denotes substrate modulus (silicon, 179 GPa). The complex interplay between elastic moduli and Poisson's ratios of the film and substrate allow for this fit [60, 61].

The open circles confirm that the Zhou-Prorok model is valid because it can accurately extract the film modulus. The solid black line data comes from previous tests using a different method, a membrane deflection experiment (MDE) [62, 63]. In these tests, elastic modulus of gold thin films was provided using a different method so as to compare with the nanoindentation tests. Some errors at low indentation depths are attributed to a loss in contact [64]. Using CSM, the indenter may not be fully in contact when oscillating at low indentation depths, usually under 100nm, which be seen in almost all of the indentation data presented.

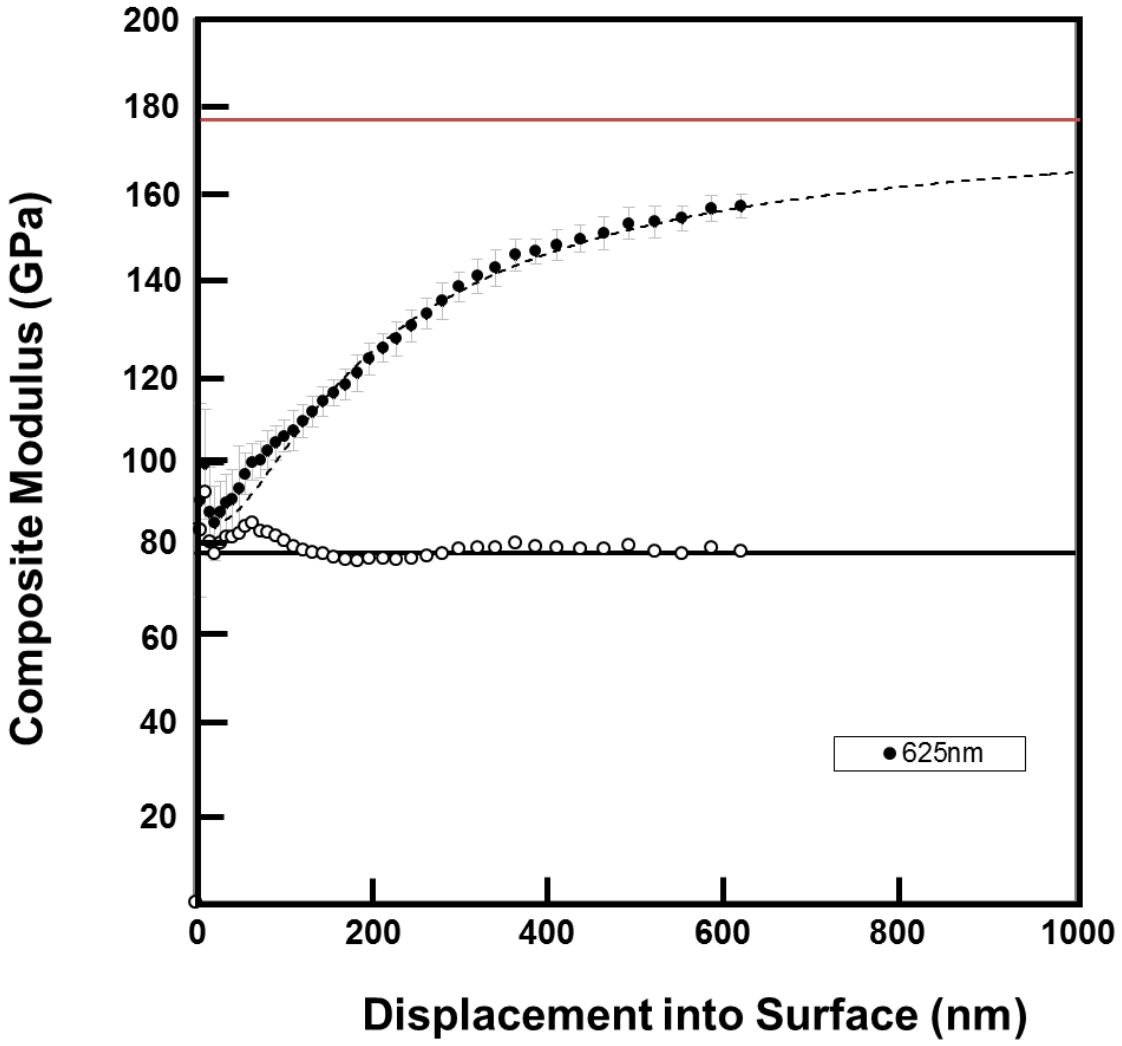

Figure 18. Gold film 625nm thick on silicon following the Zhou-Prorok model.

5.1.1 Fitting the Zhou-Prorok Model to gold films on silicon substrates

Next, different thicknesses of gold on silicon were indented and plotted along with the Zhou-Prorok model. Again, the model correctly predicts the composite modulus up to the film thickness. It is also verified by extracted film thickness, all aligned around 79GPa for gold, the solid black line. Figure 19 shows these trends. The standard deviation seems to increase with increasing thickness, which is explained by the grain size differences. If there are longer times for sputtering, then the grains may have a longer time to rearrange or grow. This has been show in previous work from the Prorok research group, utilizing electron backscatter diffraction to view grain changes with indent depth [65]. These

findings can explain the difference of the Figure 19 curve for the thickest film tested, 950nm.

With the experimental data comparing different thicknesses in Figure 19, it is evident that the film thickness is affecting the elastic modulus. In order to compare this experimental data without thickness variations, the x-axis was divided by the thickness (Figure 20), with modulus plotted against normalized displacement, h/t. The results from experimental and the model now all collapse onto the same curve. This is expected for the model because the information is solely based on material properties. The data follows the model, so it can be determined for gold on silicon substrates, the film thickness does not affect the elastic modulus. To confirm, the film elastic modulus is again extracted and follows the MDE values for gold.

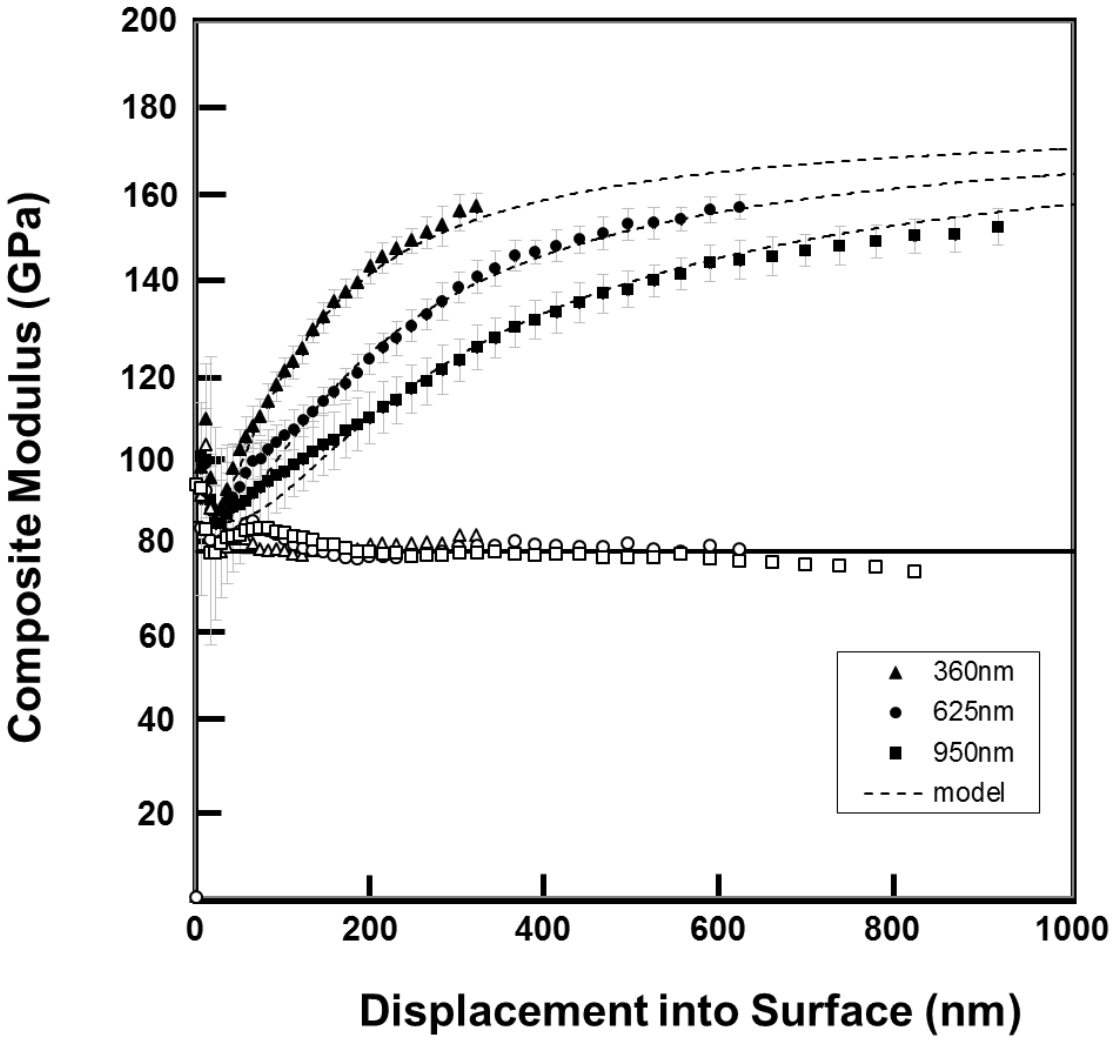

Figure 19. Experimental data of gold film of different thicknesses on silicon (solid markers) with model (dashed lines) and extracted film modulus (open markers) lining up with literature values.

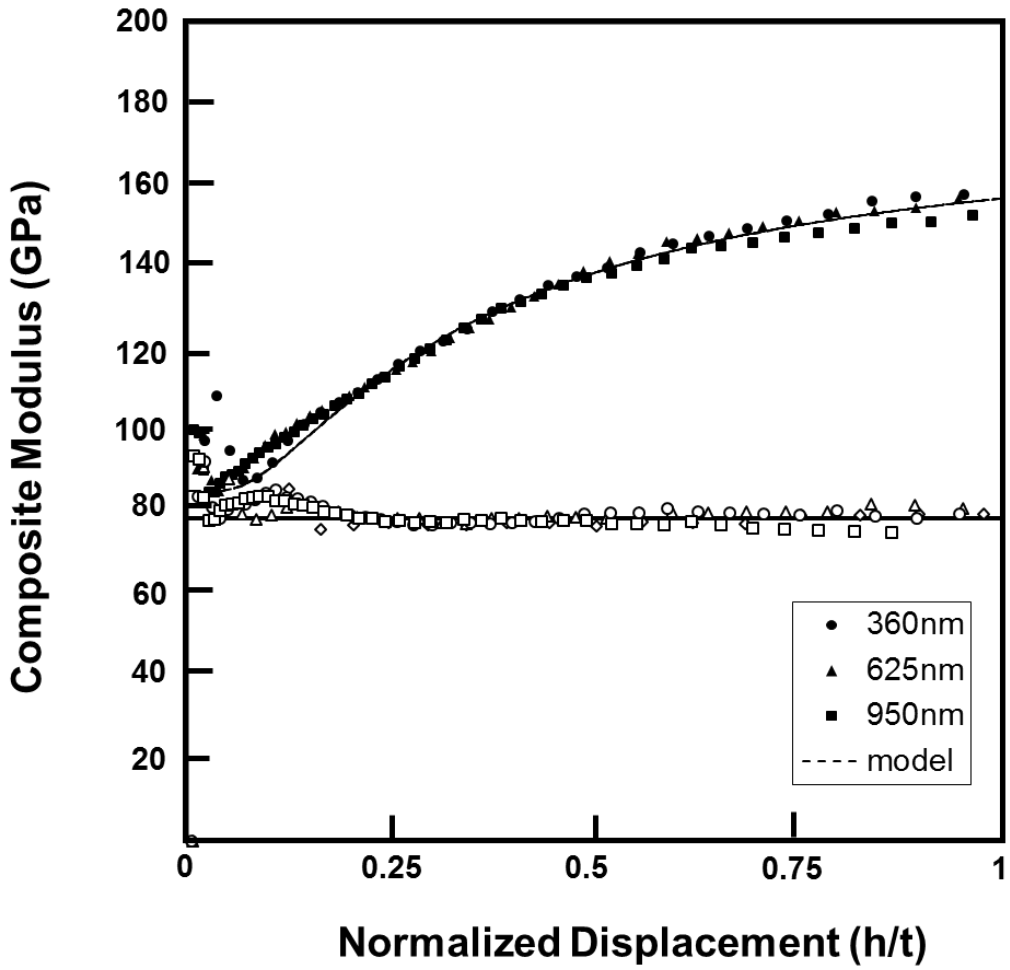

Figure 20. Composite modulus vs. normalized displacement for three different film thicknesses of gold on silicon with model fitting and extracted film modulus.

The model is accurately predicting the trend regardless of thickness and indent depth, but it is interesting when viewing the indents with SEM. Figure 21 shows the progression from 200nm to 1200nm of 625nm gold on silicon. It is evident where the film starts to peak through, after 625nm. From these images, it is clear that there is pile-up. It grows continuously as the indent depth increases for this thickness. In our cases, we start measurements around 200nm because that is where the pile-up begins to appear with our observation methods. With indents any smaller, it becomes very difficult to find in the SEM, to image clearly, and measure accurately.

Even though there is more pile-up as the indent depth increases, the model still predicts and still can extract the substrate modulus. This is unusual, and either the model is accounting for the changes, or pile-up plays no role in the elastic modulus calculations.

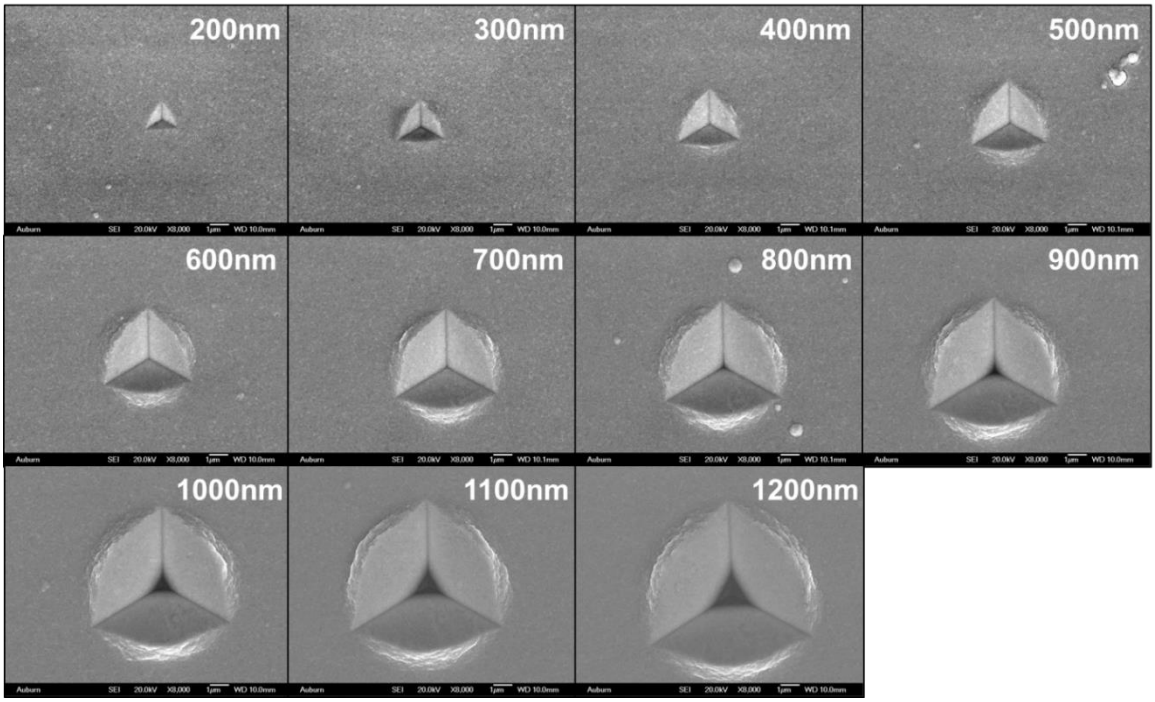

Figure 21. Progression of indents on film-substrate combination of 625nm gold on silicon.

5.1.2 Novel Measurement Techniques Utilizing ImageJ

The images taken from the SEM were imported into ImageJ software. Here, using the micron bar as calibration, the projected area was calculated by using the number of pixels. The process is seen in Figure 22 where the total area, projected area, and pile-up area can all be measured by creating an outline in the software. In Figure 22b, the Oliver-Pharr area is the residual triangular indent that is typically used for area calculations. Either the projected area is subtracted from the total area (solid lines) or the lobes of pile-up can be measured alone. The flexibility and ease-of- use of the ImageJ software is beneficial for these measurements.

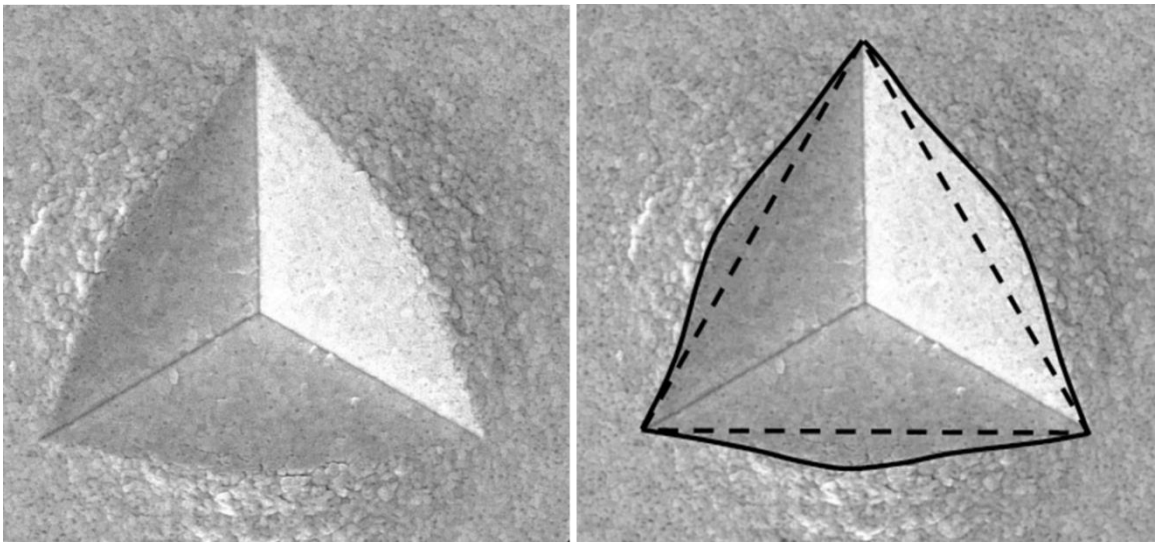

Figure 22. Outlines from ImageJ software for a) original area, b) projected area with dotted line and pile-up area the area between the dotted and solid lines.

This unique method of measuring pile-up allowed for comparisons across film-substrate combinations. It is not expected that this would be the way to determine pile-up in the future, as the motivation for nanoindentation is to eliminate the need to image the indent. Instead, these images are used as a means for characterizing the error introduced by pile-up, in order to test for robustness. The different areas in the Figure 22 can be separated and defined as projected area, total area, and pile-up area. Projected area also follows a specific equation, $A=24.5h^2$ because of the self-similar geometry of the Berkovich tip. Next, total area is measured, which is all visible deformation that may be in contact with the indenter tip. The difference between total area and projected area gives the three lobes outside the triangle, defined here as pile-up area. Figure 23 shows these three measurements plotted as area vs. displacement into surface for one specific sample, 360nm gold on silicon. The trends are all similar, and increase with increasing indent depth. The open triangles represent the projected area, and align with the geometrical equation noted with the solid line. The pile-up area is highlighted with the dark circle markers. This is the value that is a unique measurement and most important for our study. The open squares are total area, calculated as the addition of the triangles and circles, or the projected and pile-up area. This is shown for only one gold film thickness of 360nm on silicon, but more thicknesses of gold on silicon substrates were tested.

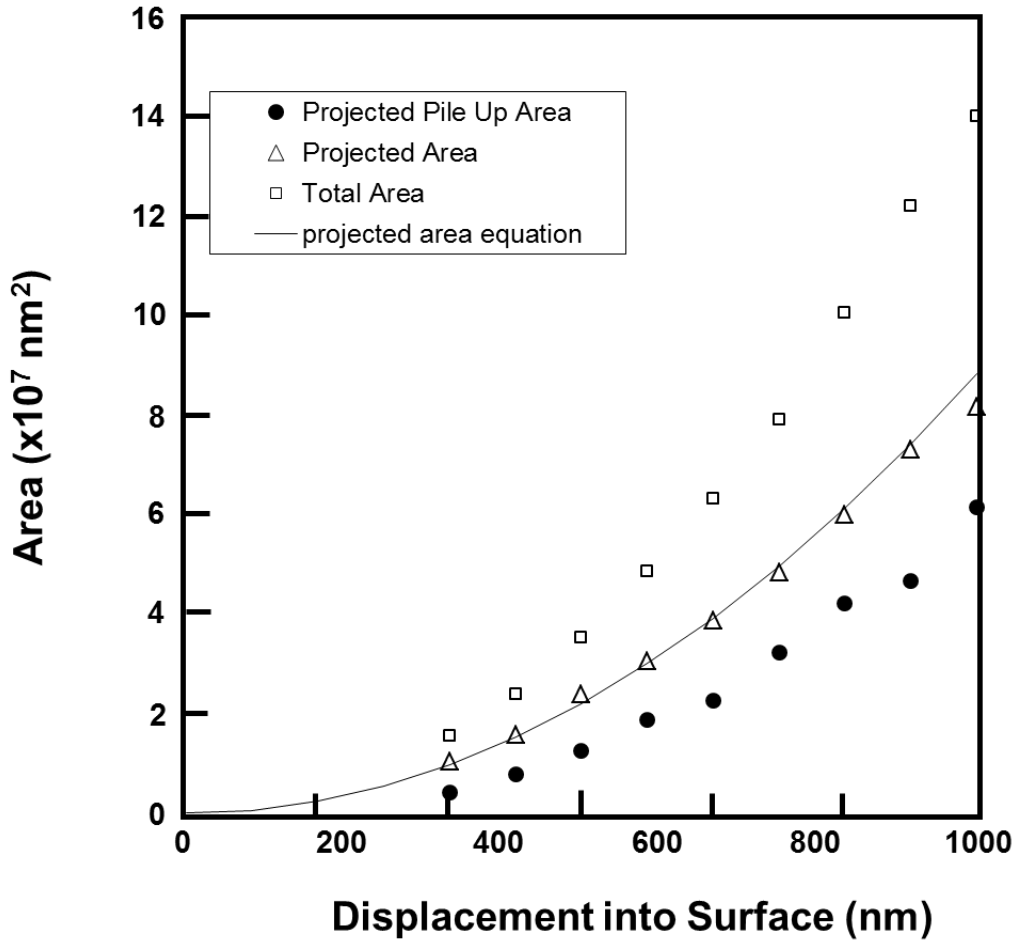

Figure 23. Projected area, total area, and pile-up area for 360nm gold film on silicon substrate. The trend still holds even past the film thickness.

5.1.3 Different Thicknesses Do Not Affect the Model

The data is even more interesting when comparing across different film thicknesses. The pile-up area was calculated the same way for all of the gold on silicon samples, and the pile-up is strikingly the same as indent depth increases. No matter the thickness, if an indent is performed at one displacement, for example 400nm, the pile-up will be identical across the samples. Figure 24 shows the numerical data, while Figure 25 visually depicts this behavior. The pile-up information was only considered up to the film thickness. An average of four indents with pile-up were measured, and the trend line is depicted on Figure 24. It is very surprising that now, no matter the film thickness, the pile-up is following the same trend for this film/substrate combination.

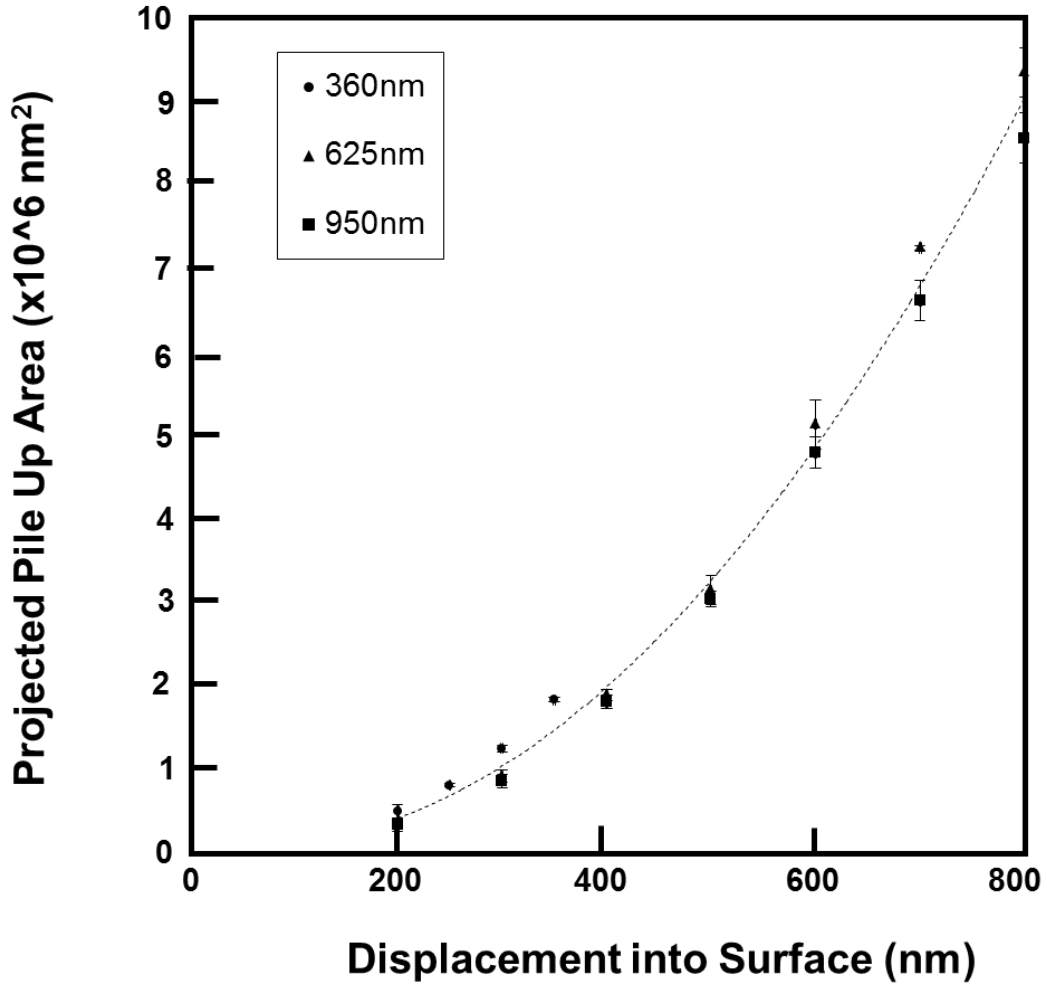

Figure 24. Pile-up area for all thicknesses of gold film on silicon substrate, following the same trends.

When using SEM to view the indents, the pile-up looks identical at the same indent depth. The SEM images are compared to a schematic of the indenter tip penetrating through the film in Figure 25. With a film thickness of 360 nm, the 400 nm indent is just hitting the substrate, or 111% into the film. For 625 nm, the indent tip is about 60% into the film, and for 950nm, about 42% into the film. However, even with the different percentages, the pile-up is identical at the 400 nm depth no matter the film thickness. This observation is very peculiar, and it leads us to believe that it may not be necessary to account for the different pile-up for this material. All researchers mentioned in the introduction have been adjusting areas because they have been using the equation from the indenter that includes

the area. However, with the Zhou-Prorok model, area is not a consideration, and the model still fits the experimental data. The distance from the substrate does not seem to play a role in dictating the pile-up; it seems as though only the film is affecting the pile-up trends.

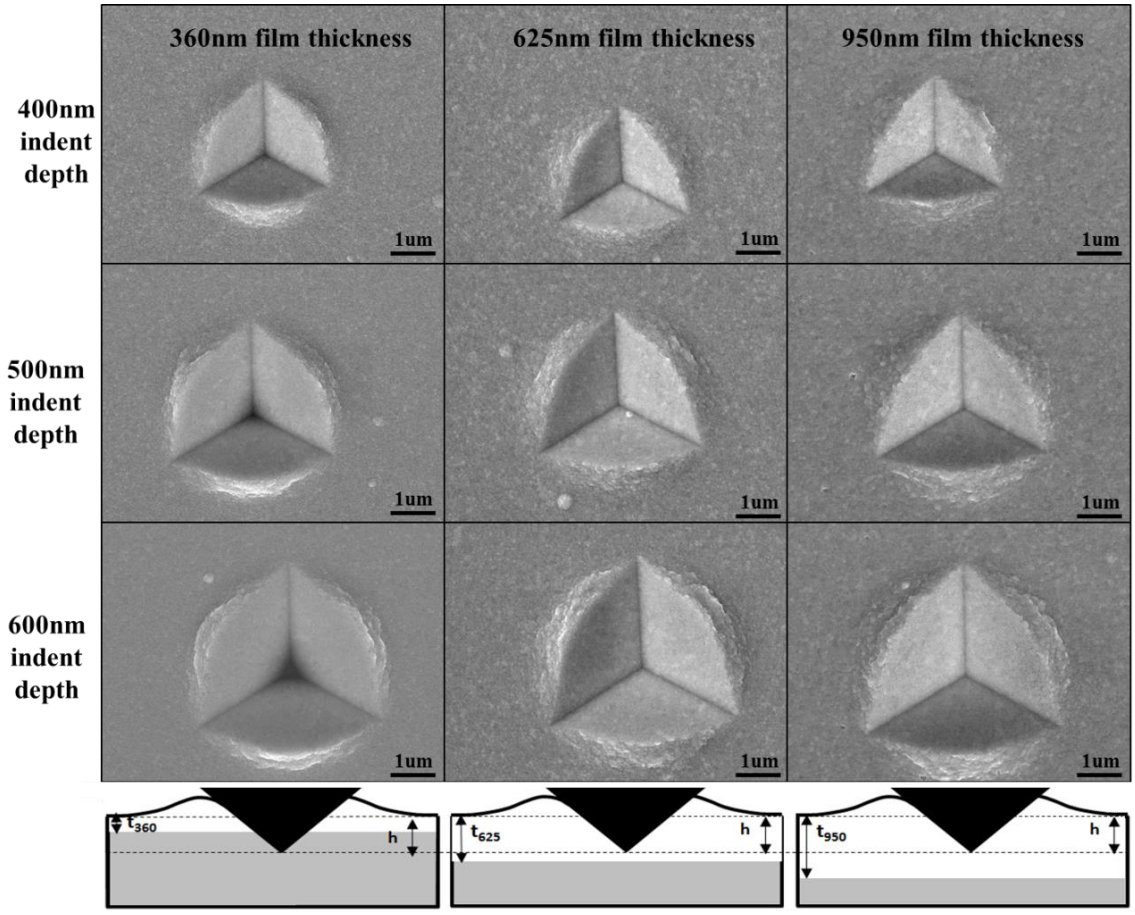

Figure 25. Pile-up across different gold film thicknesses on silicon substrate all at 400nm indent depth and identical pile-up amounts.

The next step was to try different substrate materials to see if this is the case. Initially, it was thought that the model was accounting for these parameters unlike other models, so more experiments were completed to test this hypothesis further.

5.1.4 Different Substrates' Effects

The substrates were chosen carefully to prevent any plastic deformation, and were all sputtered at the same time to ensure uniform thickness. Even though the material properties are different, the model still accurately predicts the experimental composite modulus.

Figure 26 demonstrates that the model, (dotted lines), matches the experimental data and still verifies the film elastic modulus, (open markers) as 79 GPa for gold. The film was 360nm thick, and the model was fit up until the film thickness. An array of 25 indents was completed, and averages with standard deviation are shown with the error bars. Data for the model fitting is seen in Table 5.

When the same processing was done on the indents, with SEM images and ImageJ analysis, the projected pile-up area is plotted in Figure 27. This is analogous to Figure 24, but only the pile-up area is plotted for clarity. Up until the film thickness, the pile-up area is identical at the same indent depth, no matter the substrate. Only the gold film seems to be influencing the pile-up. All of these substrates are much harder than the film, and the pile-up is surprisingly identical.

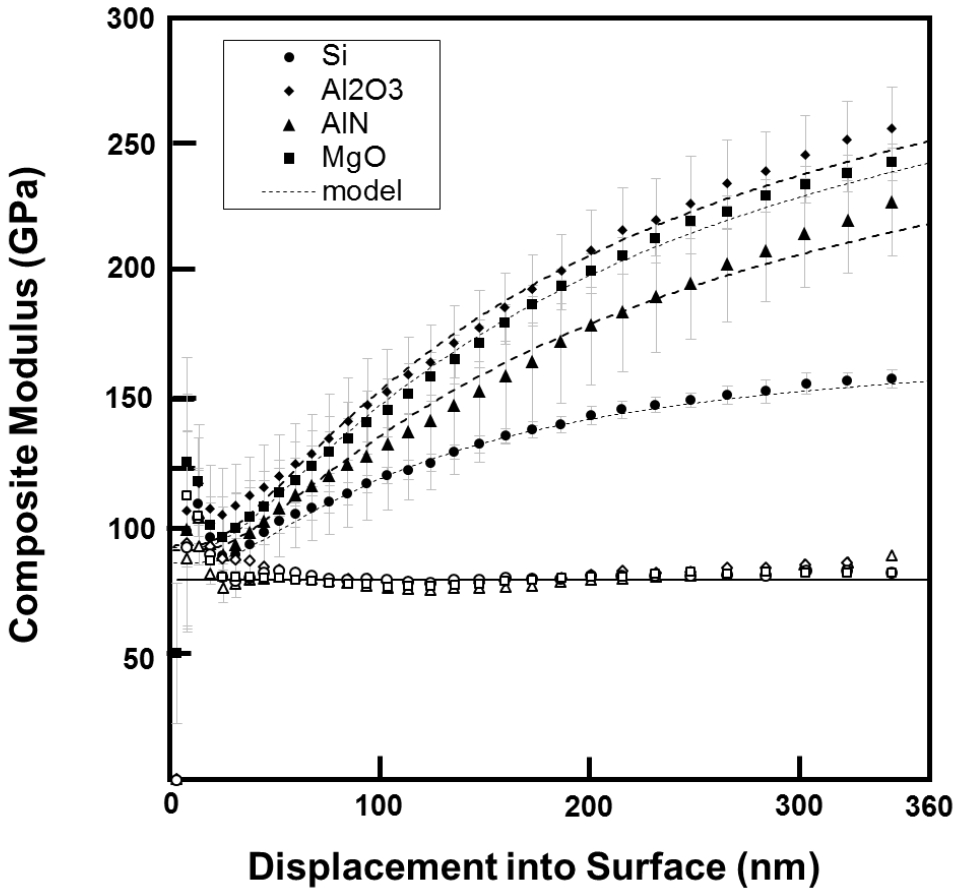

Figure 26. Gold on ceramic substrates, fitting the model and extracting correct film modulus.

Table 5. Data that fits in the model for gold film on different substrates.

Substrate material	Substrate E	Substrate v	Au Film E	Au Film v
Si	179	0.27	79	0.44
Al_2O_3	350	0.22	79	0.44
AlN	316	0.26	79	0.44
MgO	345	0.23	79	0.44

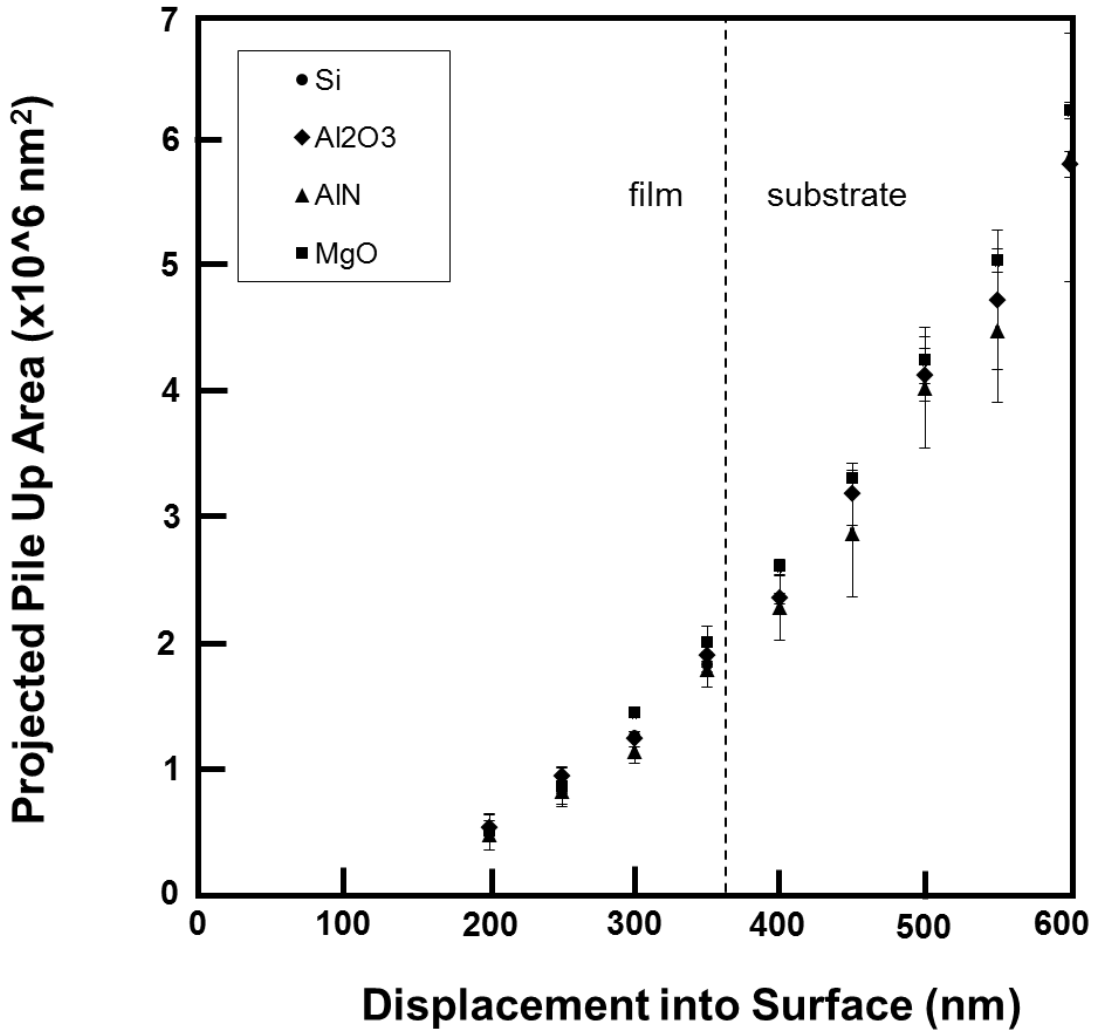

Figure 27. Pile-up area for different substrates with same gold film thickness, 360nm.

The SEM images are shown for verification in Figure 28. Although it seems error may be introduced by the roughness past the projected pile-up area, following identical measurements along the edges where the top of the pile-up is evident produces similar values. Interestingly, this experimental data indicates the substrate affects the elastic modulus, but pile-up does not. Neither the substrate nor the film thickness is affecting pile-up. It was over-zealous to assume that the Zhou-Prorok model was accounting for pile-up in some way; instead, the pile-up is not affecting the elastic measurement at all.

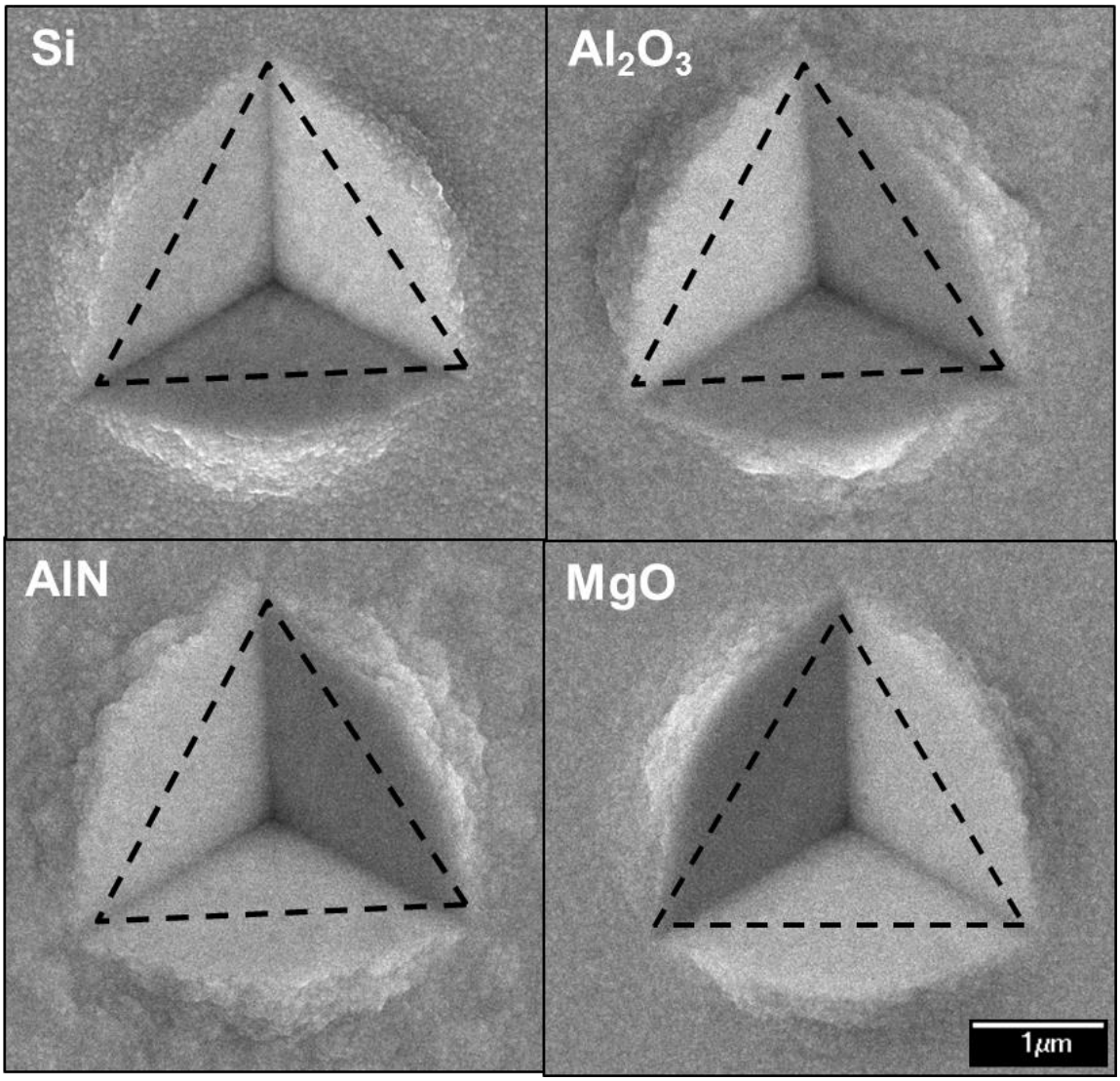

Figure 28. Visual evidence of same pile-up at 400nm indent depth for four different substrates with 360nm gold film.

5.1.5 Different Films show different results

Because the behavior of pile-up seemed consistent for gold films, the next step was to confirm this was not an abnormality with the one chosen film. Platinum is also easy to deposit, and had been previously tested in the Prorok lab [66]. The same procedure was followed for the platinum films. Four different thicknesses of 292, 590, 777, and 1014nm were achieved with the sputtering conditions seen in Tables 3 and 4 in the procedure section.

After sputtering, the films were all nanoindented and fit to the Zhou-Prorok model. Although it is assumed the material properties of E and ν will be different than gold, when inserting the parameters into the Zhou-Prorok model, the composite E is still well-predicted. The pile-up area was measured for all four thicknesses, and again, no matter the film thickness, the pile-up follows the same trend for platinum. This is seen in the open markers in Figure 29, and the short dotted line follows the trend. The platinum data is compared to the same gold data found in Figure 27. The pile-up is different for platinum than it is for gold, but the idea that film thickness and substrate material do not play a role still holds. The platinum was also tested on the ceramic substrates and follows this trend, as well. To visually compare the platinum and gold pile-up values, Figure 30 demonstrates side-by-side SEM images of the samples. They have very similar thicknesses (777nm for gold and 742nm for platinum), and are indented to the same depth, 500nm. The magnification is the same for both, as well.

The substrates are identical when comparing the gold and platinum, so it must the film material properties that are controlling the pile-up. However, elastic modulus and Poisson's ratio are used to correctly model experimental data in the Zhou-Prorok model, so there must be other factors related to the film that are controlling the pile-up. Elastic moduli are different between gold and platinum, but it is more likely plastic properties are controlling pile-up. The next step was to examine substrates of varying yield stresses that can plastically deform. Extracting the plastic properties of the substrate was the aim in order to find the plastic yield stress of the film.

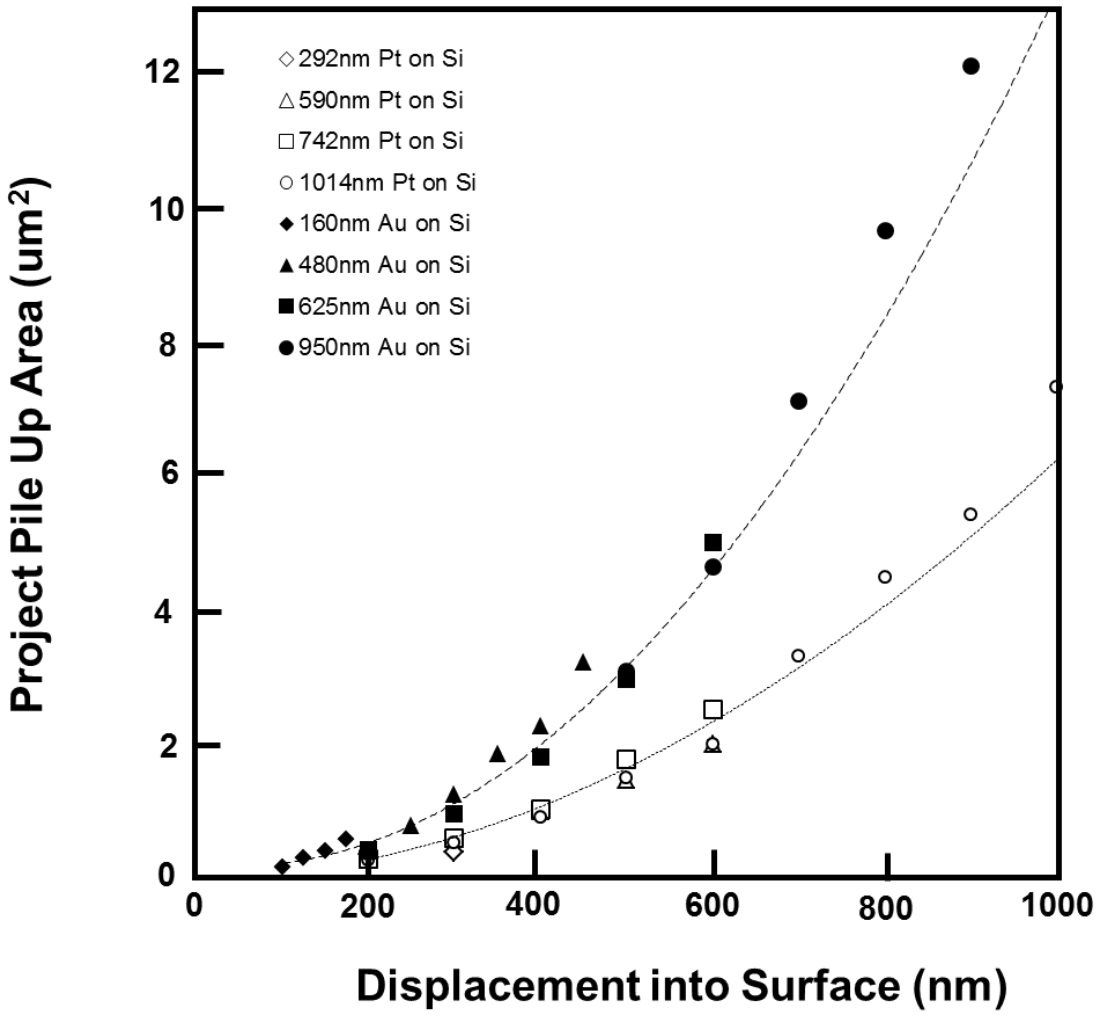

Figure 29. Comparison of pile-up for gold and platinum films on silicon substrates.

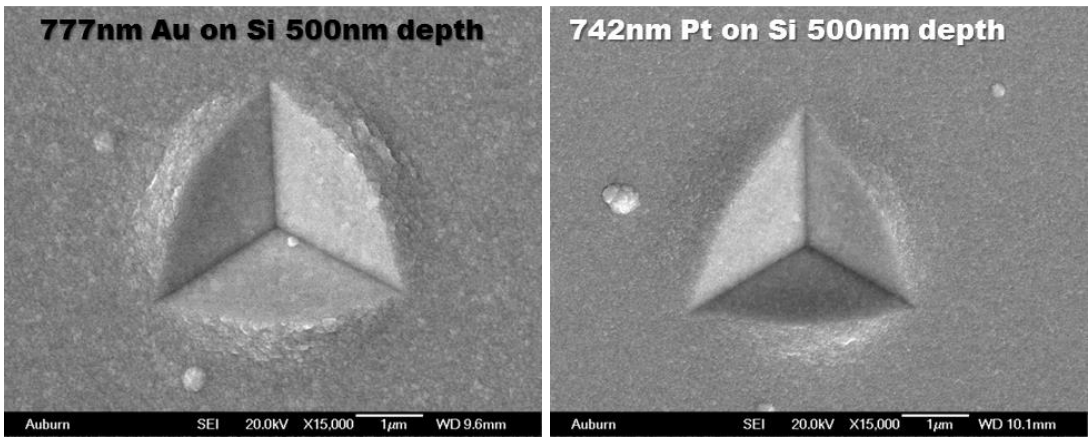

Figure 30. Side-by-side image of gold and platinum films about the same thickness and same indent depth with different pile-up behaviors.

5.2 Yield Stress Changes

A basic engineering technique was employed to test and control the yield stress of materials. In this work, nanoindentation has been the focus, but tensile testing was sought out to compare and impart differences in yield stress. It is known that when a material is loaded in the tensile direction, the yield stress can be read directly from the stress-strain curve seen in Figure 31. The point at which there is a transition from the linear elastic portion is considered the yield stress. When loaded past this point, the atoms are being rearranged instead of solely bonds being stretched, so yield stress then changes. Work hardening is occurring in the material, and yield stress increases with additional elongation.

The equipment described in the experimental procedure was utilized in this sense. Metallic coupons from Pasco were stretched manually in this way. The stress-strain curve was determined through the rotational displacement and the load sensor. The curve followed what was expected of a stress-strain curve for a metal in all cases.

In theory, if the material is loaded below the yield stress, the elastic portion of the curve is all that will be activated. Passing the yield stress, the trends still follow, but if reloaded, the yield stress increases. Annealed steel had the largest range to adjust yield stress, and the others could be loaded to about four different stresses within the range in order to obtain a variety of yield stresses of the metallic substrates.

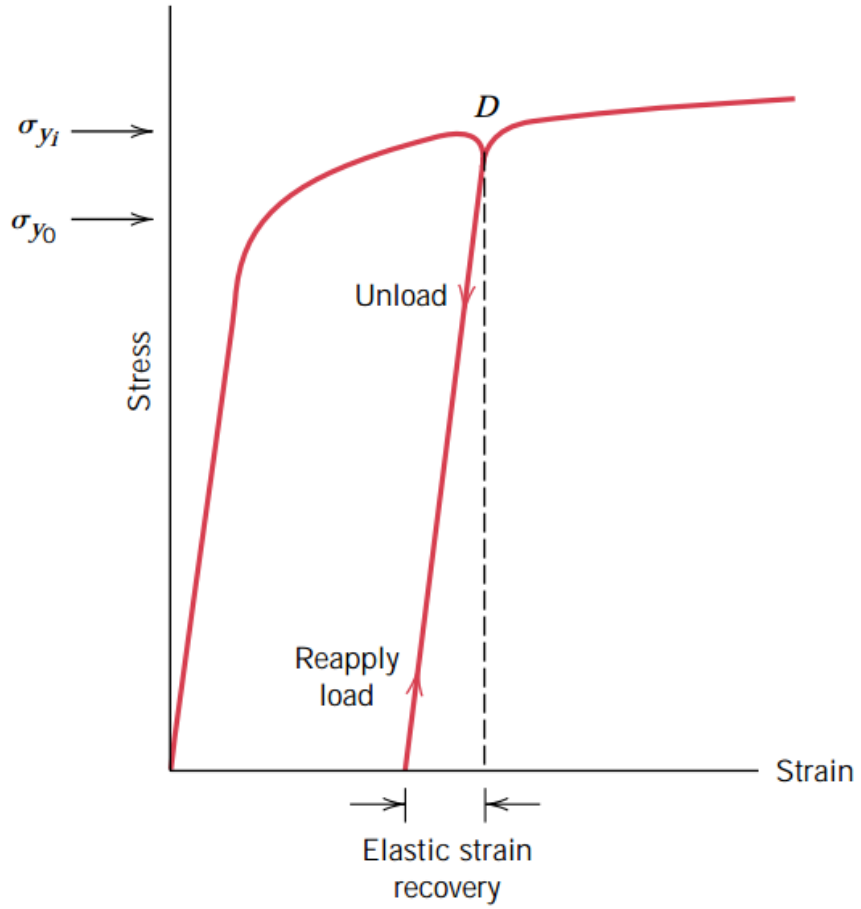

Figure 31. Elastic recovery after loading past yield stress [56].

Pulling each metal resulted in elongation of each coupon with progressively greater length as some plasticity was introduced. Annealed steel had a great opportunity for plastic deformation. Between each yield stress, there was not a greatly noticeable change in length, but in the final pull, the material failed after elongation, seen in Figure 32. The material failed at a 45 degree angle, which is typically in a steel as the maximum shear stress is at an angle 45 degrees from the tensile direction. The progression of yield stresses shown here are untested around 160 MPa, then tested 175, 225, 275, 300 MPa, and to failure at 320 MPa.

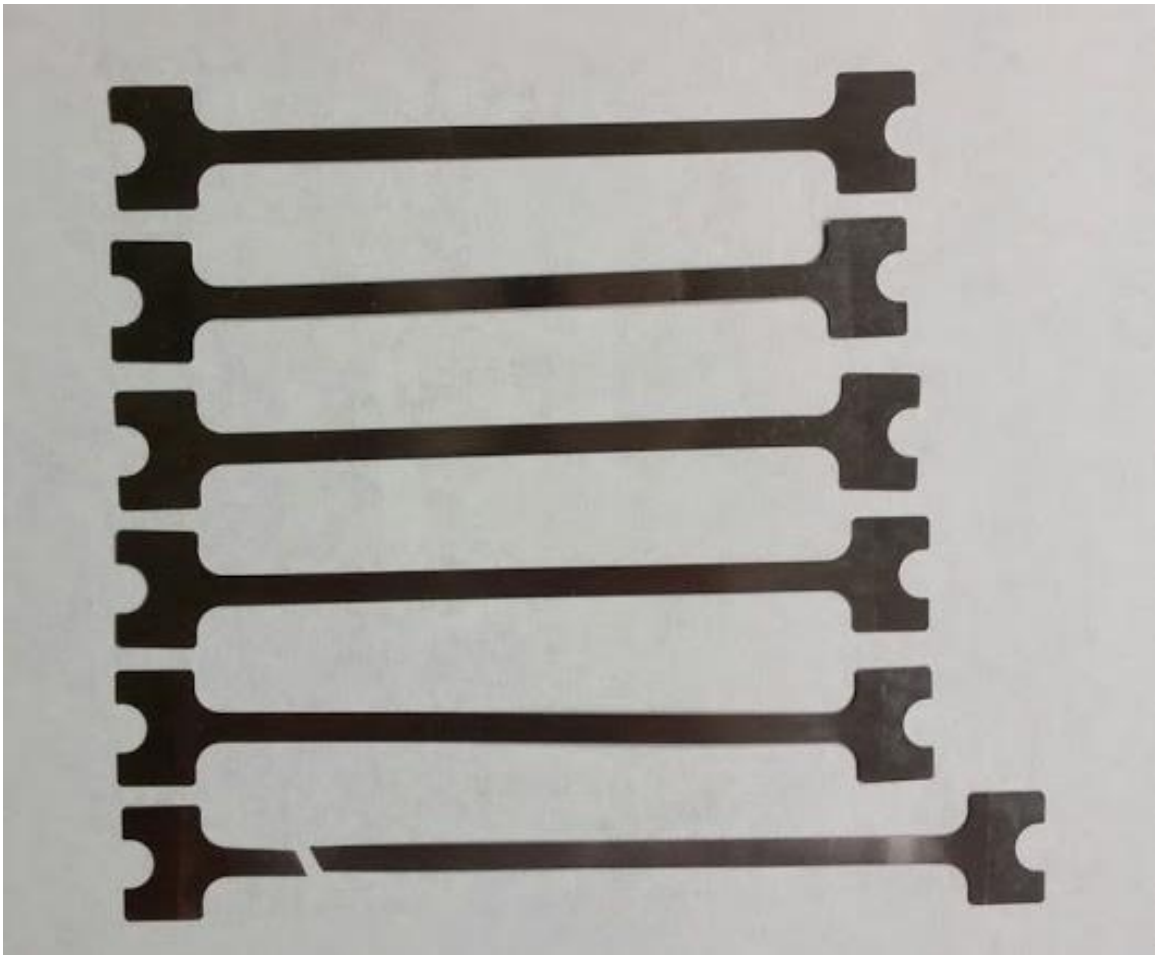

Figure 32. Elongation of annealed steel with progressively longer coupons with added plasticity.

All of the metal coupons were tested with the handheld tensile setup by Pasco explained in the experimental procedure. First, the stress-strain curve for aluminum is shown. It had a capacity of 62 MPa to failure, so points were chosen to stop testing below this value. The data is shown in Figure 33. The run to failure of 62 MPa is expressed, and has no unloading curve. The other values of 45, 50, and 60 MPa are shown with an unloading segment. With increasing plasticity, the yield stress was changing slightly by 5 MPa. The loading curves are all identical as these follow the elastic response of aluminum, measured to be about 69 GPa, matching literature values. Each unloading curve also has the same slope, and it is reassuring that each of the tests fall on each other, showing the material acted uniformly across samples. This sample is least clear on when the exact yield stress may be occurring, as it appears very early in the stress strain curve. It was assumed the original

yield stress was around 15 MPa, as the slope was measured at 69 GPa for elastic modulus and deviated past this stress..

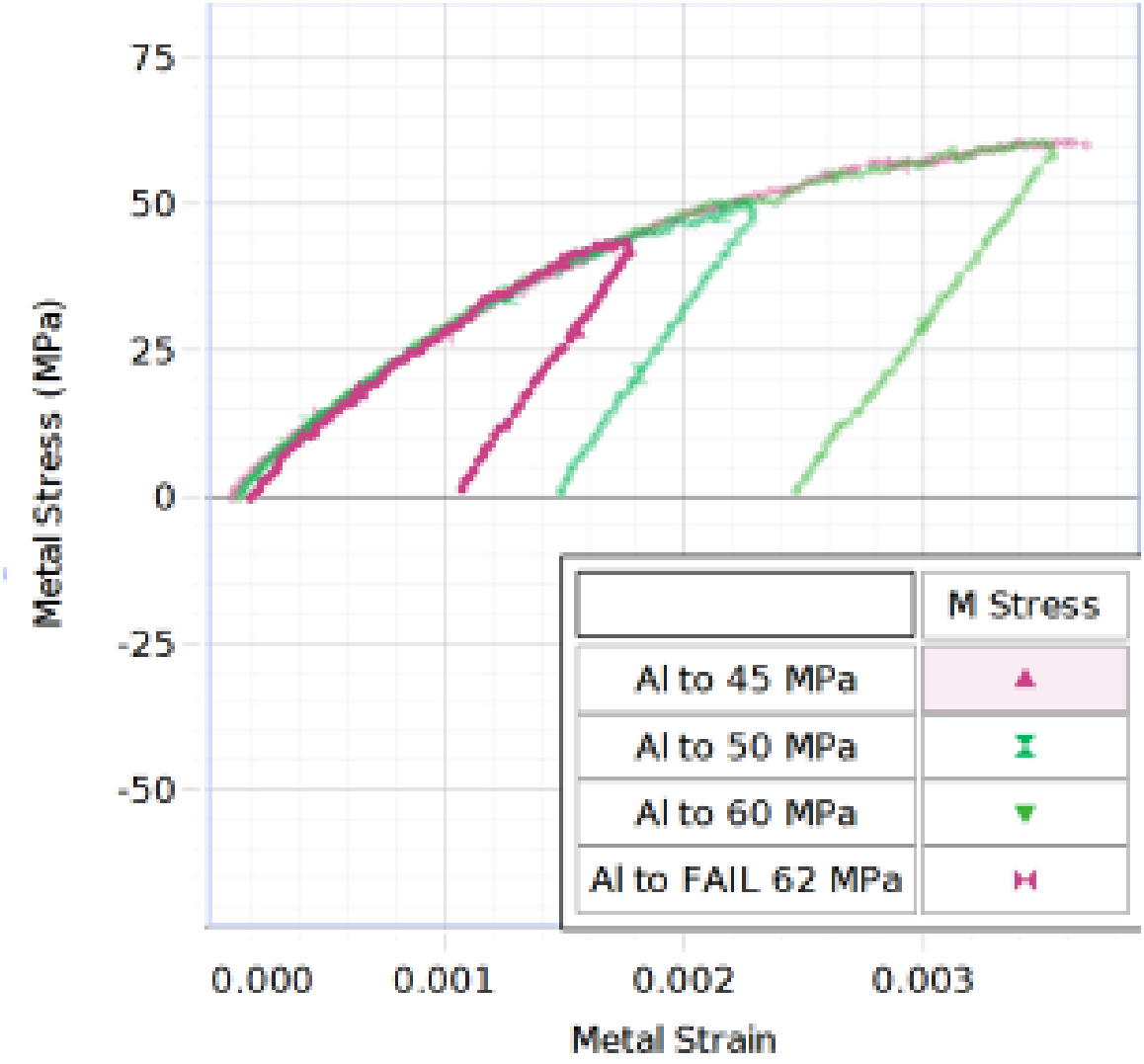

Figure 33. Stress-strain data for aluminum.

Figure 34 shows the same elastic loading to plastic yield stress points for brass. Similarly, the coupons were pulled to increasing yield stresses within the plastic zone. However, brass has a much lower capacity for plastic deformation, so the range was from 275 MPa, the original yield stress, to 290, 300, and 310 MPa. The ultimate tensile stress was at 318 MPa. The elastic modulus for all of the tested coupons was uniform at 117 GPa. The only slight variation in this data is that the final brass tested to failure did not yield at the same

point as the others. As it was close to the 310 MPa that was tested, however, this data was not included in the later measurements of pile-up.

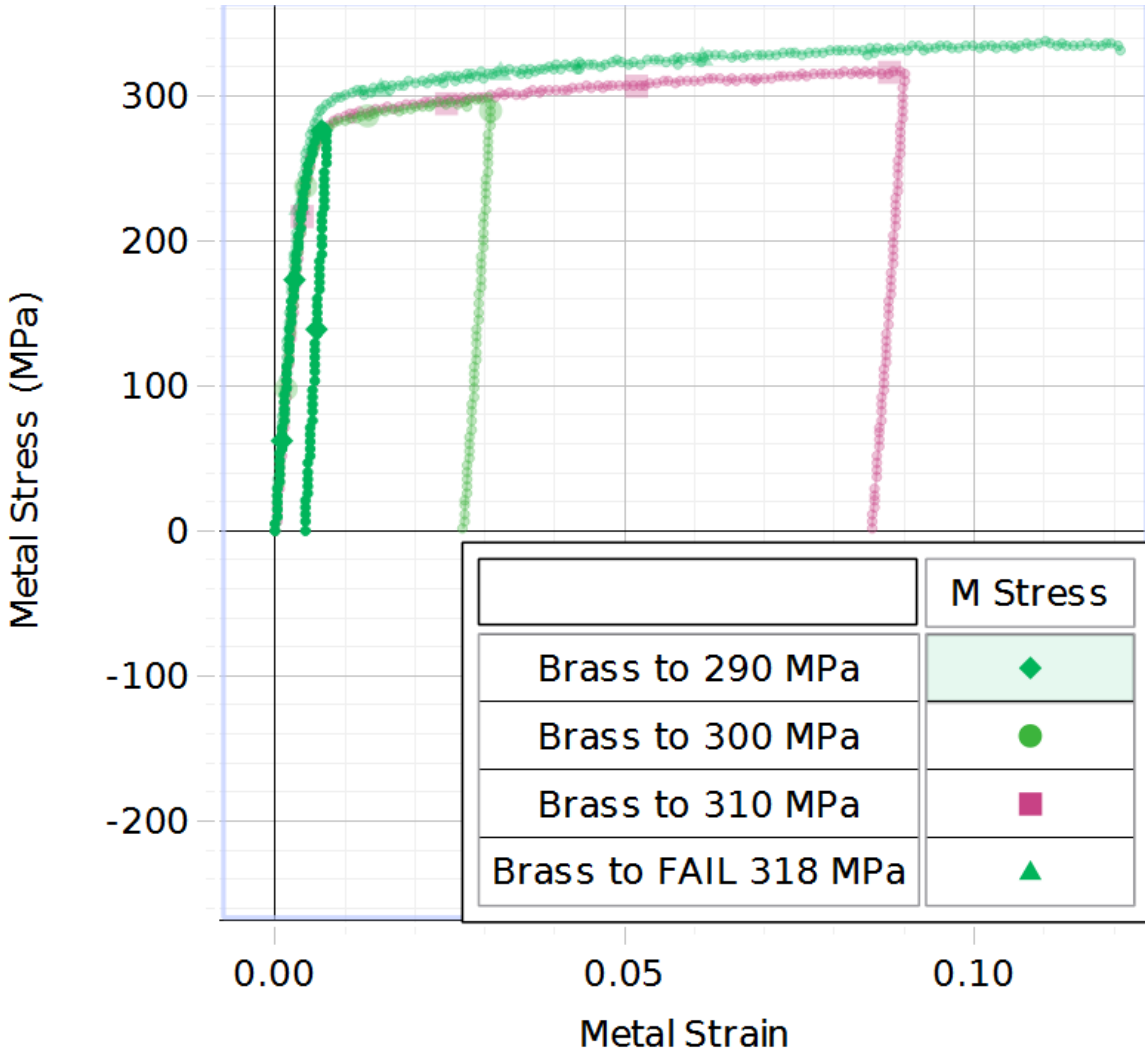

Figure 34. Stress-strain data for brass.

Next, cold rolled steel was tested in the same manner, seen in Figure 35. It similarly did not have much room for plastic deformation, but it was an interesting choice because there were also annealed steel tested coupons for comparison. First, the cold rolled streel showed that there was about a 300 MPa original yield stress. As the material's plasticity range was so short, only 400 and 500 MPa samples were created, and failure occurred at 510 MPa. It is also interesting to note the very small strain, as the material did not deform much. When

pulling in the tensile tester, it was a very abrupt failure, as some of the other materials stretched before breaking, the cold rolled steel had minimal stretching.

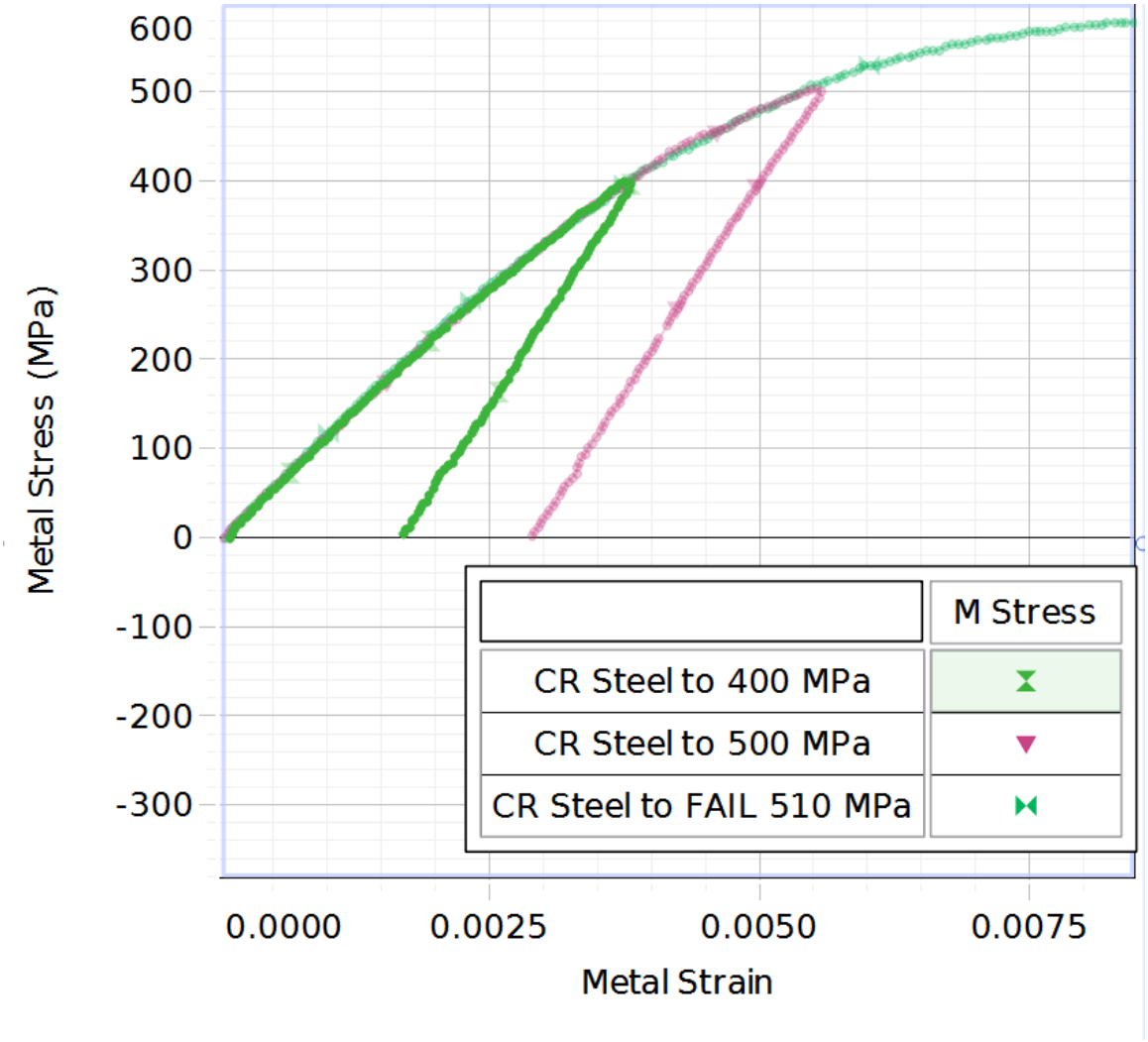

Figure 35. Stress-strain data for cold rolled steel.

Finally, annealed steel showed the most interesting results as it could be pulled over a long range before failure, seen in Figure 36. To note first, the material exhibited some behavior typical for Luder bands. When pulled to around 175 MPa, the stress was constant while strain was still increasing. The material was deforming at a constant rate, and this could be due to dislocations forming and reforming that do not allow for an increase of stress yet. However, when this capacity is full, then the stress begins to increase, and can hold through a large amount of strain. The annealed steel was tested to 175, 225, 275, and 300 MPa.

The stress was then constant as the material kept stretching, and finally failed at 320 MPa. The samples were previously shown in Figure 32, with the final coupon to failure extending much farther past its original length. The elastic modulus of the annealed steel is identical to the cold rolled steel and matches literature values at 200 GPa. It is very interesting that the steel can act with these two strikingly different behaviors based on their processing. The cold rolled steel had been dramatically deformed previous to testing, so there was less room in the material for changes in yield stress. The annealed steel, however, had been able to relax during the process of heat treatment, and acted much more ductile. These basic material responses show that the yield stress can drastically change based on the processing, and in this work we can show that the plasticity depends on this as well. The steel samples were most interesting because they have the same elastic modulus, but plastic properties have an enormous range between annealed and cold rolled. These phenomena between the two steel samples are later examined even further in depth.

The Pasco tensile tester was an excellent tool for creating materials with different yield stresses. The trend of increasing yield stress due to imparting dislocations has proved very useful for this research, and since the substrate yield stress is well-known, it is much easier to predict or extract film properties.

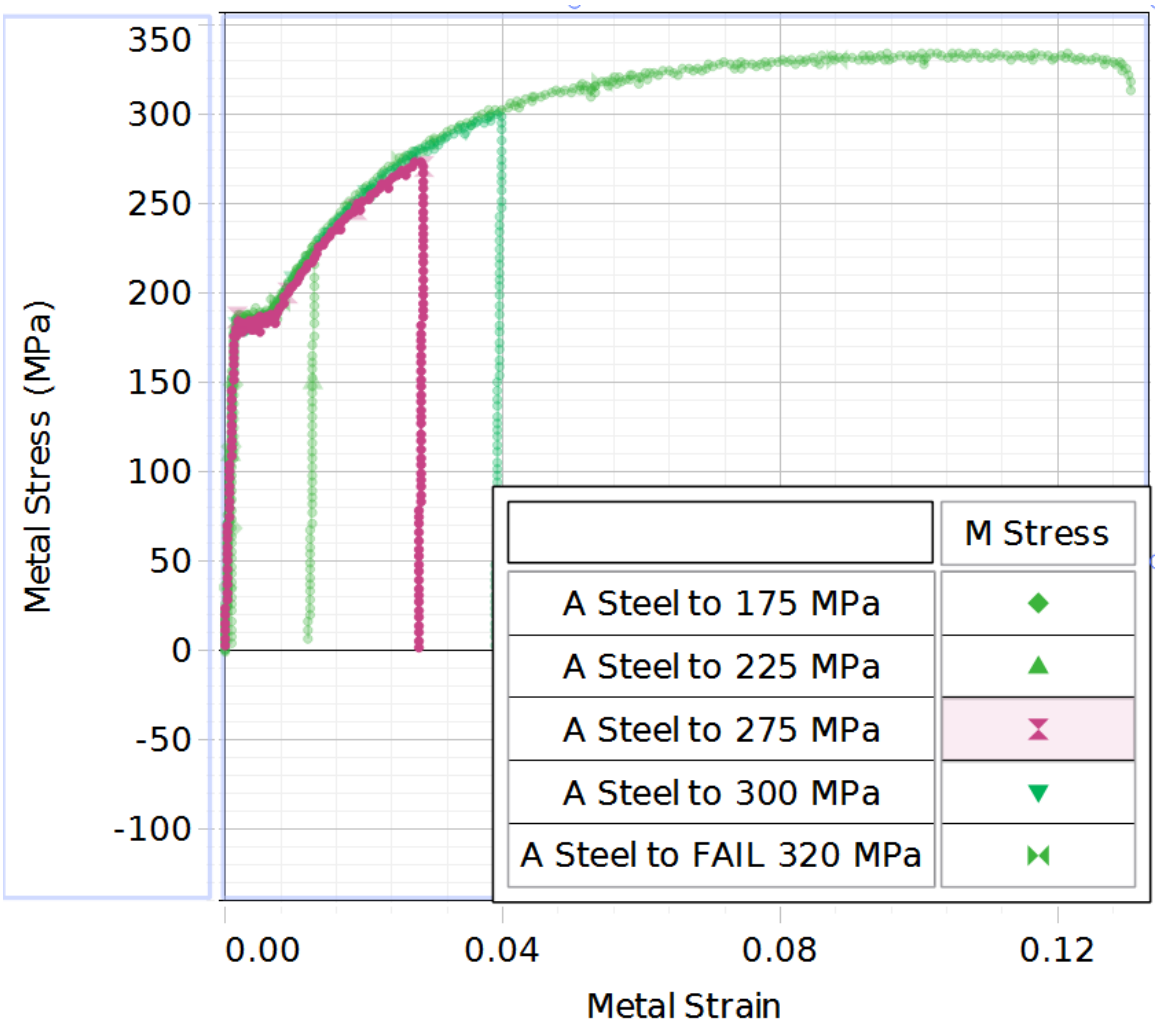

Figure 36. Stress-strain data for annealed steel.

5.2.1 Pile-Up in Metallic Substrates

The first comparisons of pile-up were completed on sole metallic substrates. This was not possible for ceramic substrates because first, they are non-conductive and cannot be viewed in the SEM without coating, and second, there is limited plasticity in the ceramic substrate. In most cases indenting on solely a ceramic substrate resulted in cracking instead of pile-up; the energy is distributed differently, and put into forming new surface instead of creating dislocations in the material. However, the coupons utilized, aluminum, brass, annealed steel, and cold rolled steel, all were studied up to different indent depths. The indents are presented, which shows the increasing pile-up in the substrates alone with

increasing indent depth. The depths chosen for every test are 200, 300, 400, 500, 600, and 1000 nm into the sample. This was selected because when films are added, the thickness aim was 500 nm. This allowed for most of the indents to be within the film thickness. For bulk samples, however, this is not an issue, and these were chosen to compare against the film/substrate combinations indented to the same depths.

After programming in multiple yield stresses, nanoindentation was completed on each sample. Elastic modulus averages of 25 indents are plotted vs. displacement into surface for each of the varying programmed yield stresses. As expected, the elastic modulus is constant in all of these cases, across all displacements into the surface. To prove this, first, the indentation data from a single set of indents, 200 – 1000 nm are plotted together in Figure 37. The data lines up at every indent depth, which confirms the CSM method and shows that the elastic modulus is constant at a particular indent depth. In this case, below 200 nm there may be loss of contact, as the indenter is oscillating in the beginning, and may not be fully engaging the surface. This noise in the initial region of indentation is expected and seen across all samples. That is another reason why indents at 200 nm are the lowest indents analyzed.

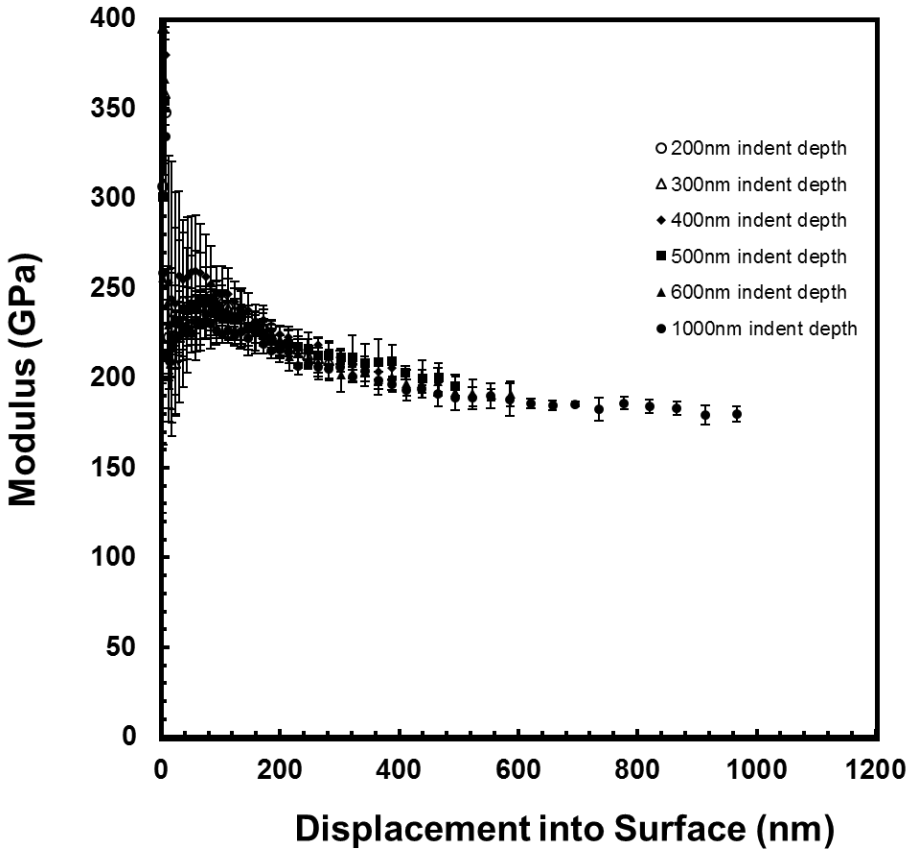

Figure 37. Indentation data of annealed steel 175 MPa yield stress with increasing indent depth.

As seen in the Figure 37-40, the materials pile-up similarly when there is no film. This was a surprising discovery because it was expected that the pile-up would be varying, as it is when there is a film/substrate combination.

The data for aluminum is seen in Figure 38. No matter the yield stress changes, the elastic modulus matches at 69 GPa. This follows for brass, with an elastic modulus of 117 GPa, seen in Figure 39 with the progression of yield stresses. Both cold rolled and annealed steel have the same elastic modulus which matches the literature value of 200GPa, and also the tested value with the Pasco tensile tester. These are seen in Figure 40 for cold rolled steel and Figure 41 for annealed steel.

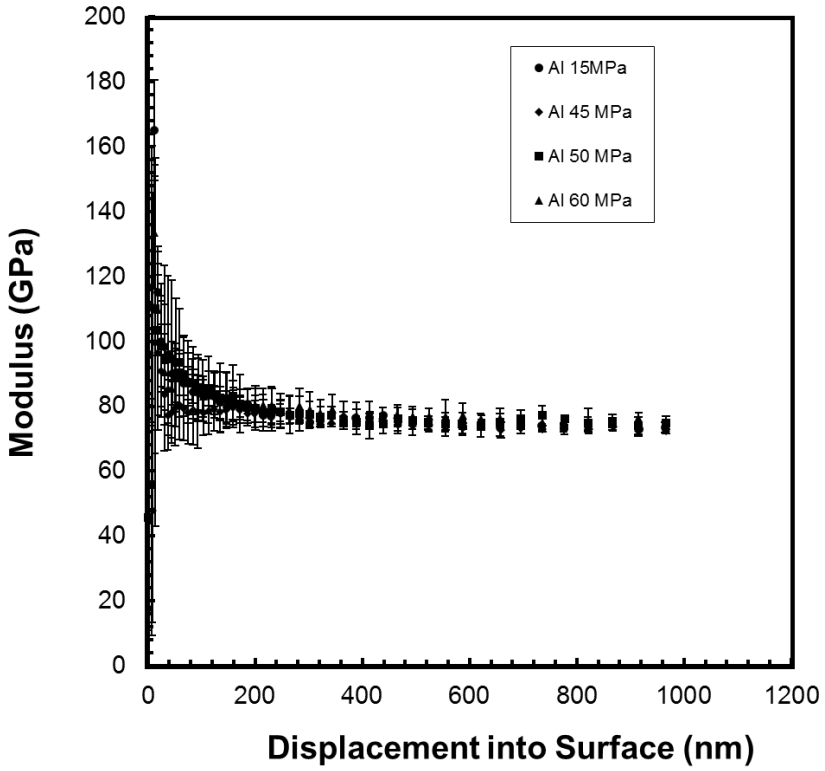

Figure 38. Bulk aluminum nanoindentation data compared at different yield stresses.

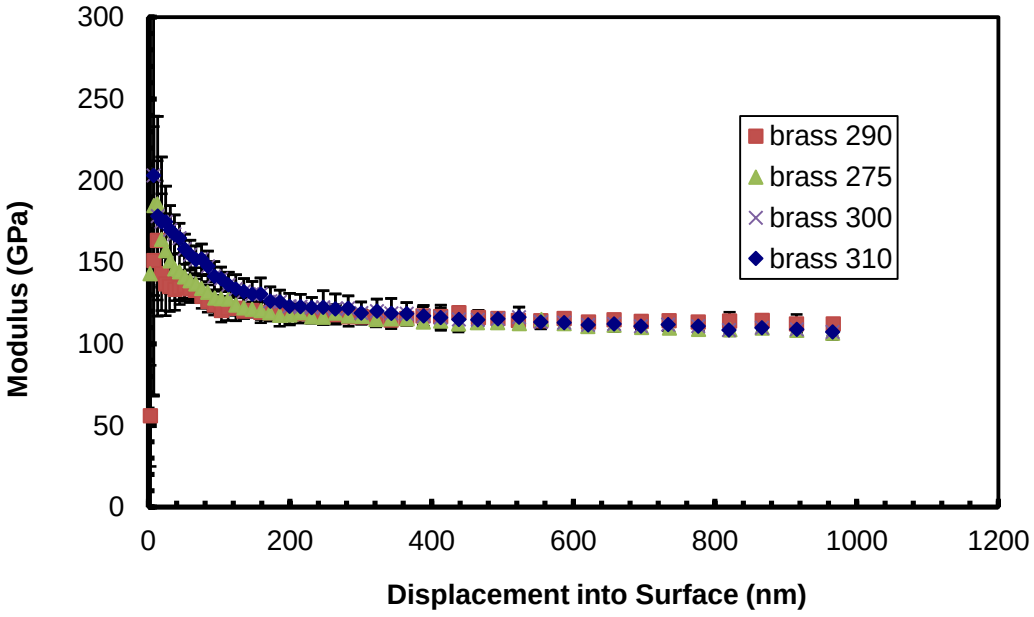

Figure 39. Bulk brass nanoindentation data compared at different yield stresses.

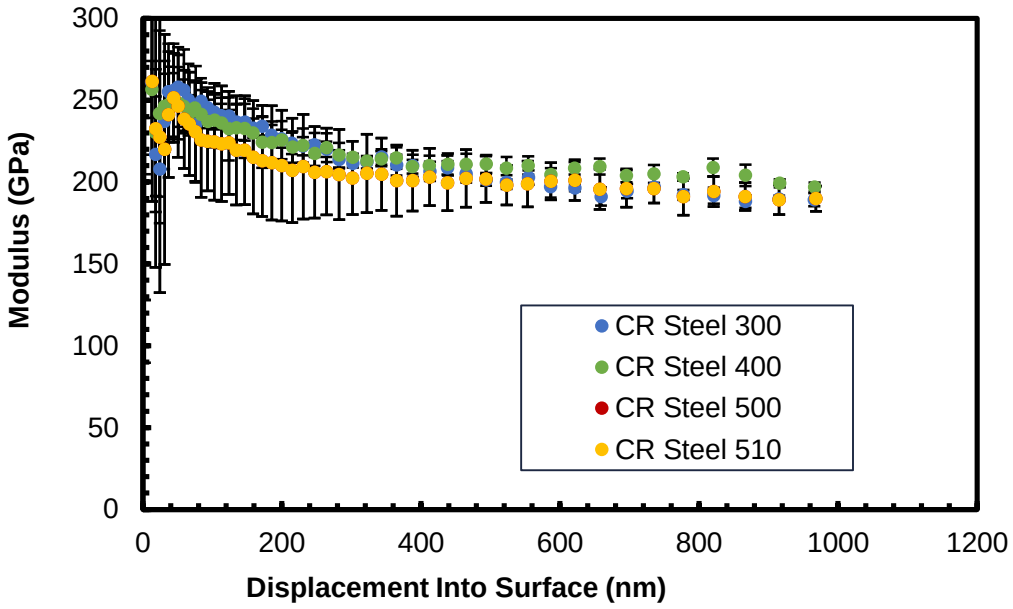

Figure 40. Bulk cold rolled steel nanoindentation data compared at different yield stresses.

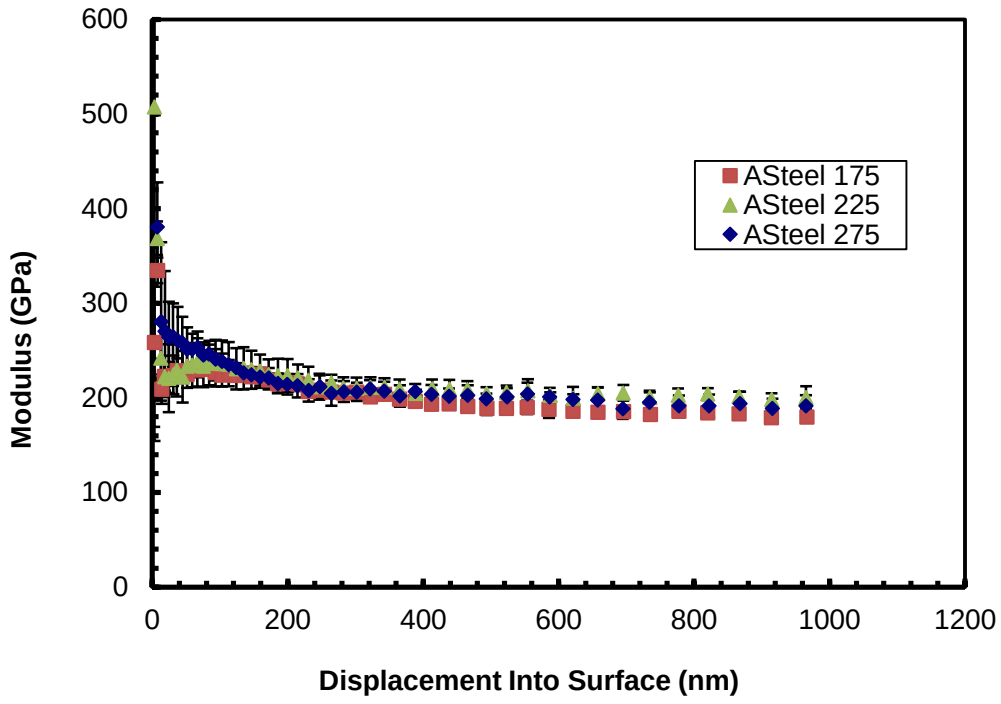

Figure 41. Bulk annealed steel nanoindentation data compared at different yield stresses.

The indents were imaged at identical magnifications with increasing indent depths. The SEM micrographs are seen in Figures 42 – 45 for aluminum, brass, annealed steel, and cold rolled steel. The ImageJ method previously outlined for measuring the topography for the earlier images of gold on ceramic substrates was used again. The numerical results are seen in Figures 46 – 49 for the different yield stresses on each individual indent. There are at least four indents averaged in this data.

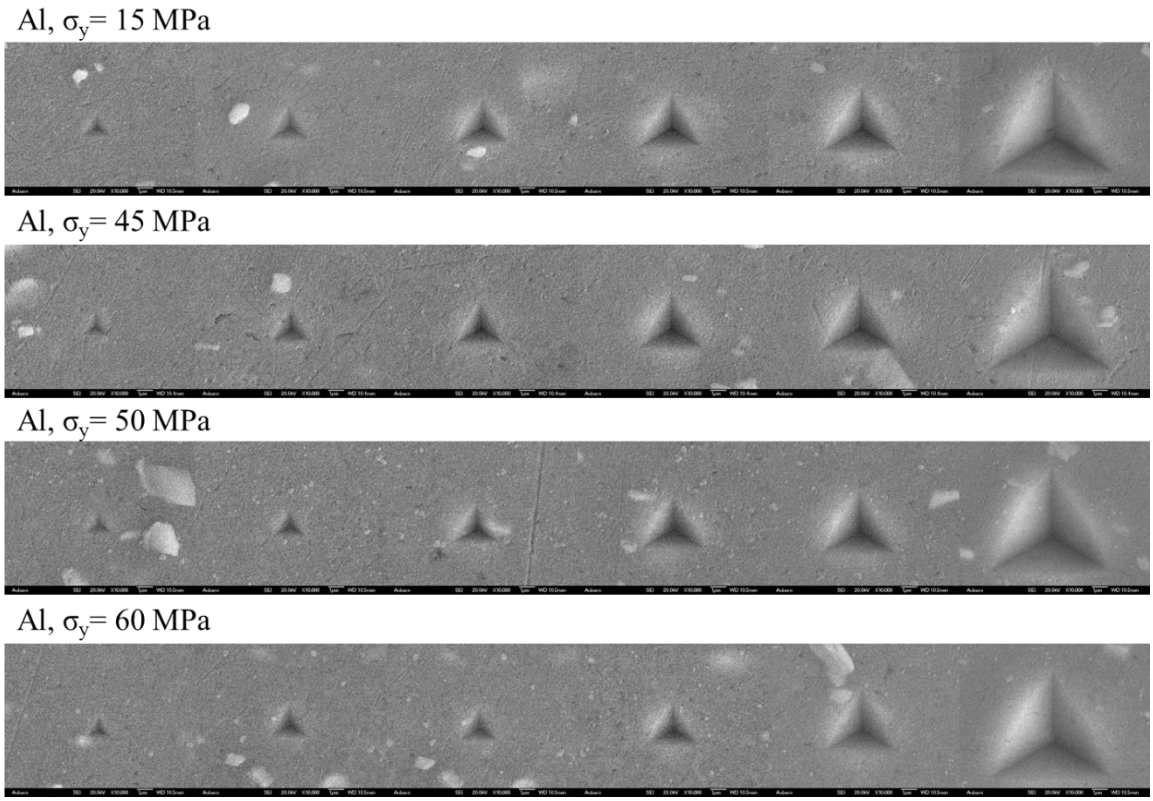

Figure 42. SEM images of increasing indent depth for each yield stress of aluminum substrate.

Brass, σ_y= 275 MPa

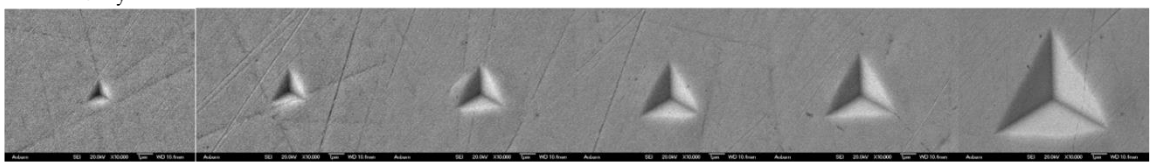

Brass, σ_y= 290 MPa

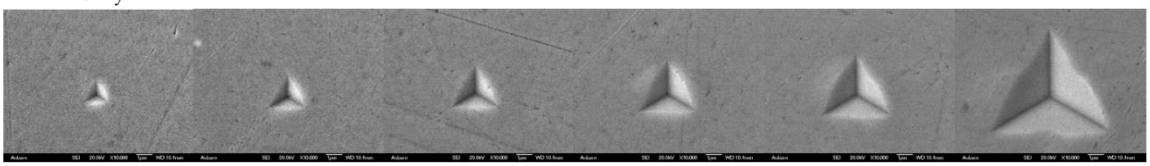

Brass, σ_y= 300 MPa

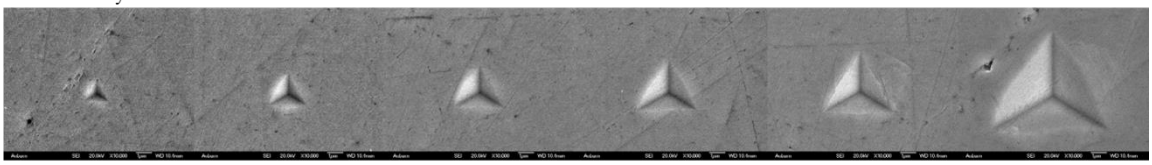

Brass, σ_y= 310 MPa

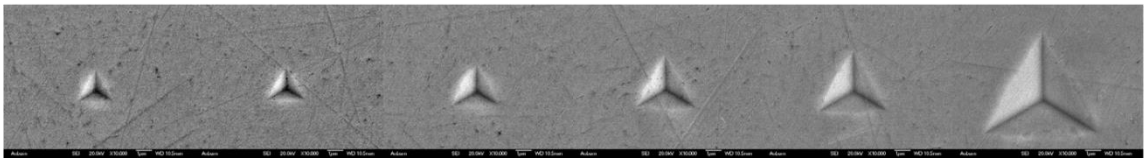

Figure 43. SEM images of increasing indent depth for each yield stress of brass substrate.

Asteel, σ_y= 175 MPa

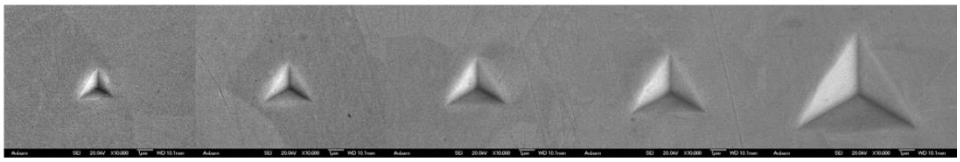

Asteel, σ_y= 225 MPa

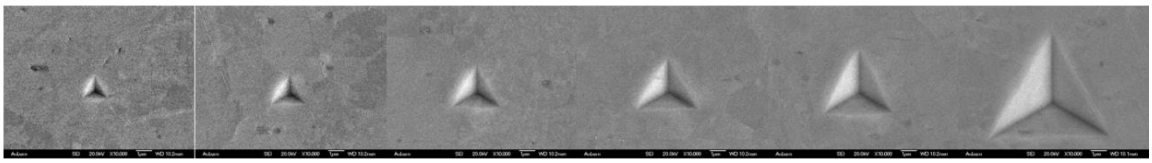

Asteel, σ_y= 275 MPa

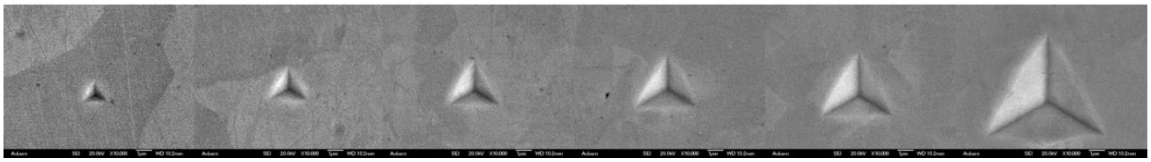

Figure 44. SEM images of increasing indent depth for each yield stress of annealed steel substrate.

CR Steel, σ_y= 300 MPa

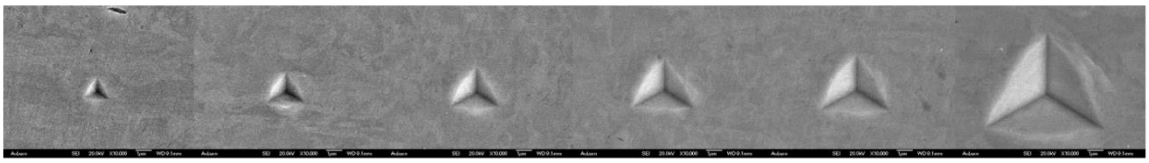

CR Steel, σ_y= 400 MPa

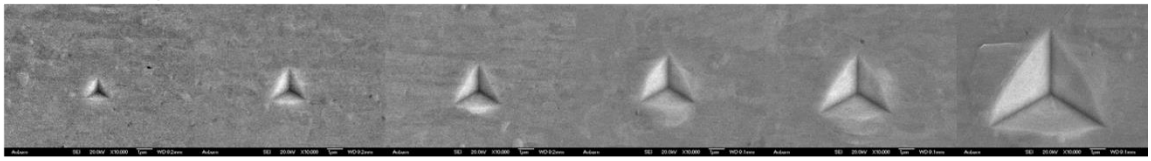

CR Steel, σ_y= 500 MPa

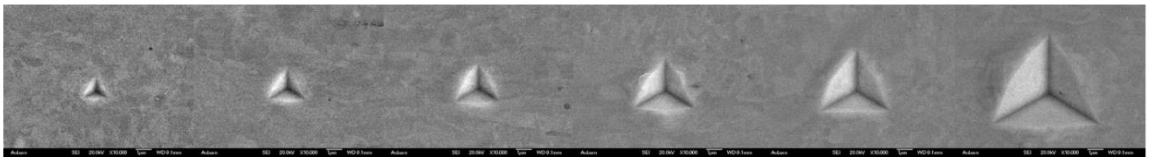

Figure 45. SEM images of increasing indent depth for each yield stress of cold rolled steel substrate.

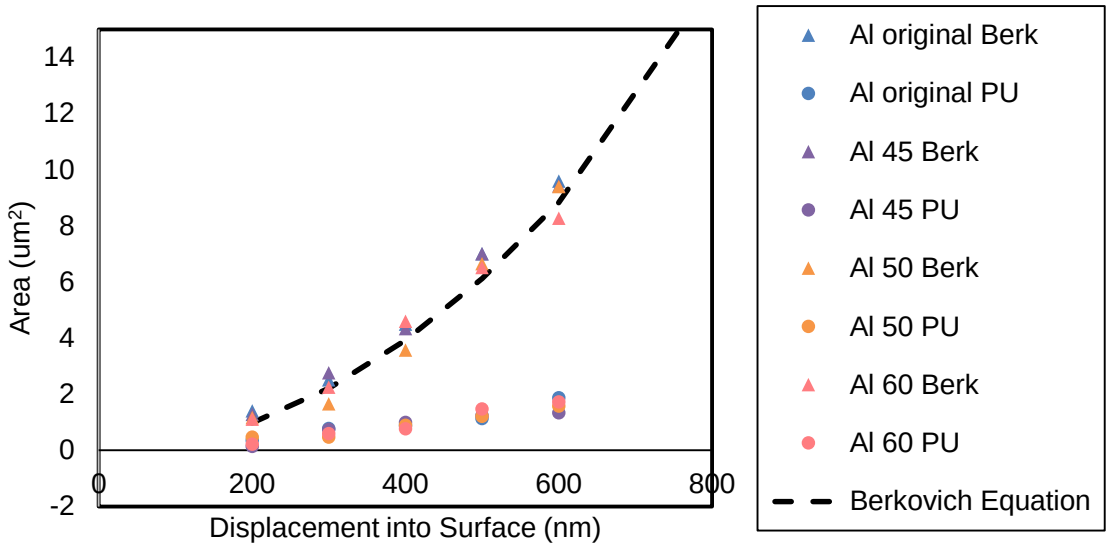

Figure 46. Quantitative results of pile-up area of aluminum substrate pulled to different yield stresses vs. displacement into surface.

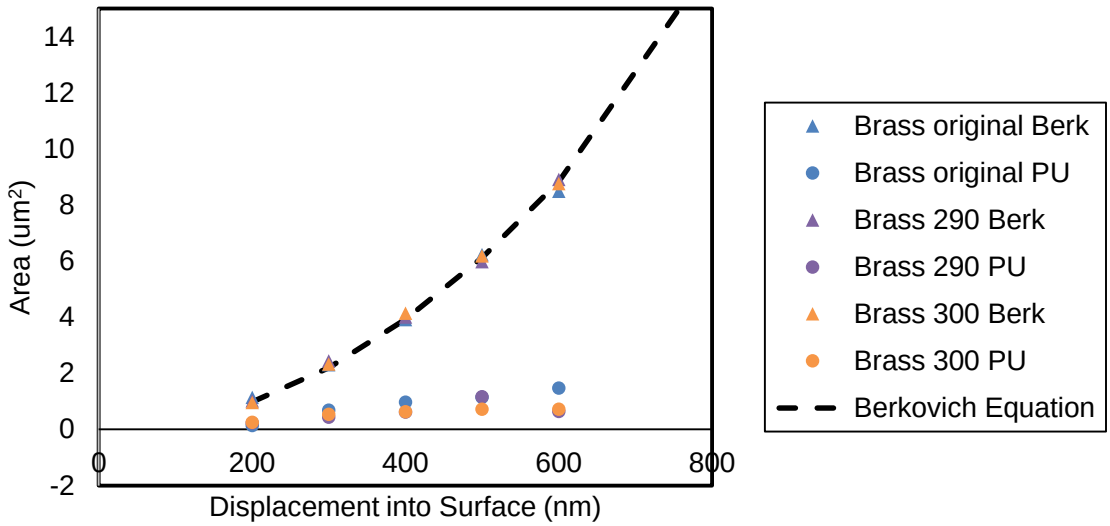

Figure 47. Quantitative results of pile-up area of brass substrate pulled to different yield stresses vs. displacement into surface.

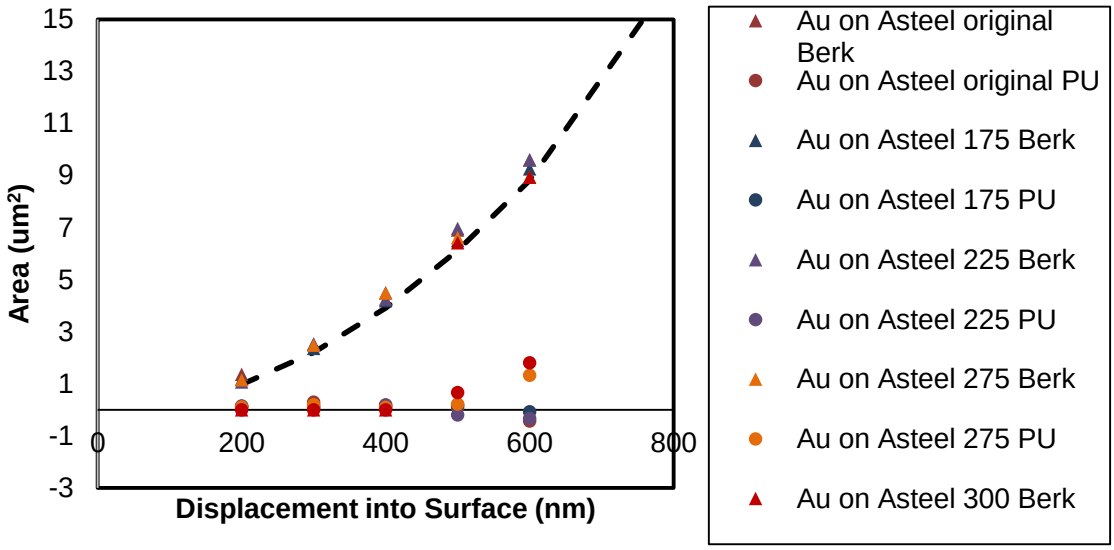

Figure 48. Quantitative results of pile-up area of annealed steel substrate pulled to different yield stresses vs. displacement into surface.

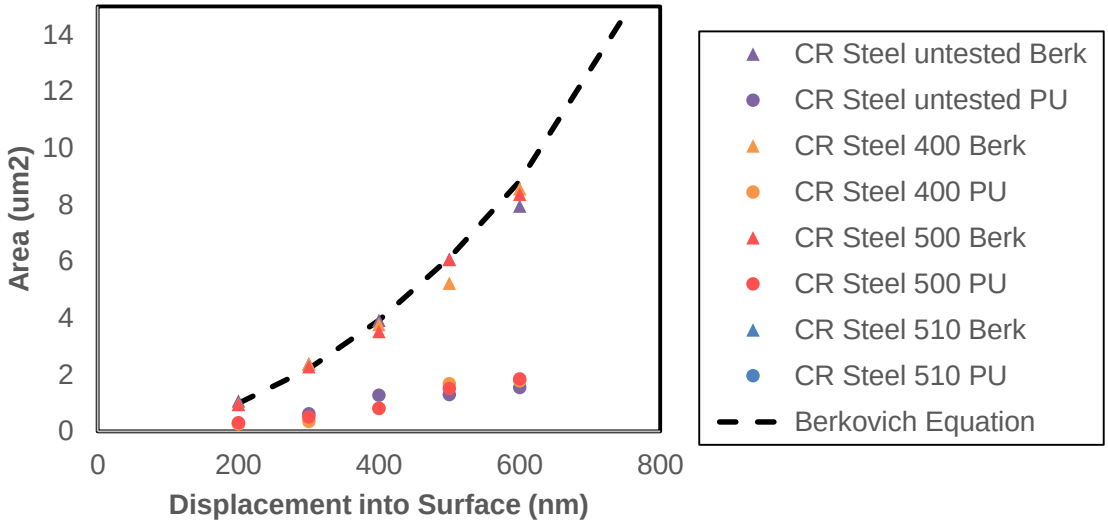

Figure 49. Quantitative results of pile-up area of cold rolled steel substrate pulled to different yield stresses vs. displacement into surface.

While it was thought that there would be an obvious trend when changing yield stress, the results are showing that the yield stress of a single material did not greatly affect the pile-up. However, when comparing all of the materials, there is an interesting trend that all of the materials pile-up in very similar manners. There is not enough of a difference to confidently conclude that the yield stress is affecting the pile-up of these metals when they are solely the substrate. However, when adding a film onto the materials, even more interesting results occurred.

5.2.2 Pile-Up in Gold on Metallic Substrates

After testing the substrates alone, gold was deposited onto the substrates as film properties are sought after in this work. All of the samples were created in the same run at the same time, so film thickness is assumed constant across the samples because of the rotating sample holder employed. The film thickness is about 520 nm as tested with a cross-sectional view of one of the samples using SEM and profilometer readings. The same samples that are seen in the first batch that had pulled to different stresses were utilized in the same pile-up analysis. First, nanoindentation was completed to confirm the elastic modulus was uniform across all samples, even with varying the yield stress. Nanoindentation results of gold on the samples to varying yield stresses are seen in Figures 50 – 53. Gold on aluminum, brass, annealed steel and cold rolled steel were all examined. As seen in the charts, modulus is plotted vs. displacement into surface. The Zhou-Prorok model previously discussed fits all of these combinations. As the parameters used are solely elastic modulus and Poisson's ratio, the yield stress changes will not affect the model, and also do not affect the data for the elastic properties. The information from the nanoindenter solely extracts the elastic response, therefore it is not affected by the initial pulling of the samples in the tensile tester. All of these samples pulled to various stresses are not affected, except cold rolled steel had one mistake that is included to show that it is important to compare the experimental data that may affect indentation indent images. In Figure 53, the sample indented for 500 MPa yield stress follows a lower response. In this case, it could be due to the sample preparation, so care is followed to avoid this data that may be inaccurate from indentation.

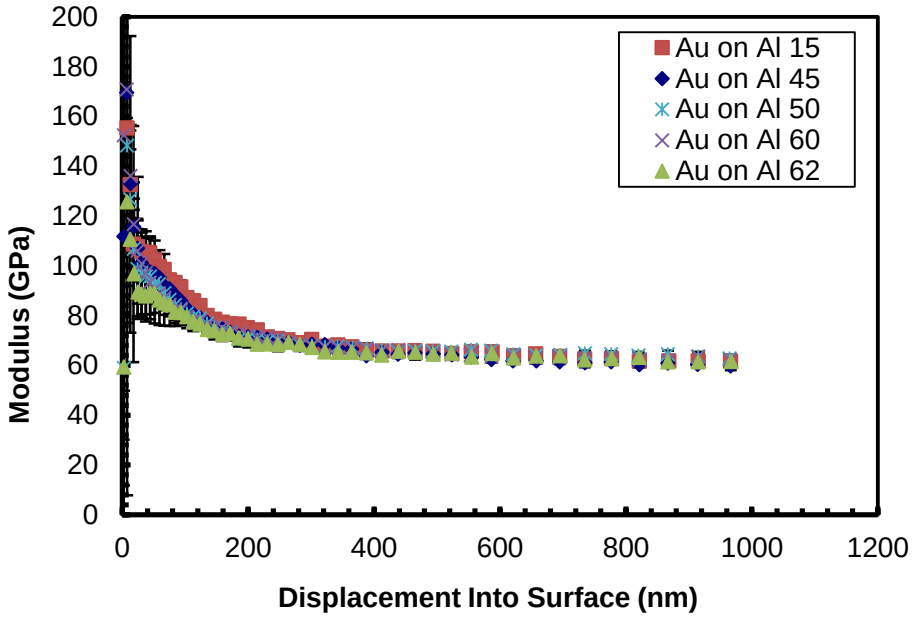

Figure 50. Gold on aluminum nanoindentation data.

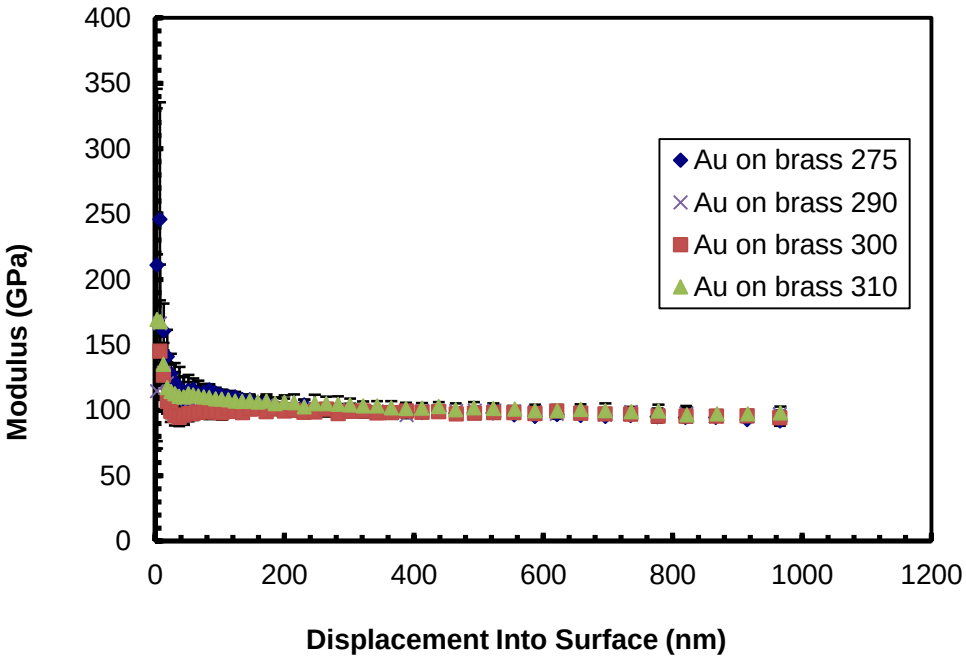

Figure 51. Gold on brass nanoindentation data.

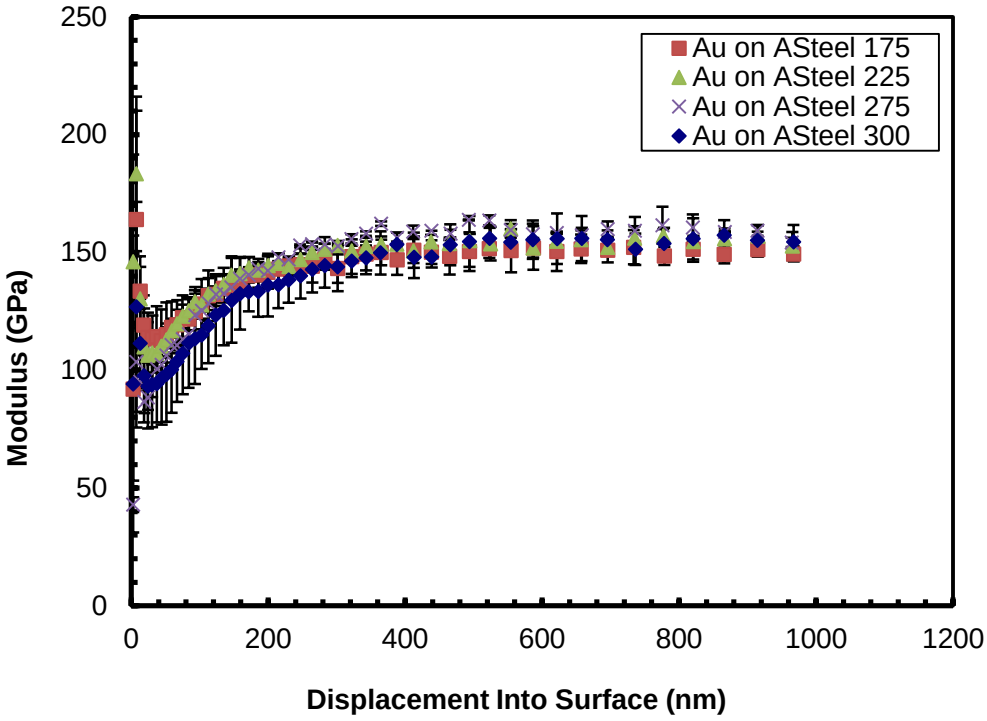

Figure 52. Gold on annealed steel nanoindentation data.

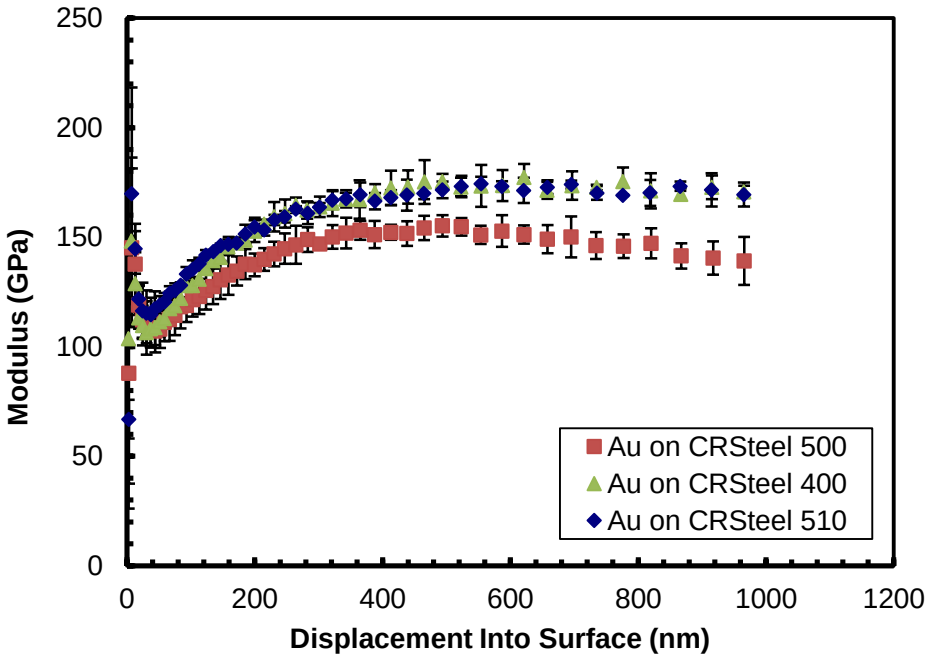

Figure 53. Gold on cold rolled steel nanoindentation data.

Nanoindentation data is shown to 1000nm indent depth in the previous figures. However, when indenting, a series was created to test to increasing indent depths. The indent depth does not affect the elastic data, and will follow any of the trends seen in Figures 50 – 53. With indents to increasing depths, pile-up trends can be visualized. These are seen in series in Figures 54 – 57. First, gold on aluminum to yield stresses of 15, 45, 50, and 60 MPa are shown. This is the one set where it is clear that most of the indentation on this system results in sink-in. Brass follows, at 275, 290, 300, and 310 MPa, and exhibits slight pile-up in these cases. Annealed steel looks slightly similar at 175, 225 and 275 MPa. Some indents may not be pictured that did not give good results, and were omitted from the analysis, as well. Finally, cold rolled steel has evidence of much more pile-up at its higher yield stresses of 300, 400, 500, and 510 MPa.

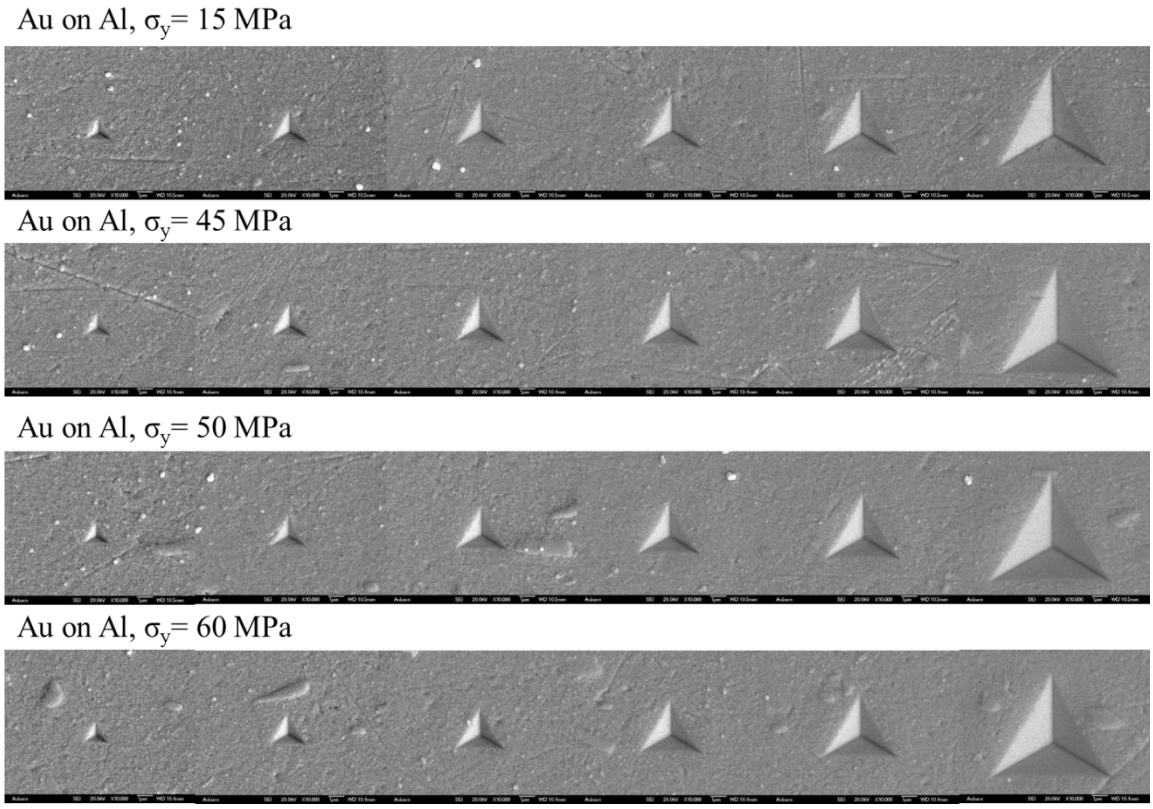

Figure 54. Gold on aluminum to varying yield stress pile-up progressions.

Au on Brass, σ_y= 275 MPa

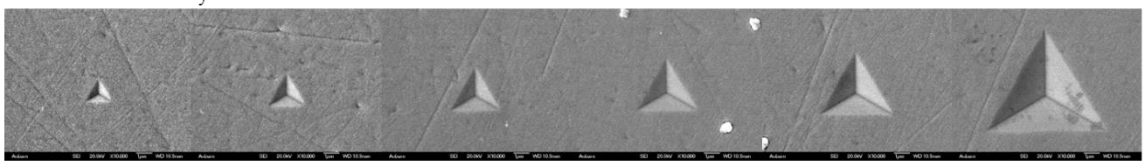

Au on Brass, σ_y= 290 MPa

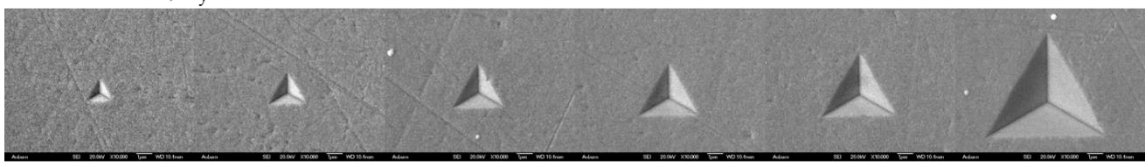

Au on Brass, σ_y= 300 MPa

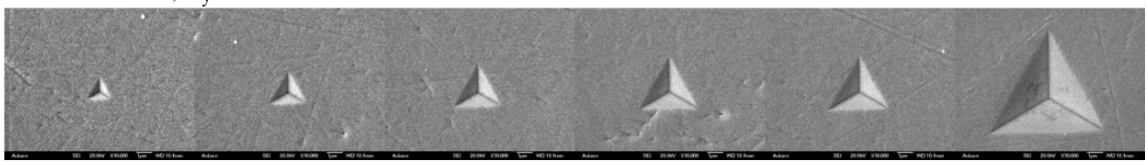

Au on Brass, σ_y= 310 MPa

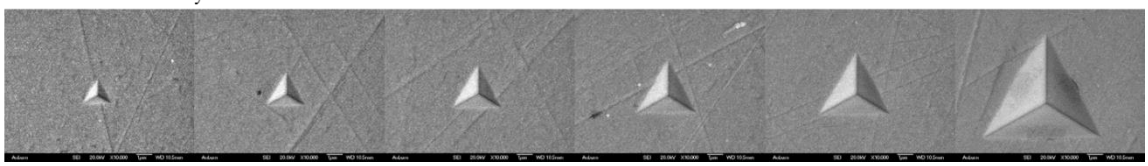

Figure 55. Gold on brass to varying yield stress pile-up progressions.

Au on Asteel. σ_y= 175 MPa

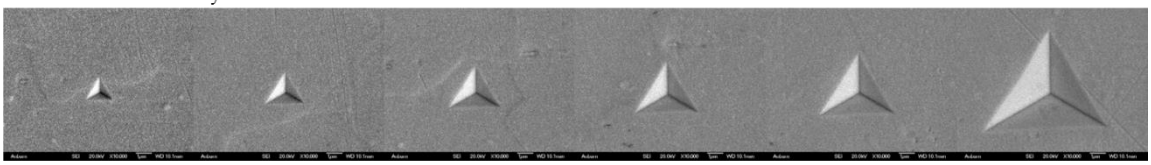

Au on Asteel. σ_y= 225 MPa

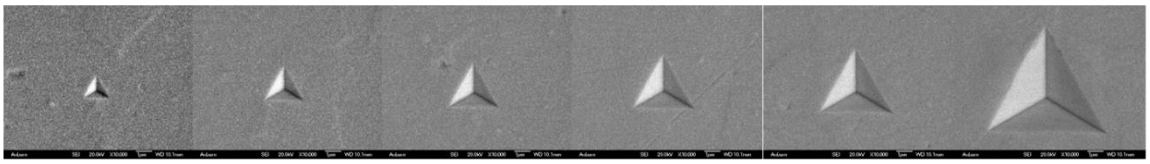

Au on Asteel, σ_y= 275 MPa

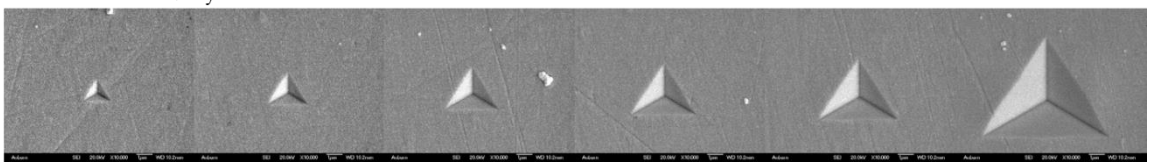

Figure 56. Gold on annealed steel to varying yield stress pile-up progressions.

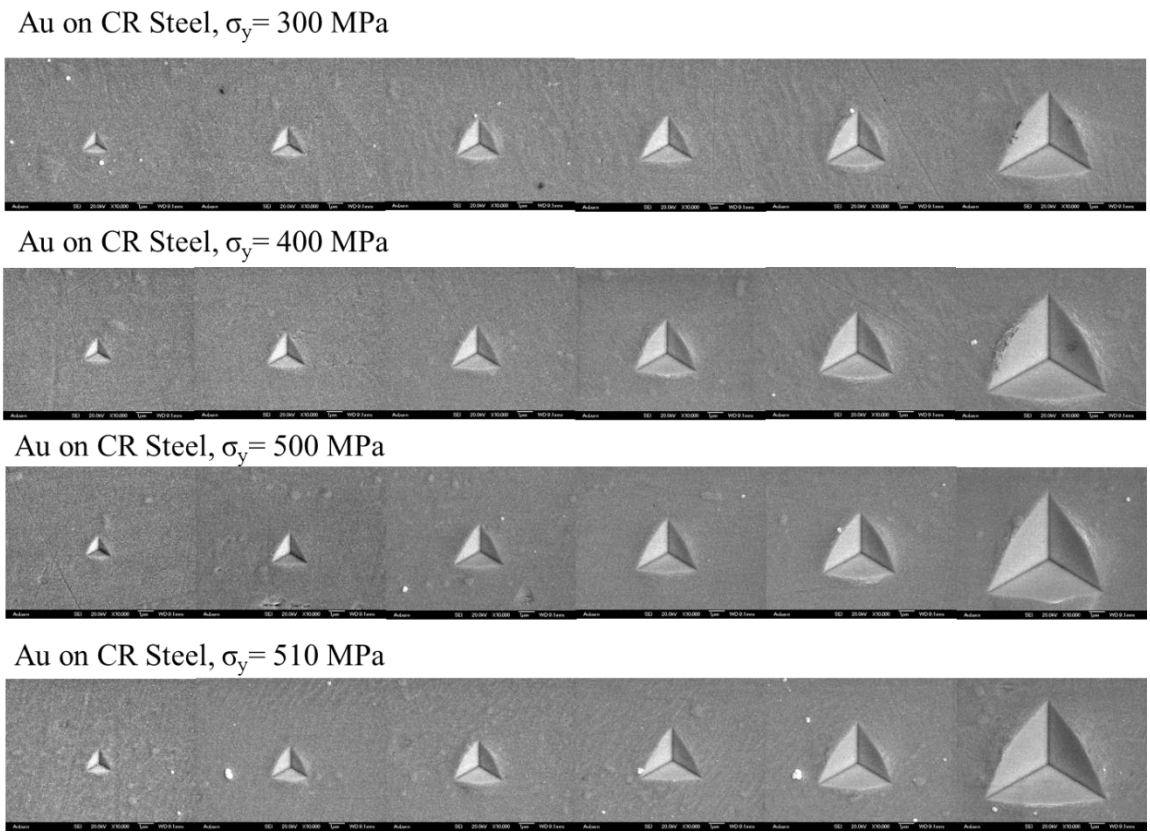

Figure 57. Gold on cold rolled steel to varying yield stress pile-up progressions.

From these figures, the ImageJ analysis process described in the experimental procedure was used. Some of the materials clearly exhibit pile-up, such as the gold on cold rolled steel, whereas others show clear sink-in, such as the aluminum. It is interesting to compare the pile-up from the pure metallic substrates in the previous section, as even the aluminum exhibited pile-up alone. With the added film, however, the behavior changes. It is evident that there is an interplay between film and substrate that controls this behavior of sink-in or pile-up. In this work, the claim is that the elastic properties are irrelevant, and it is solely plastic properties of the materials and their imbalance that will create the pile-up or sink-in phenomena.

When viewing the amounts of pile-up or sink-in, there is not a clear trend within one material substrate type. It was expected that increasing the yield stress with tensile testing would greatly affect the pile-up. There is a slight trend with an increase in pile-up/sink-in depending on the materials with increasing yield stress, but it is not enough to strongly

claim that the yield stress tests changed the material enough to change the pile-up. Between materials however, there is a very striking difference.

First, to show the pile-up and sink-in measurements of the individual materials with varying yield stresses, pile-up was measured directly from ImageJ and compared to the indent depth. One very clear distinction is that with increasing indent depth, either the pile-up or sink-in increase. This has been the trend in previous samples, as well, and correlates to the expected area. However, when viewing Figures 58 – 61, the trends are visualized quantitatively, as compared to Figures 54 – 57 where the images show qualitative differences. Additionally, the measured Berkovich area is plotted with the expected Berkovich area, dependent on the indent depth and predicted based on the calculated area. These were compared first, because if there was a large difference in this area, then the pile-up measurements would be skewed. In these cases, however, they are well-predicted by the equation, and are seen in the plots following the dotted line that represents the equation for the Berkovich area.

The progression begins with gold on aluminum. From the SEM images, it is clear that all of the indents exhibit sink-in. The numbers extracted from the ImageJ analysis are plotted in Figure 58. It seems that with increasing yield stress, there may be a trend in increasing sink-in, but not enough of a statistical difference in which to make a confident confirmation. This is the only substrate tested that completely results in sink-in with gold films. This material also has the lowest modulus and yield stress of the tested samples.

Figure 59 shows the gold on brass pile-up trends, Figure 60 the gold on annealed steel series, and finally Figure 61 shows the amounts of gold cold rolled steel pile-up. Unlike aluminum, most of these exhibit pile-up. There seems to be a transition in the annealed steel from sink-in to pile-up at small indent depths, but is slightly difficult to discern in the images as 200nm is a small indent, and the pile-up or sink-in from this indent depth is also very small.

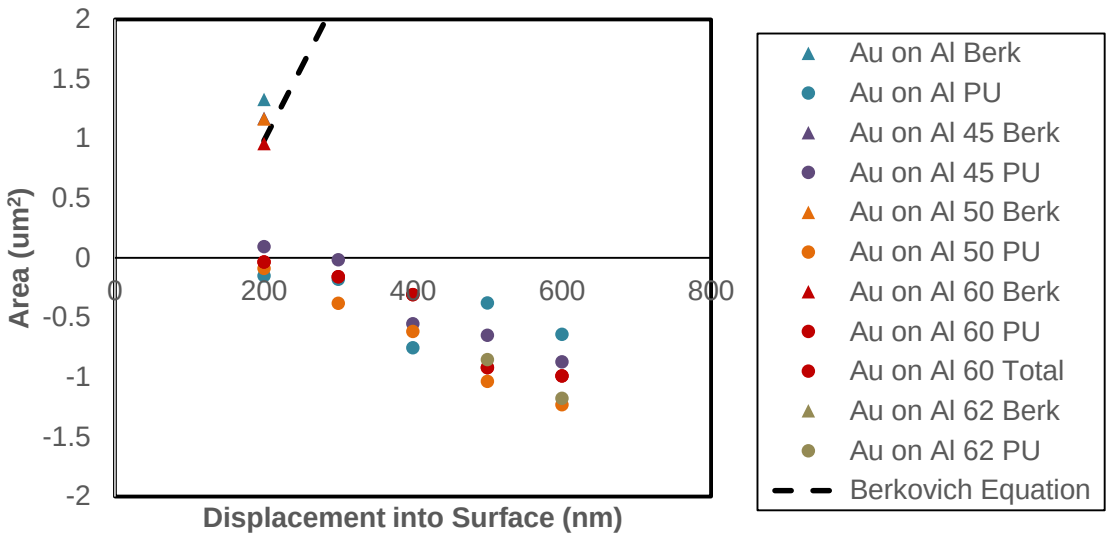

Figure 58. Pile-up area vs. displacement into surface for gold on aluminum to varying yield stresses.

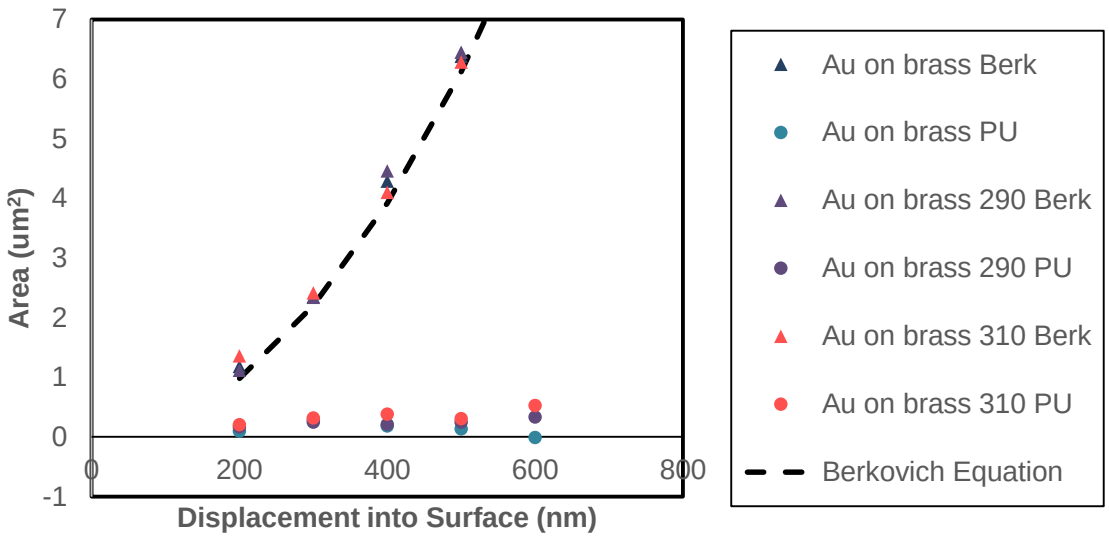

Figure 59. Pile-up area vs. displacement into surface for gold on brass to varying yield stresses.

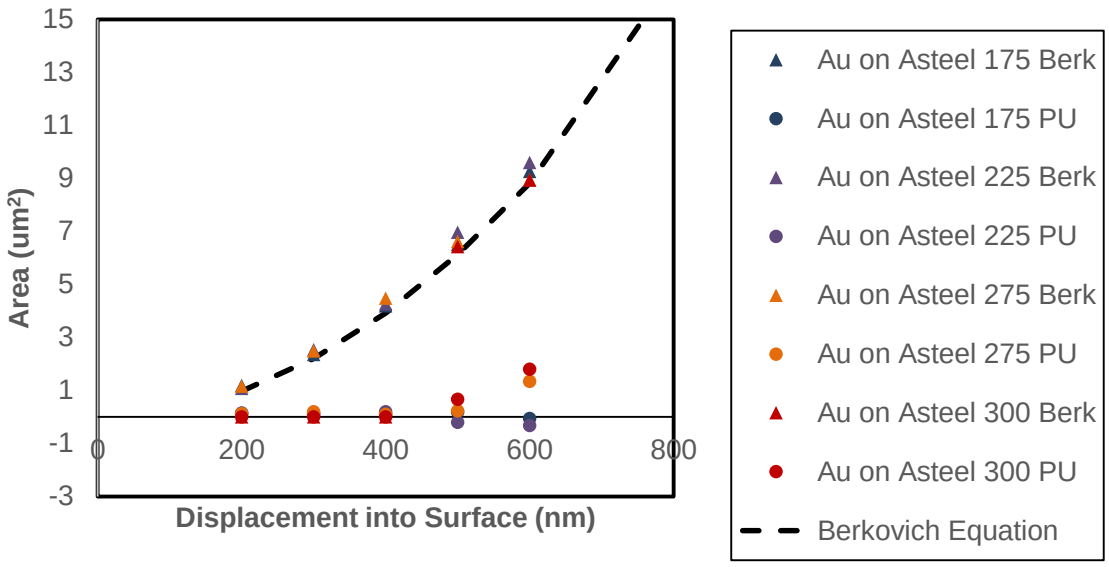

Figure 60. Pile-up area vs. displacement into surface for gold on annealed steel to varying yield stresses.

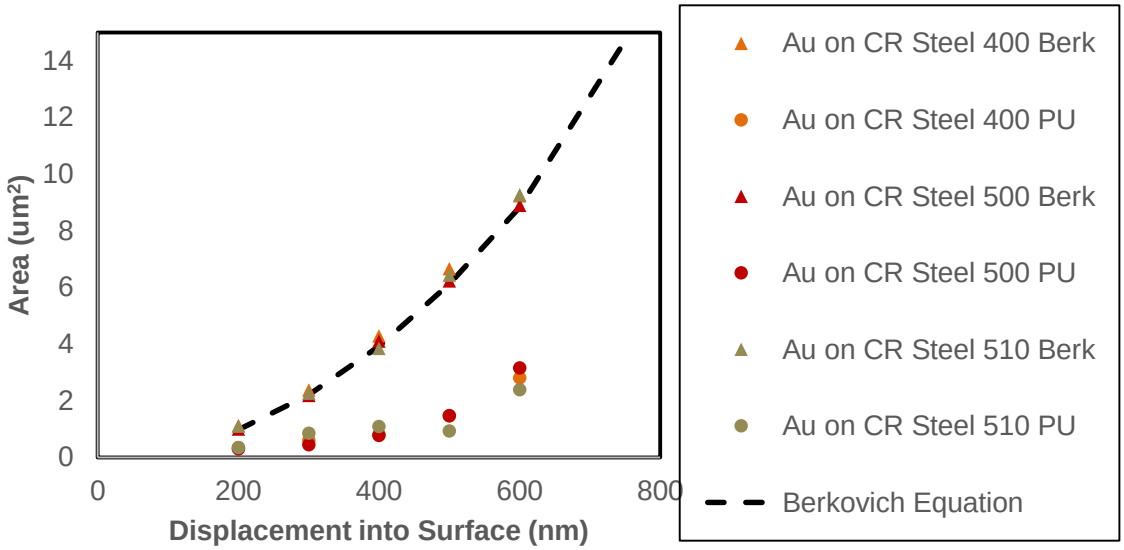

Figure 61. Pile-up area vs. displacement into surface for gold on cold rolled steel to varying yield stresses.

After assessing the materials individually, it was prudent to compare them altogether. As yield stress only slightly changed between individual samples, between each metallic coupon there are much larger yield stress differences. They range from aluminum to brass to annealed steel to cold rolled steel in order of increasing yield stress. Pile-up area vs.

yield stress was compared, but now there are different indent depths to consider. Figures 62 – 67 exhibit each of the indent depths and the trends seen in order of increasing yield stress.

The y-axis is a normalized pile-up area. In order to remove the units from the y-axis, the pile-up area (um^2) was divided by the expected Berkovich area at this indent depth (also um^2). For example, Figure 62 has a y-axis of the measured pile-up area with ImageJ divided by $24.5h^2$, or $24.5*(200um)^2$. Figures 62 – 67 follow the same trend.

On each of these plots in the following figures, the metallic coupons are shown as different colors. Aluminum is yellow, brass is blue, annealed steel is purple, and cold rolled steel is red. In this fashion, is it easy to see that the materials have an increasing yield stress over a large range, from 15 MPa to 510 MPa. There are only a few yield stresses that overlap between materials, and this will be crucial to explain some further details about the pile-up at these specific points. Additionally, a linear line is fit to each of these plots. The trends seemed linear, and mostly fit the linearization. Table 6 shows a comparison from the normalized data of the y-axis, slope, and x-axis of all of these normalized plots.

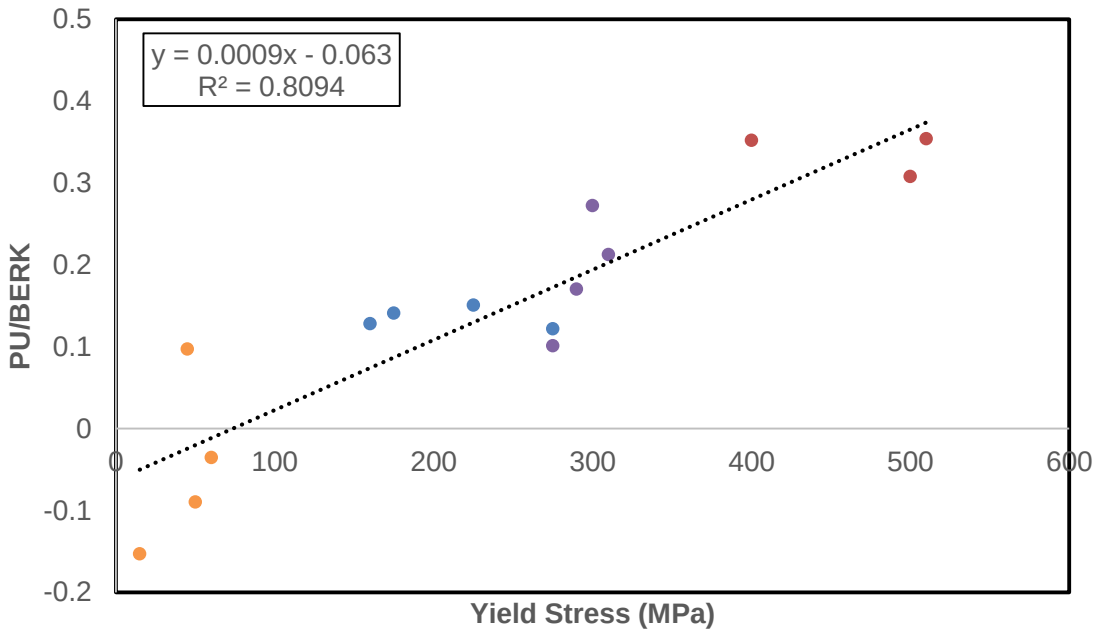

Figure 62. Normalized pile-up area vs yield stress for gold on all metallic substrates at 200nm indent depth.

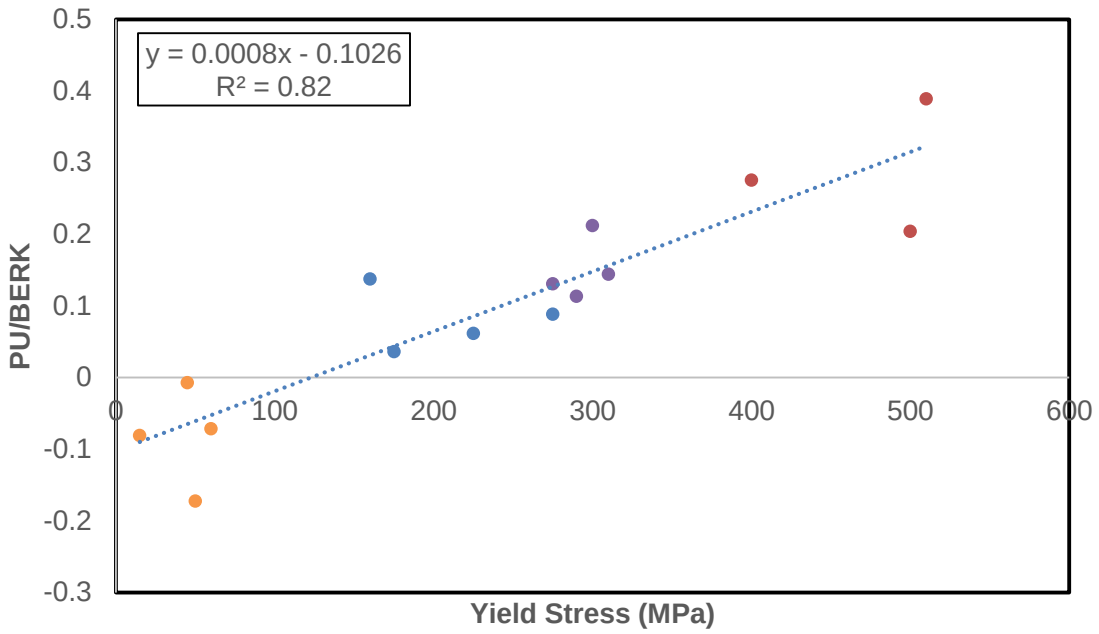

Figure 63. Normalized pile-up area vs yield stress for gold on all metallic substrates at 300nm indent depth.

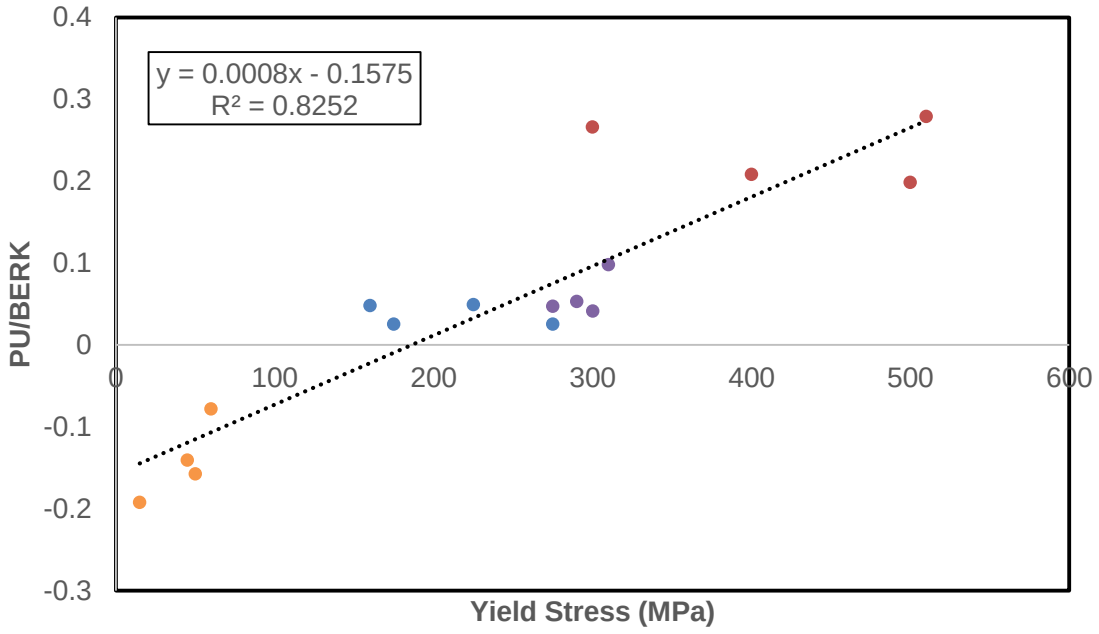

Figure 64. Normalized pile-up area vs yield stress for gold on all metallic substrates at 400nm indent depth.

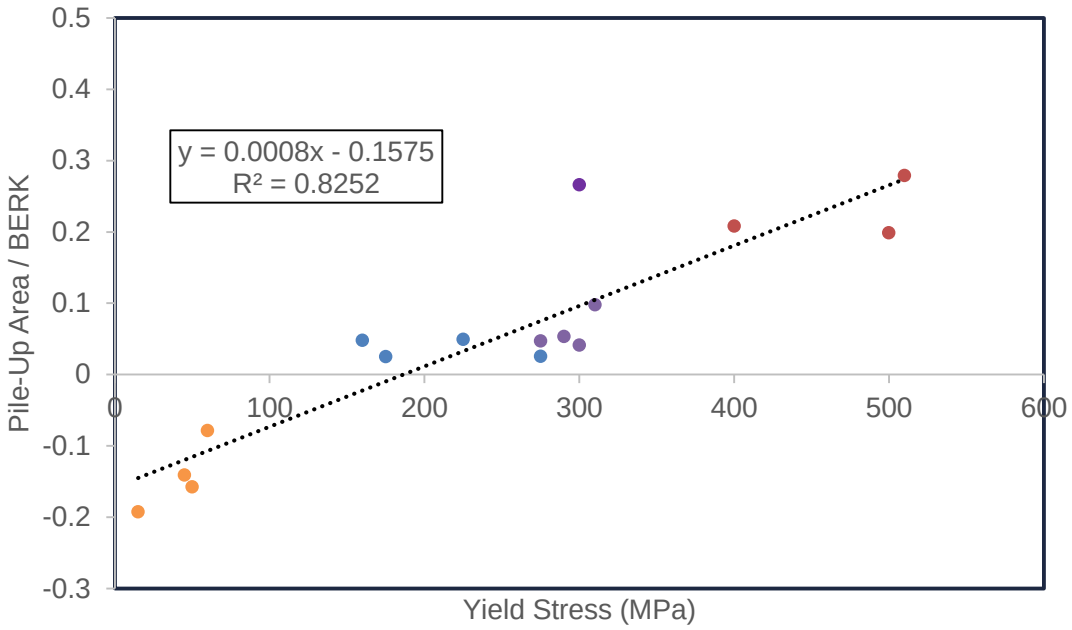

Figure 65. Normalized pile-up area vs yield stress for gold on all metallic substrates at 500nm indent depth.

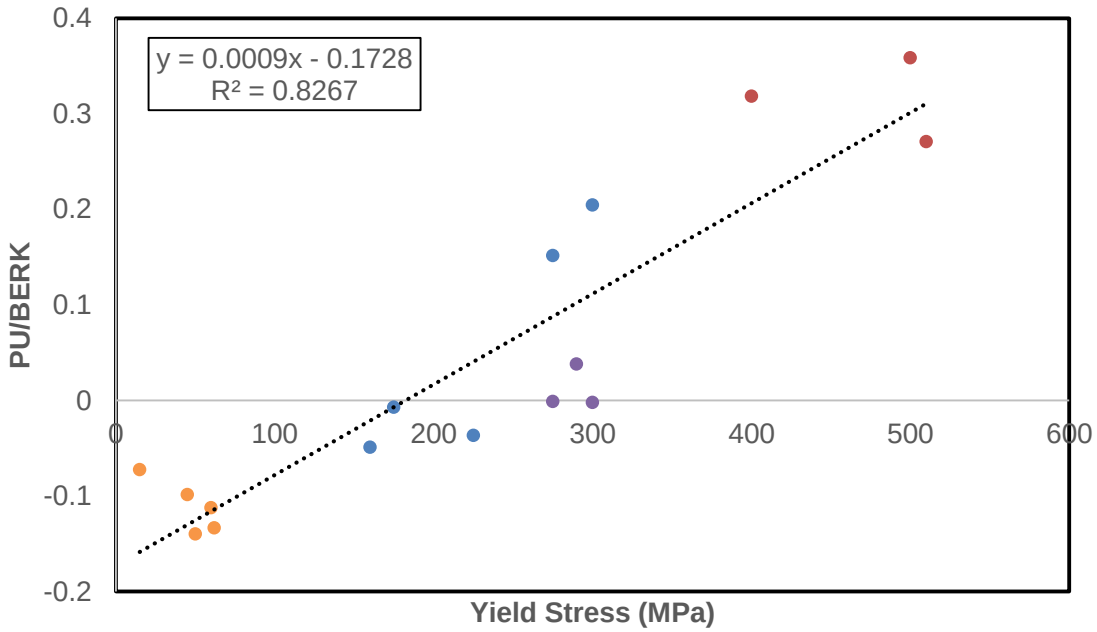

Figure 66. Normalized pile-up area vs yield stress for gold on all metallic substrates at 600nm indent depth.

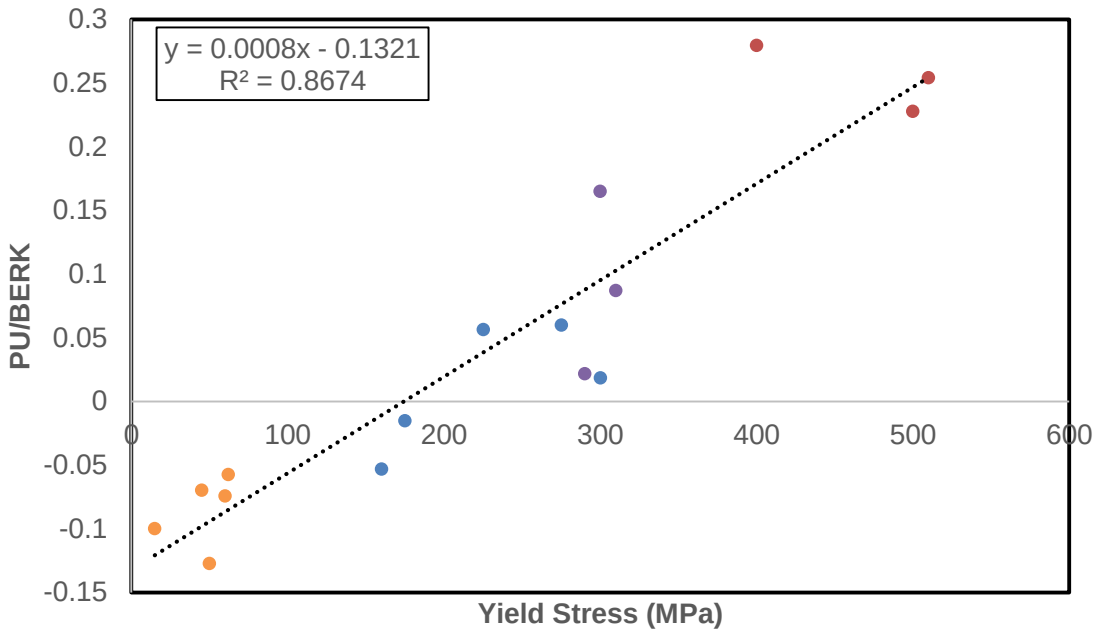

Figure 67. Normalized pile-up area vs yield stress for gold on all metallic substrates at 1000nm indent depth.

Before normalizing the data, all of the individual lines from each indent depth are compared on the same chart in Figure 68. This information is from the raw data taken from ImageJ to calculate the pile-up area. The y-axis may be titled pile-up area in some of these charts, but if it is negative, it is indicative of sink-in. A value of zero would mean no pile-up or sink-in. All of the lines in Figure 68 increase with increasing indent depth. There is a large jump from 500 – 600 nm, and again between 600 – 1000 nm. The first can be explained because the indenter should be at the film thickness are 500 nm, and past it at 600 nm. The depth of 1000 nm was used to compare trends that followed double the film thickness, and they seem to agree quite well. In this plot, however, it was hard to compare the materials based on their indent depth, and the properties should be identical at increasing indent depths, so that is why all of the previous figures were plotted with the normalized area.

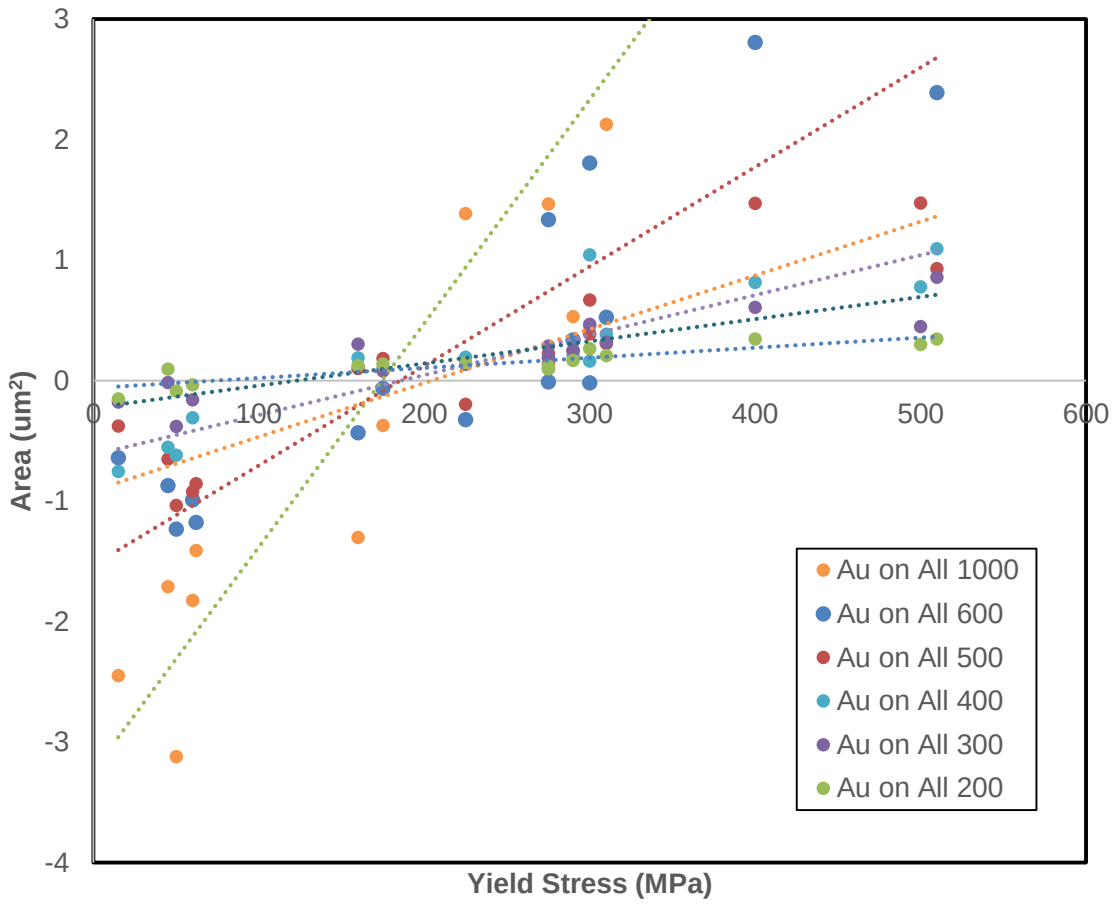

Figure 68. All indent depths for measured pile-up area vs. yield stress.

With normalized y-axes, it is possible to compare the linear trends of yield stress vs. normalized pile-up for all indent depths on the same chart. This is visualized in Figure 68, which is Figures 62 – 67 superimposed on one another.

After dissecting all of this information, the most interesting point on all of these charts is that there is a cross-over of all the lines on the x-axis. A negative pile-up value demonstrates sink-in, and positive is pile-up. It is curious to examine the zero point on the x-axis because this would mean no pile-up or sink-in; it represents a perfect indent based on the Berkovich tip indent area. This point does change slightly for all of the indent depths, where the slope is very similar, shown in Table 6. To visualize the change in the cross over point with indent depth, the x-intercept is plotted against indent depth, or the first and last columns of Table 6 in Figure 70.

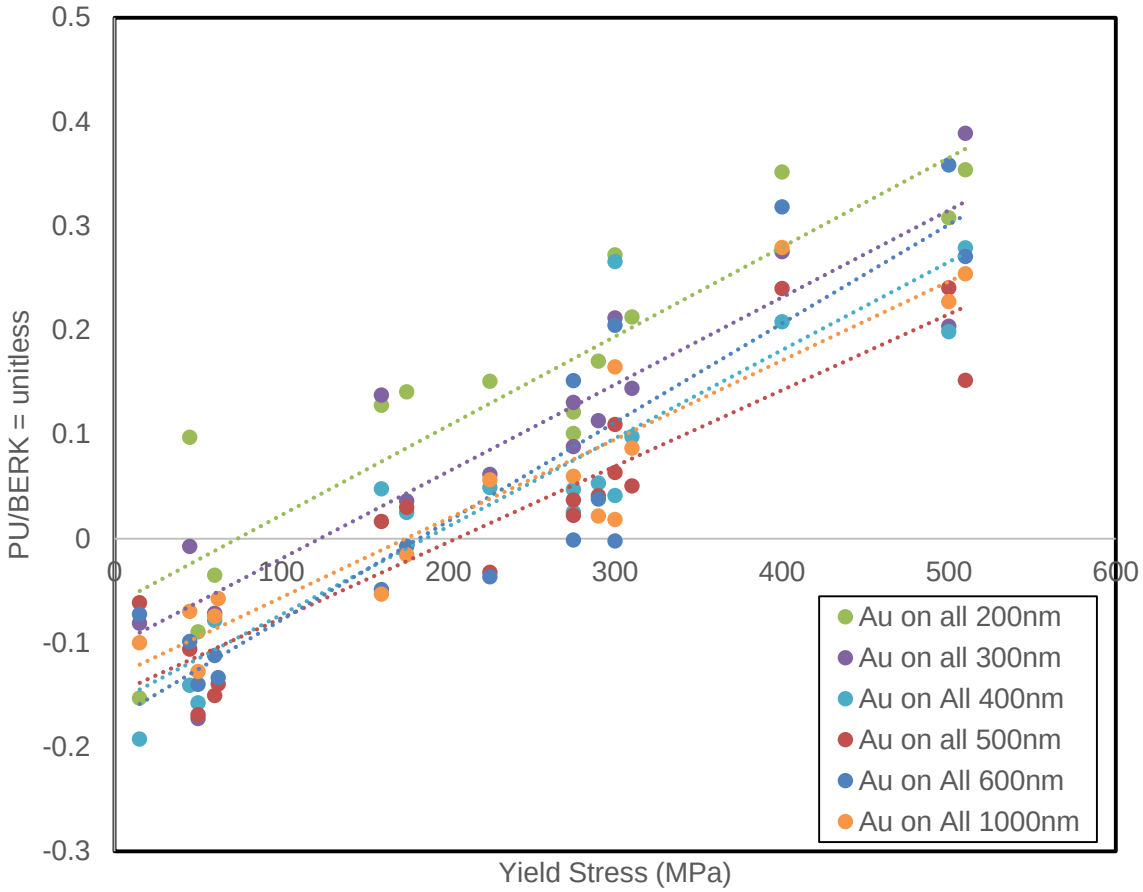

Figure 69. Normalized indent depth vs. yield stress of all gold on metallic coupons at all indent depths.

Table 6. Comparison of linear lines for each indent depth.

Indent depth (nm)	**y-intercept (unitless)**	**slope (1/MPa)**	**x-intercept (MPa)**
200	-0.063	0.0009	70.0
300	-0.0126	0.0008	132.5
400	-0.1575	0.0008	196.9
500	-0.1492	0.0007	213.1
600	-0.1728	0.0009	192.0
1000	-0.1361	0.0007	194.4

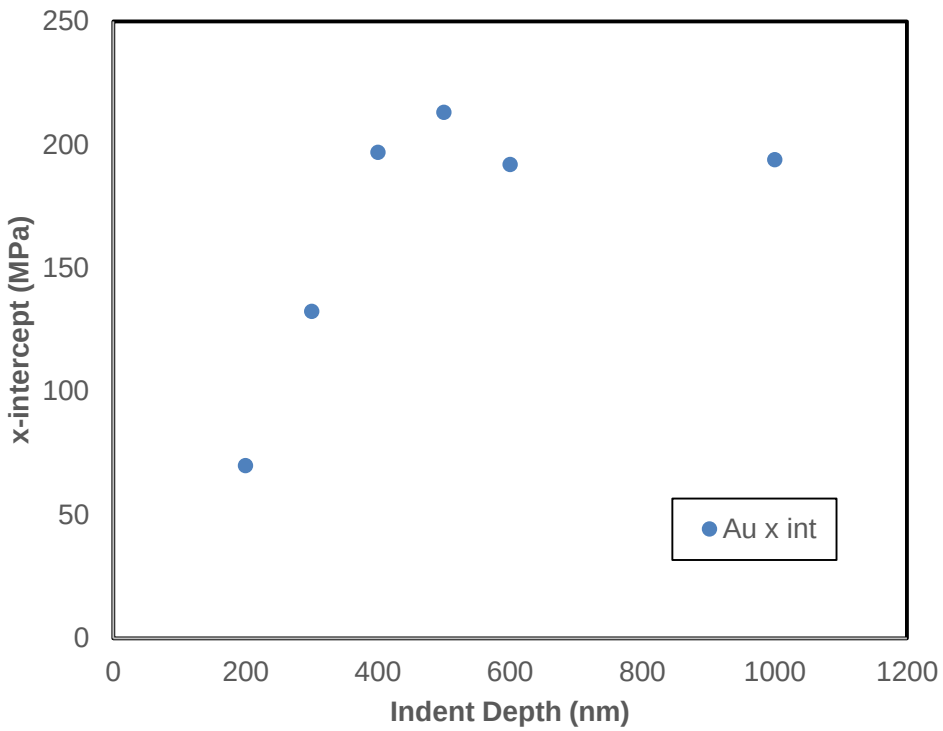

Figure 70. X-intercept vs. indent depth of normalized linearization of all metallic coupons with gold film.

The x-intercept is so intriguing because the units are in MPa, and can possibly relate to the yield stress of the film. It is evident there is a balance of the plastic properties at this point, to allow for zero pile-up or sink-in. Figure 70 is very fascinating when plotting the change in this x-intercept yield stress with indent depth. As the film thickness is approached (480nm), the intercept is increasing at a linear rate. After the film thickness, however, the number seems to level off; the film is not playing as much of a role in this cross-over no pile-up point. This is indicative of an inherent property of the film, and it is possible it could relate to the yield stress of the film directly.

Previous work studying gold films through electron beam scattered diffraction (EBSD) were able to extract film properties and compare them to tests done using membrane deflection. The Hall-Petch relation and the variables relating to this specific sputtered gold film were uncovered. In previous work, however, the yield stress was seen to be closer to 300 MPa for sputter deposited films of this thickness [62, 63, 65]. The parameters may

have been the same, but the equipment has changed over the years, so it is possible this comparison may be slightly off.

5.2.3 Pile-Up in Platinum on Metallic Substrates

The process was completed in the exact same manner on the metallic substrates with platinum. The coupons were masked off in a way to only deposit on one area, leaving two other areas free for gold and un-coated. In these cases of platinum films, sink-in occurred in almost all of the samples. To compare with gold, platinum has a higher elastic modulus, and also a higher yield stress. It is believed the yield stress ratio is affecting the pile-up or sink-in tendencies, and comparing two film materials, gold and platinum, can reveal the differences that occur.

First, the images are visualized in the following figures. Platinum was deposited on aluminum, brass, annealed steel, and cold rolled steel to all of the same yield stresses. Figures 71 – 74 show the SEM images that correlate. Figure 71 exhibits platinum on aluminum, where sink-in is very clear through the samples. Also, the surface of these do not seem very clean, but when SEM images were taken, the best ones were chosen, and only the indents that appear to be normal were utilized in calculations of the sink-in or pile-up. Next, Figure 72 shows platinum on brass, which has a few problems with indentation, but are shown here to symbolize how difficult this entire process of indenting then imaging can be, and how it needs to be avoided for future researchers. With the platinum on brass film, there could have been poor adhesion, resulting in the indenter tip removing part of the film while testing. Another problem could have been the tip was not clean, if it had occurring in the indent prior, and re-deposits some of the film on the new indentation area. Brass had the most problems, but most of the indents appeared to be correct. Figure 73 exhibits platinum on annealed steel, while Figure 74 demonstrate the progression for platinum on cold rolled steel. These now are very different from the gold film analyses, as there is mostly sink-in, and possibly some pile-up in the deeper indents tested.

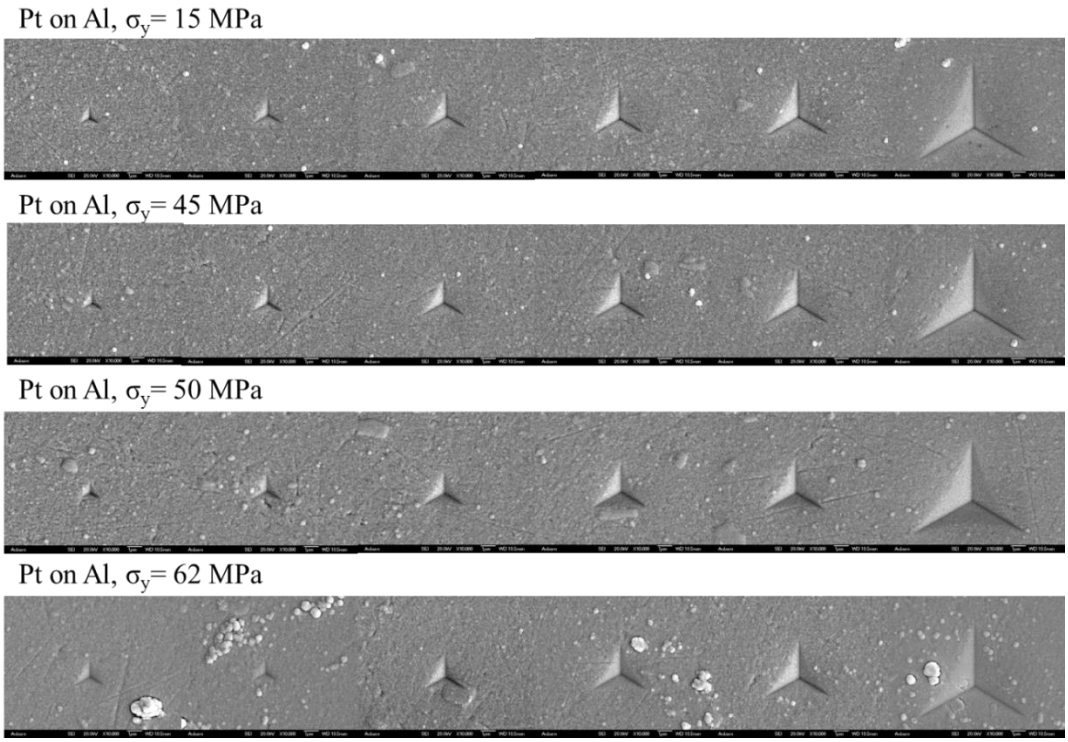

Figure 71. Platinum on aluminum to varying stresses and increasing indent depths.

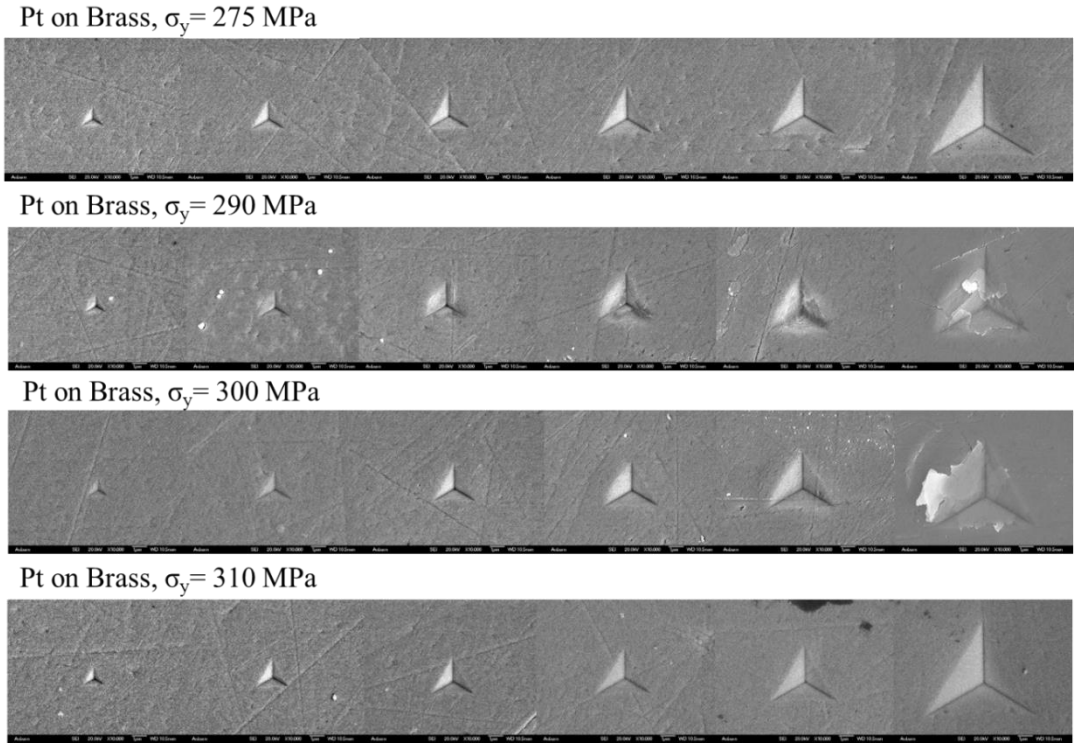

Figure 72. Platinum on brass to varying stresses and increasing indent depths.

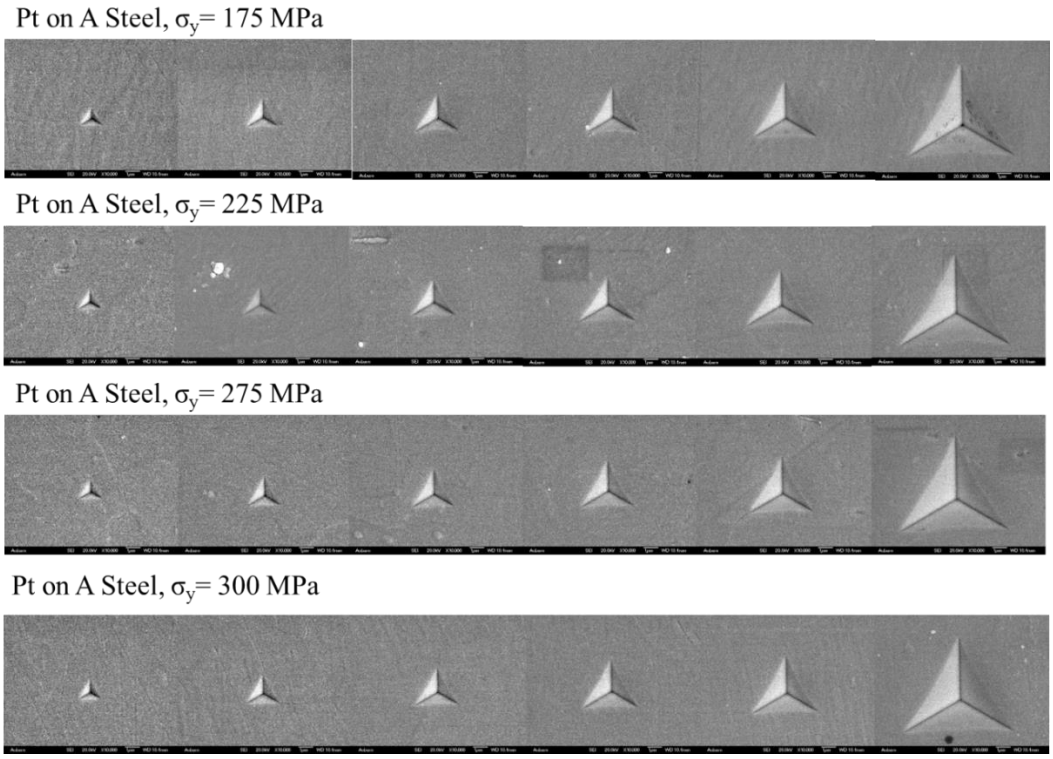

Figure 73. Platinum on annealed steel to varying stresses and increasing indent depths.

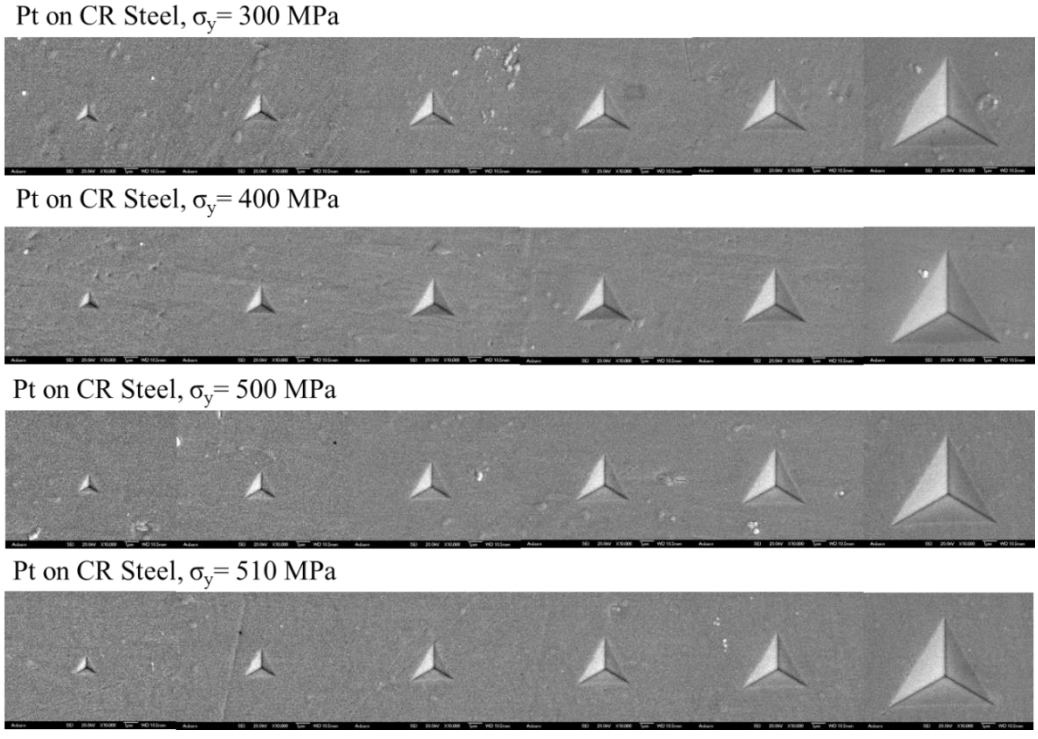

Figure 74. Platinum on cold rolled steel to varying stresses and increasing indent depths.

The idents are visualized because the indentation data was completed on each sample at increasing indent depths. These are shown in Figures 75 – 78. Similar to the tests on bulk metallic substrates or gold on the metallic substrates, all of these are identical in elastic properties and adhere to the Zhou-Prorok model. Brass is one exception, as it can be seen there may have been a problem with the initial nanoindentation testing, which led to incorrect imaging, shown previously.

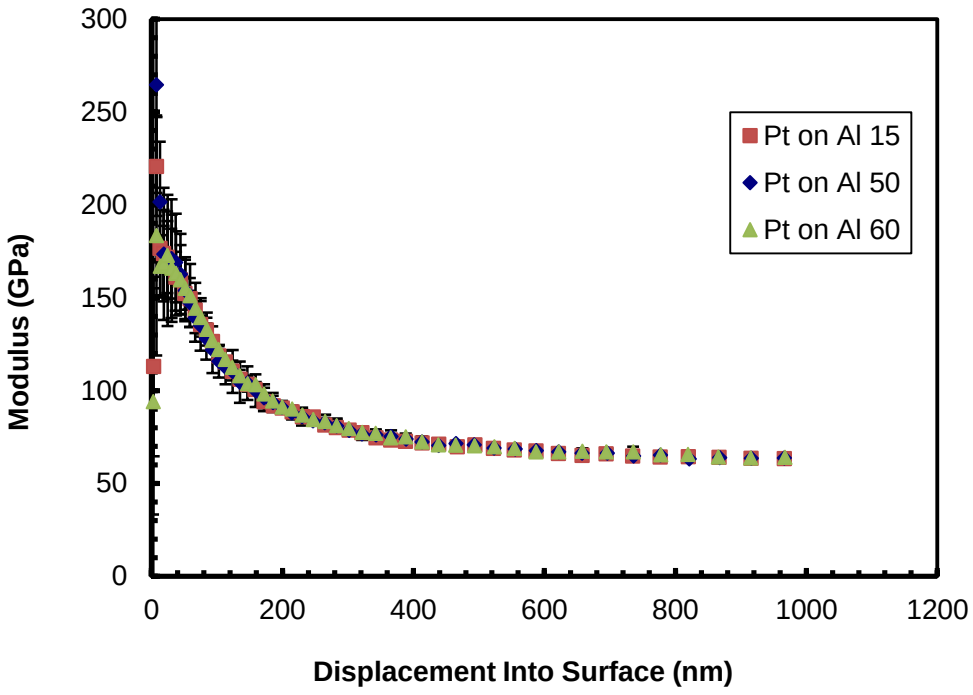

Figure 75. Indentation data of platinum on aluminum to varying stresses.

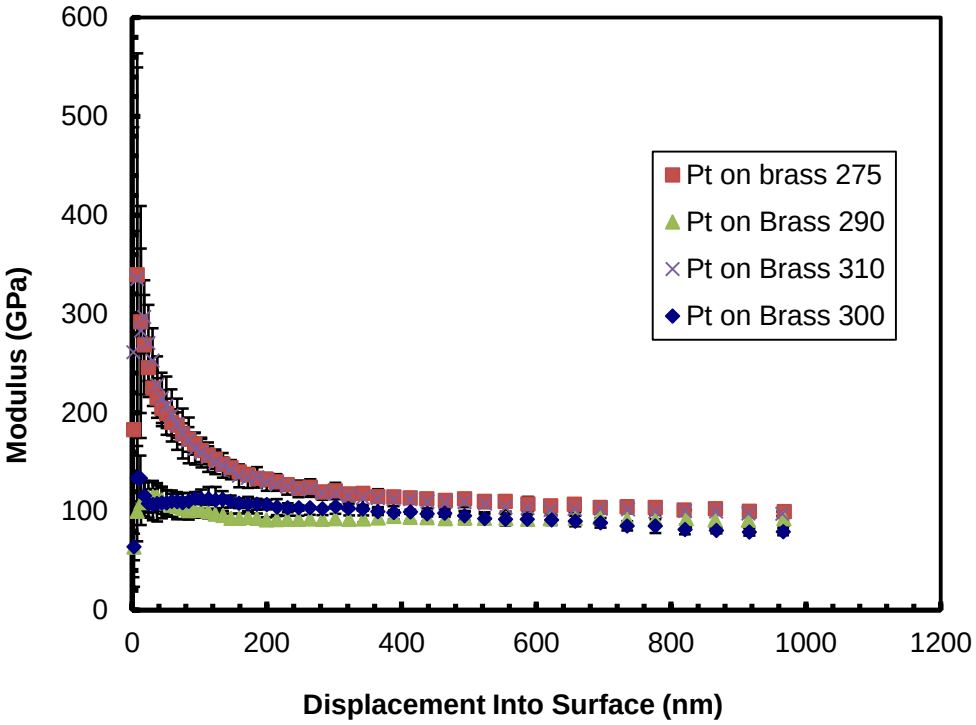

Figure 76. Indentation data of platinum on brass to varying stresses.

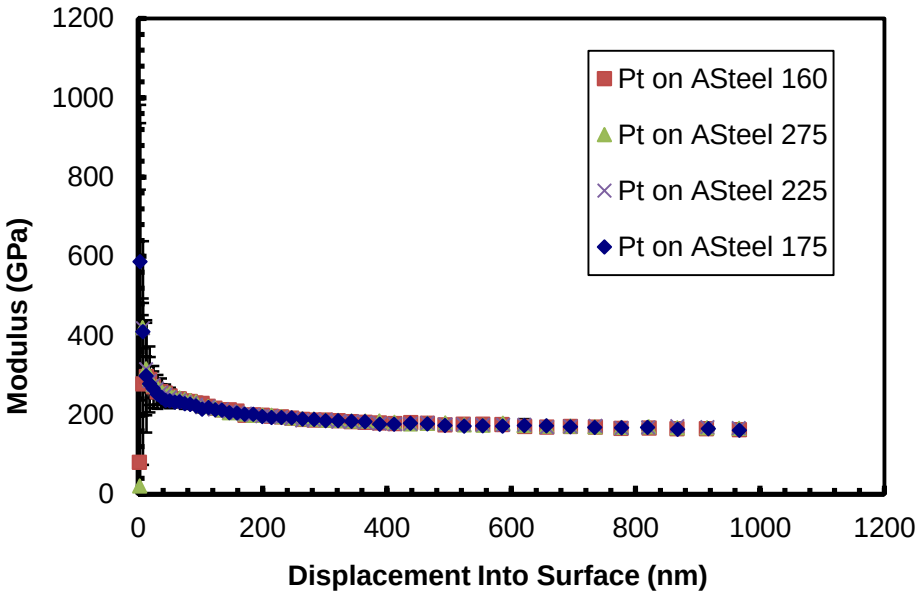

Figure 77. Indentation data of platinum on annealed steel to varying stresses.

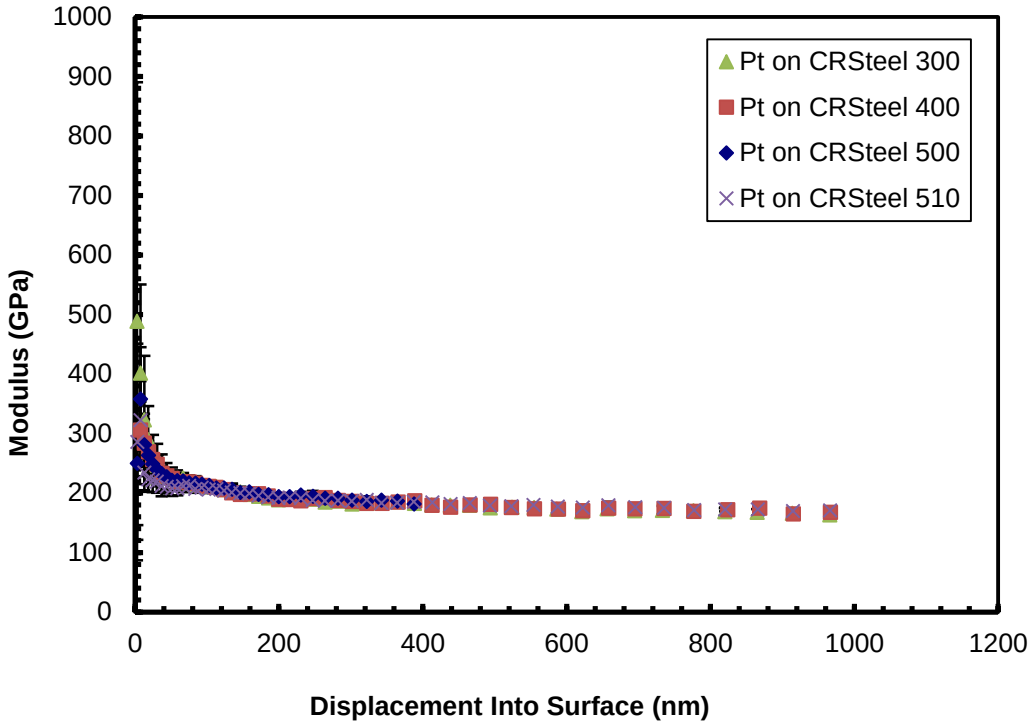

Figure 78. Indentation data of platinum on cold rolled steel to varying stresses.

ImageJ protocol was utilized again, and at each indent depth, the pile-up was compared to the yield stress as it was for the gold on metallic substrates. It is seen for platinum on aluminum, Figure 79, brass, Figure 80, annealed steel, Figure 81, and cold rolled steel, Figure 82, similarly compared to the expected Berkovich area, as well. Mostly all of these film/substrate combinations result in sink-in, where some showed some very slight pile-up, or no phenomena at all.

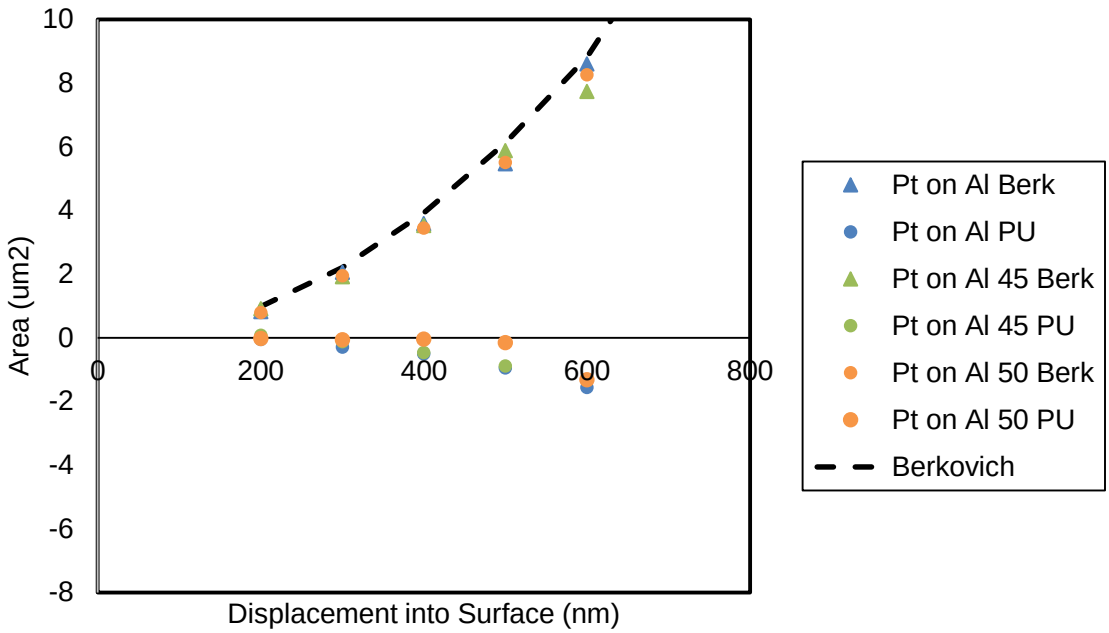

Figure 79. Quantitative data of sink-in of platinum on aluminum.

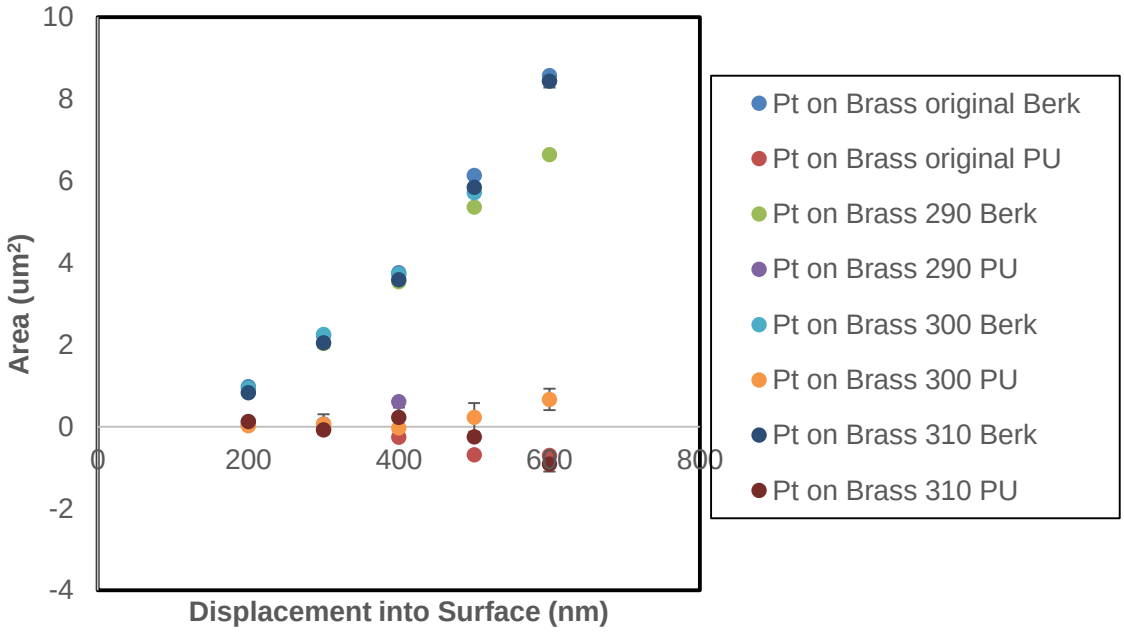

Figure 80. Quantitative data of sink-in of platinum on brass.

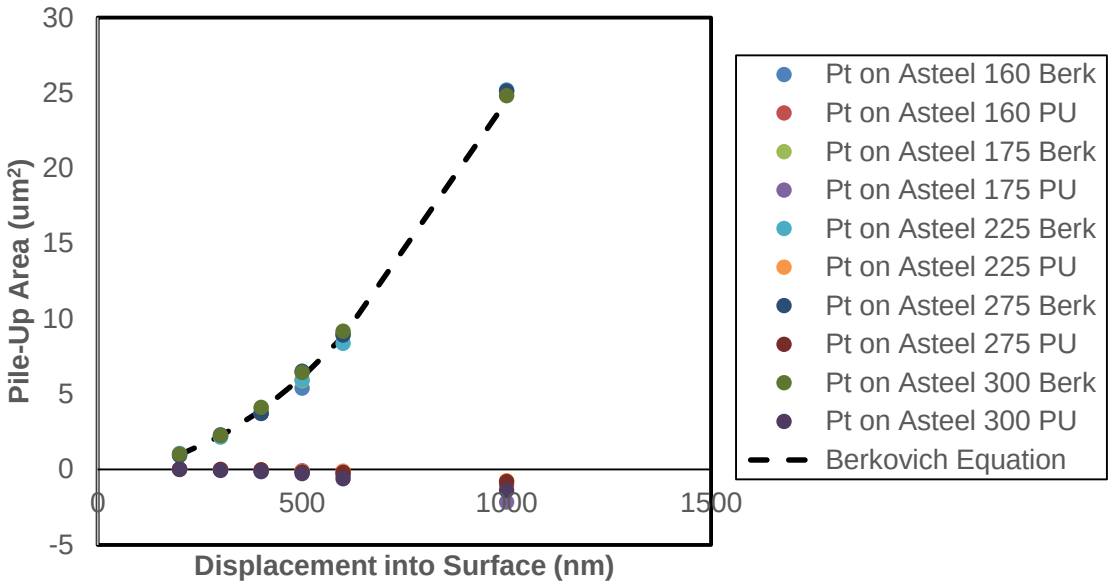

Figure 81. Quantitative data of sink-in of platinum on annealed steel.

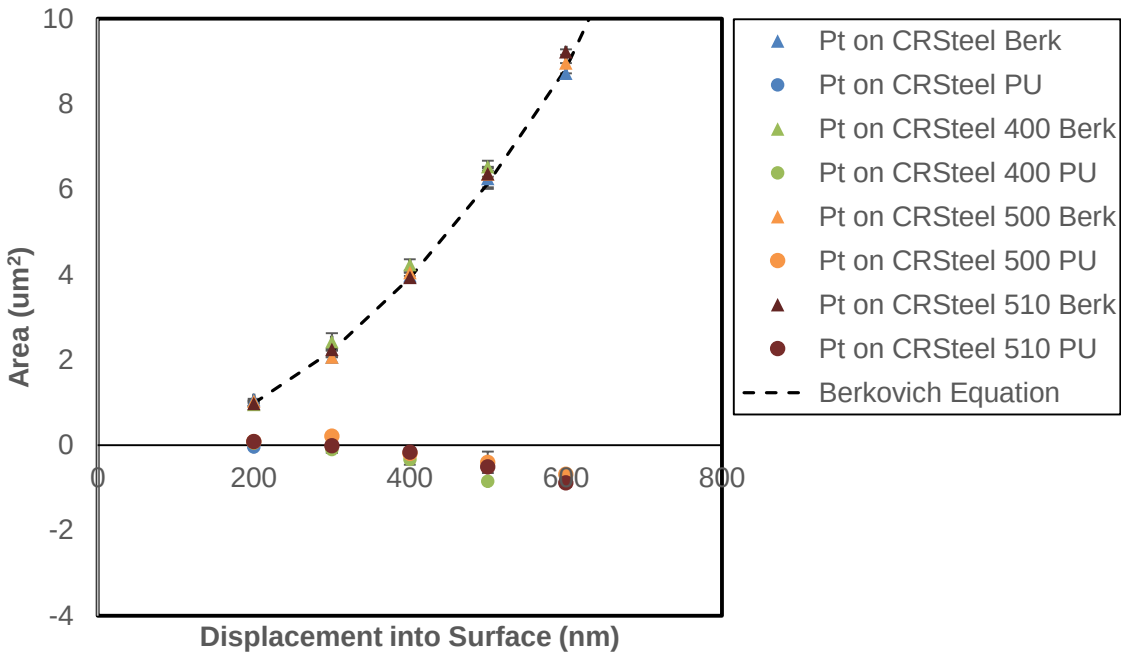

Figure 82. Quantitative data of sink-in of platinum on cold rolled steel.

The samples were similar compared altogether on the same plot in Figure 83. Each indent depth has a linear line associated with it. The trend is the same as gold; with an increase in indent depth, the slope increases. The cross-section with the x-axis is much larger in the platinum film samples than the gold, however.

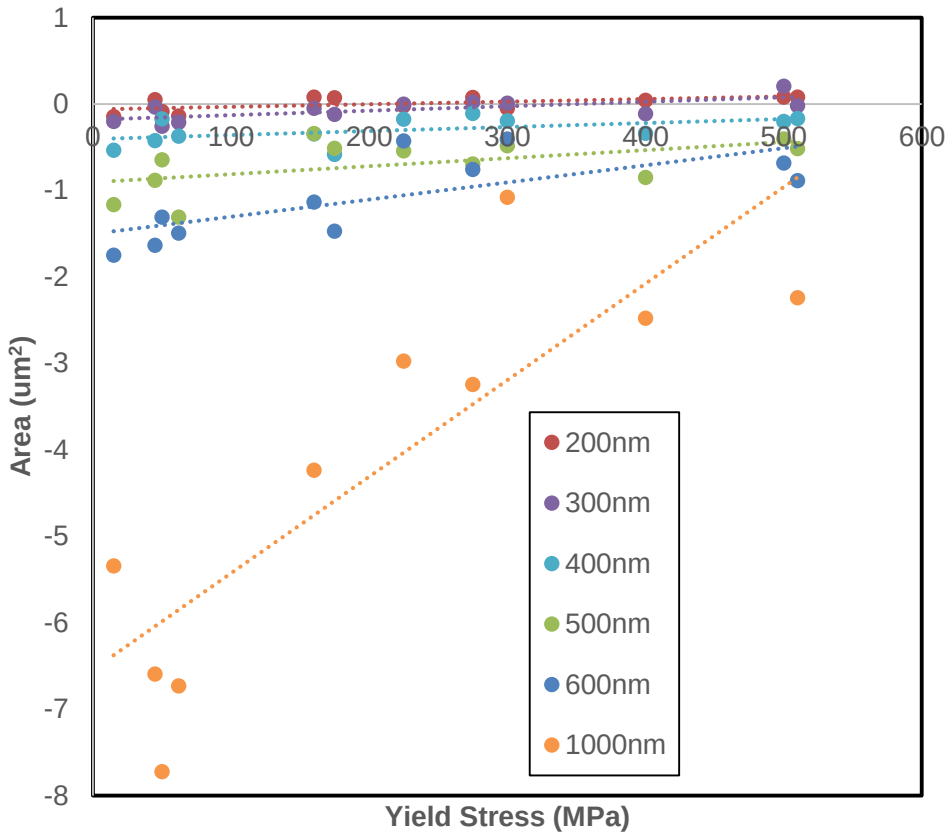

Figure 83. Platinum films on all metallic coupons at all indent depths.

When normalizing the pile-up by the expected Berkovich area, the lines also collapse to the same slope, with a shift at the intercepts, seen in Figure 84. This does not collapse as smoothly as the gold films had, however, so it is a little more difficult to interpret the results. However, it is clear that when penetrating past the film thickness in the case, the slope changes more.

Table 7. Parameters for normalized platinum on substrates.

Indent depth (nm)	y-intercept (unitless)	slope (1/MPa)	x-intercept (MPa)
200	-0.064	0.0003	213.3333
300	-0.1796	0.0005	359.2
400	-0.404	0.0005	808
500	-0.9039	0.0009	1004.333
600	-1.5025	0.002	751.25
1000	-6.5415	0.0112	584.0625

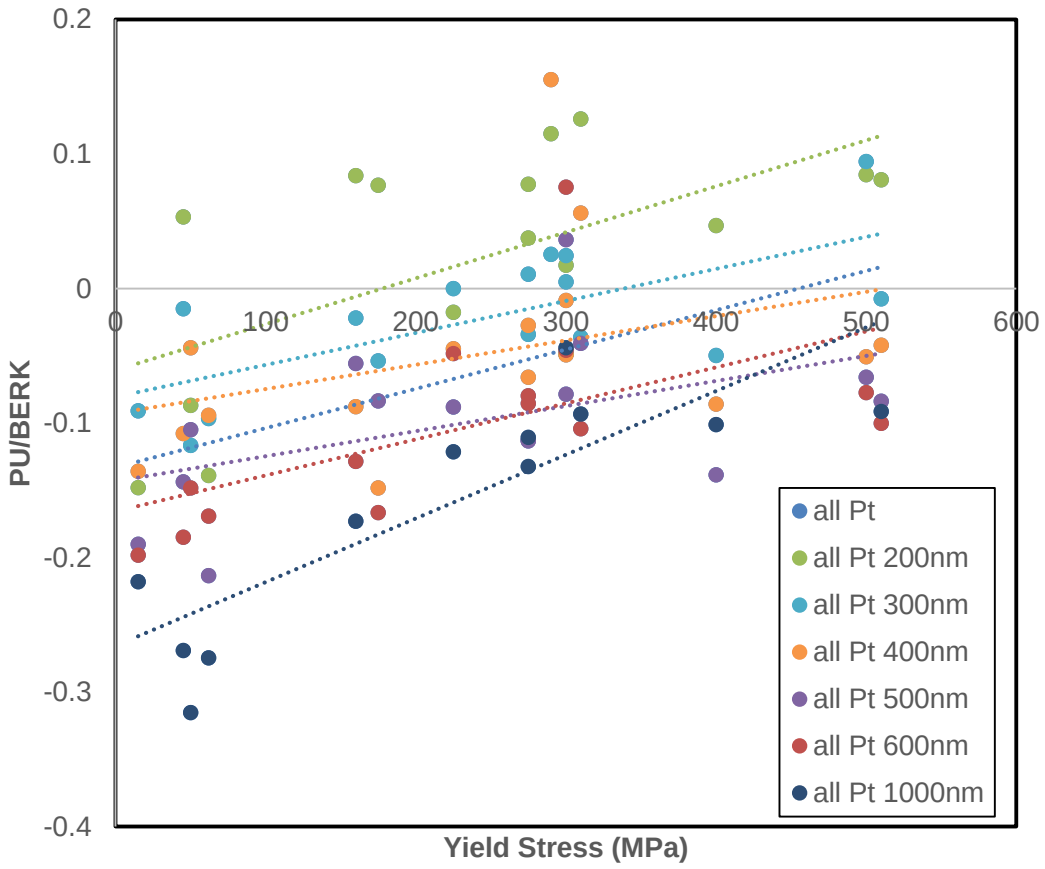

Figure 84. Platinum on all metallic coupons at all indent depths normalized to the expected Berkovich area.

Table 8. Parameters for normalized platinum on substrates.

Indent depth (nm)	y-intercept (unitless)	slope (1/MPa)	x-intercept (MPa)
200	-0.0606	0.0003	202
300	-0.0806	0.0002	403
400	-0.0928	0.0002	464
500	-0.1433	0.0002	716.5
600	-0.1656	0.0003	552
1000	-0.2656	0.0005	531.2

The intercept is much higher than it was in gold, and can be attributed to a higher yield stress in platinum than gold. Although it is difficult to measure the yield stress of the film to confirm, with the same yield stresses in the substrates, between the two film tests, there is a clear difference when the film material properties change. The results from the gold which were previously seen in Figure 70 are compared with the cross section from the platinum results in Figure 85. Although the platinum shows a much higher stress at the cross section, it exhibits a similar trend of leveling off after reaching the film thickness. It is a possibility that this could mean the film yield stress in platinum, although it is very high. It is an extremely interesting result that came from many tests at many yield stresses to get the one single plot. Although yield stress may not be able to be directly extracted confidently from this information, it has broken into the realm of nanoindentation and shown that yield stress of the substrate will results in an increase in pile-up, or a decrease in sink-in, and it is dependent on the interplay between the film and substrate plastic properties. Elastic properties have not been mentioned in these results, as the permanent deformation of pile-up or sink-in is finally described using this method. In the future, it will be unnecessary to do the complete image and measurement analysis, and the film yield stress will be determined from indentation of these materials when the substrate yield stress is known.

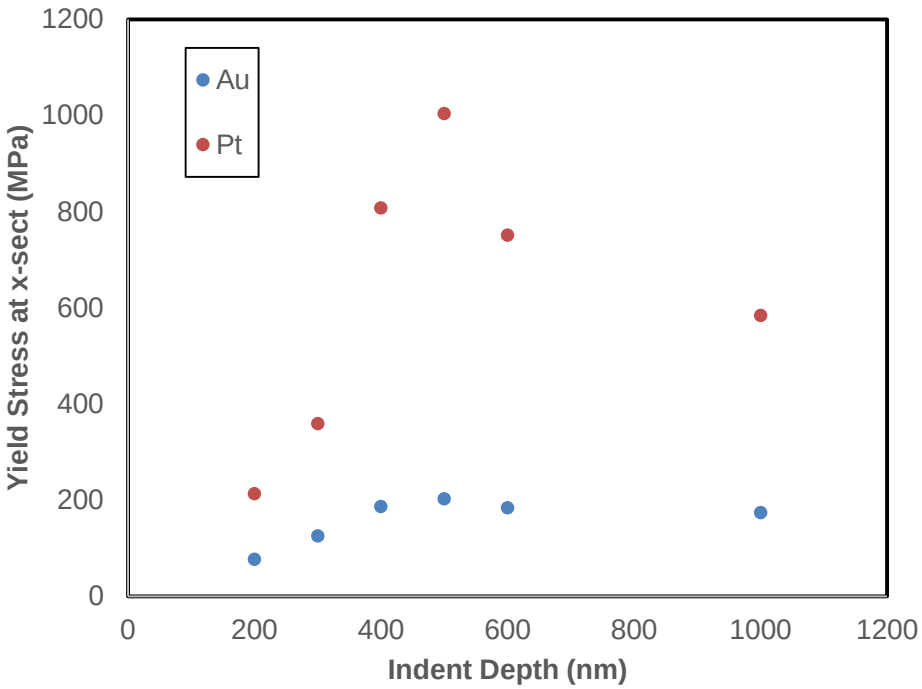

Figure 85. Comparison of the x-axis cross-section of gold and platinum films to increasing indent depths.

5.2.4 X-ray Diffraction Analysis

The most interesting samples to compare further are the annealed and cold rolled steel. They are the same material, created with very different processing techniques. The samples came directly from the company, Pasco, so some of the processing parameters are unknown. The amount of cold rolling or annealing is not specified by the company, but the coupons utilized were the perfect shape and size for these tests. When viewing the trends in each indent depth, it seems that cold rolled steel is unaffected by the tensile stress changes. There is a smaller range of plasticity, so there is less room for tensile yield stress changes. Annealed steel began at a low yield stress, as tested by the tensile machine, at about 175 MPa and failed around 310 MPa. The cold rolled steel began at 300 MPa and increased to 510 MPa until failure. The pile-up in the annealed steel is more affected than that of the cold rolled steel. To explain this difference, it is prudent to explain what is physically happening in the steel substrate during these processes.

However, in the testing method that has been completed in this work, directly comparing pile-up between the metallic substrates with films, yield stress can also be compared. In the steel samples, cold rolled greatly piles up compared to the annealed steel. The reason for this is that the material that is cold rolled has used up all of its capabilities for plastic deformation in the substrate, as there are many dislocations and the material is greatly strained. Any extra energy put into the material, as it is in nanoindentation, cannot be accommodated. Instead, the substrate pushes back and up around the indenter tip, piling up. The annealed steel has much more capability to deform, as it has been relaxed in the processing techniques. The fight between the gold film and steel substrate is still occurring, however, so slight pile-up is still visible. However, it is to a much smaller extent than it is for the cold rolled steel. These can be seen in the images compared with side by side SEM images in Figure 86.

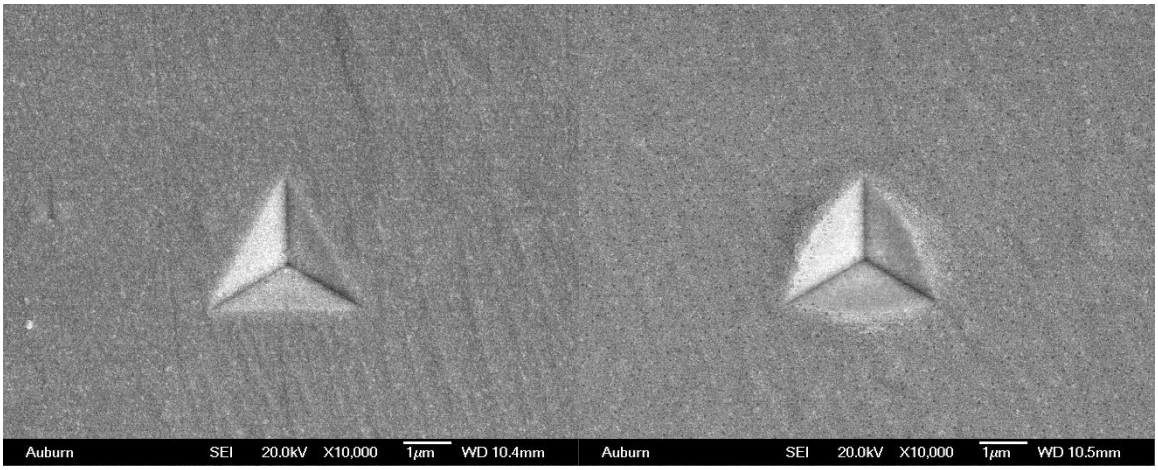

Figure 86. Annealed steel (left) and cold rolled steel (right) at 400nm indent depth.

The samples were scanned with x-ray diffraction from two conditions: un-tested with the tensile tester, and to tensile tested to failure. The chart for comparison of the x-ray scans is seen in Figure 87. For the annealed steel alone, the full width half maximum value (FWHM) did not change. Similarly, for the cold-rolled steel, the FWHM did not change between the untested sample and the one pulled to failure. Between the two samples, however, there is a difference, seen in Figure 88. These differences are directly related to the increased strain in the material that is caused by the cold rolling. The annealed steel crystallites have been able to relax, but the cold rolled steel has many dislocations, probably

excessively, as this material was initially used as a teaching tool to show the difference in the elastic properties. Having the excess knowledge of the XRD patterns allows for the understanding of the pile-up difference when plastic properties changes, yet elastic modulus is constant as it is in these steel samples.

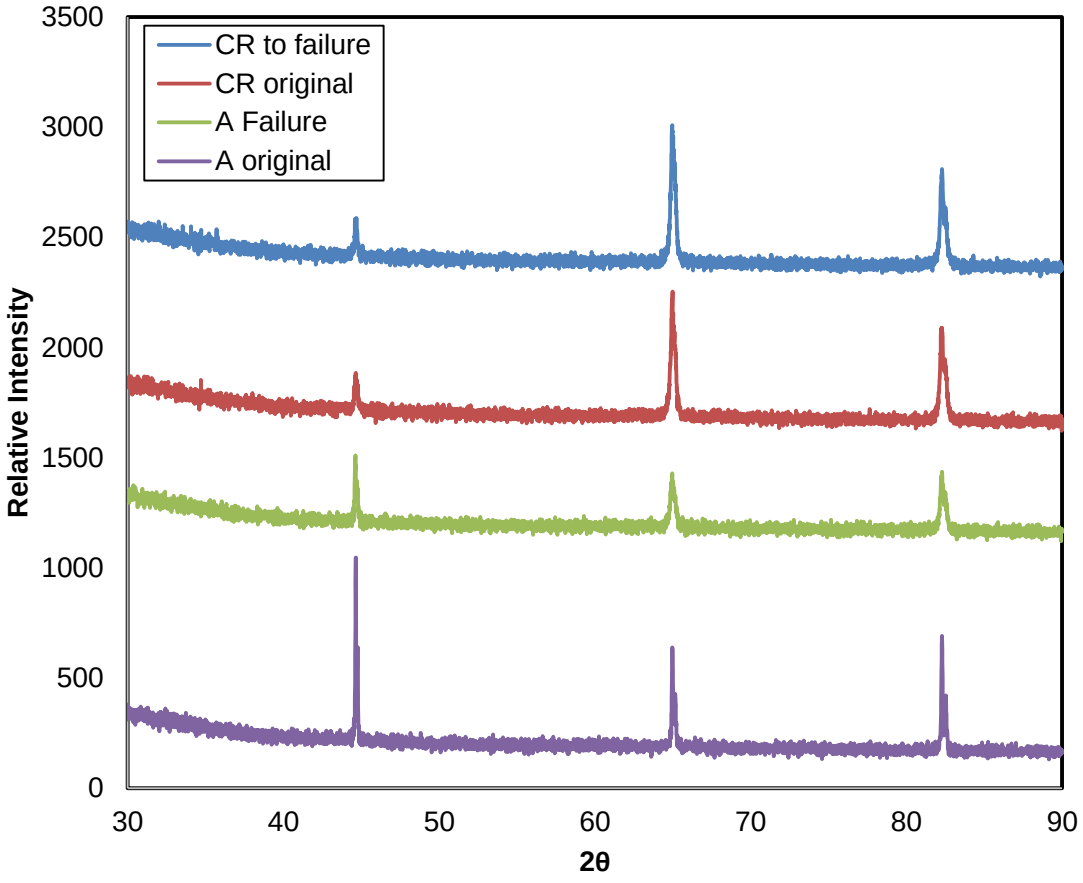

Figure 87. XRD scans for cold rolled and annealed steel, original and post tensile test to failure.

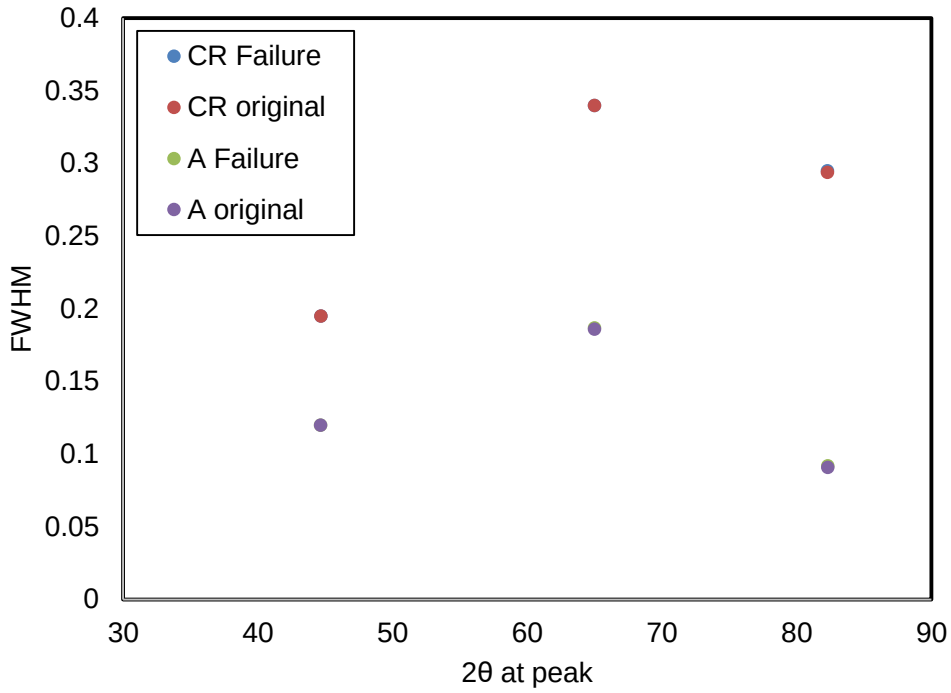

Figure 88. XRD FWHM peaks for cold rolled and annealed steel, original and post tensile test to failure.

5.2.5 Sink-In and FIB Cross-Sections

In previous work, platinum films were tested in the same manner on metallic substrates. The film was thin, at 230 nm thickness, and when penetrating into the substrate, it is curious that the substrate was not seen with SEM imaging. Previously, it was shown that the ceramic substrates are visible when punching through to the substrate with gold films. This also occurs with platinum films when the substrate is non-plastically deforming. With more compliant substrates, such as the ones seen in Figure 89, an indent double the film thickness at 400nm deep, does not visually show the substrate. Even when completing EDS on these areas, there is no sign of the substrate, seen in the next Figure 91. This is curious because it is obvious that the indent in engaging the substrate, but strange that it will not puncture through the metallic film.

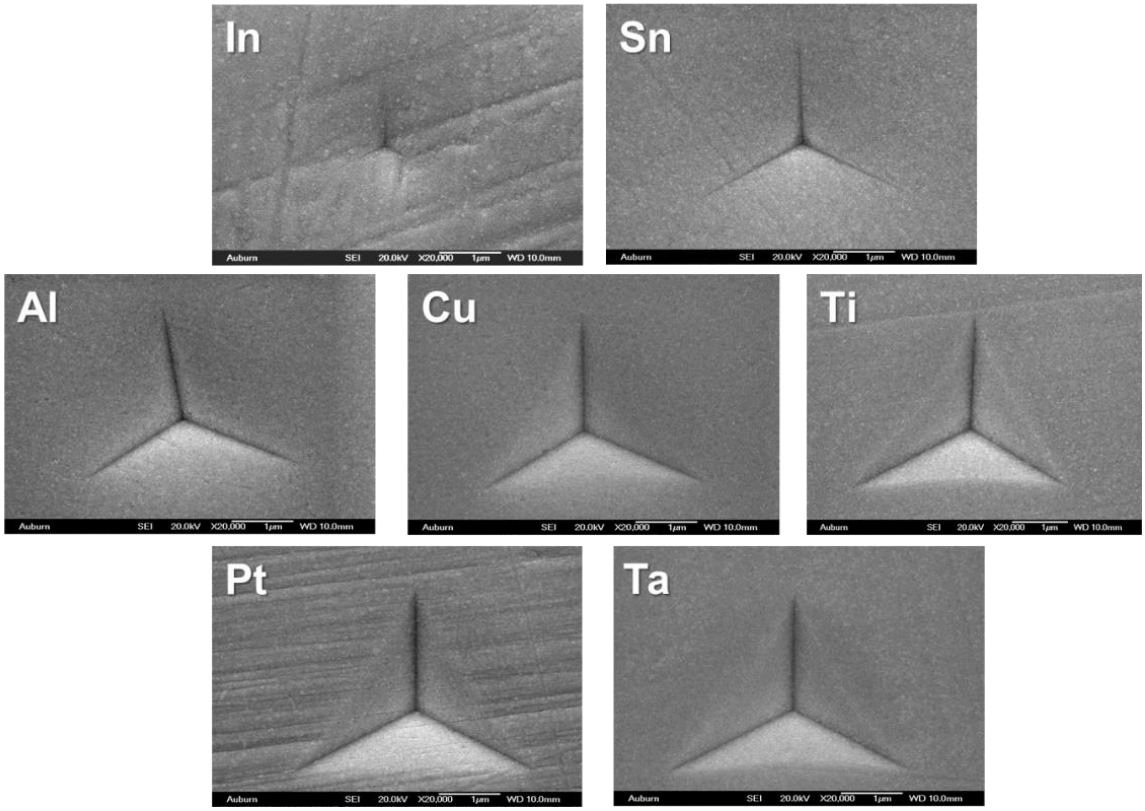

Figure 89. 230nm platinum films on metallic substrates exhibiting sink-in.

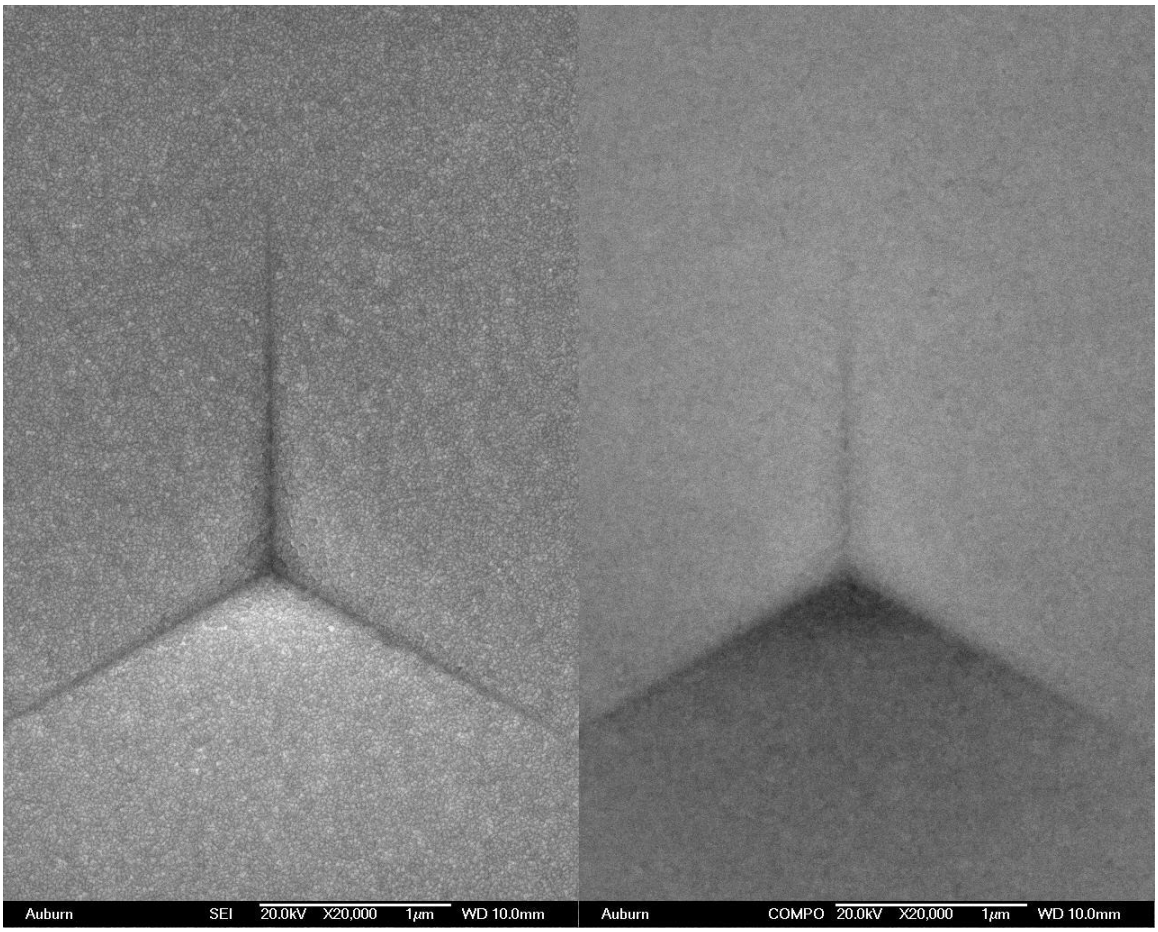

Figure 90. Backscattered image compared to one secondary electrons; if the indent had penetrated, the substrate would be clearly visible [66].

In order to understand what could be happening in the cross-section, FIB was implemented. The profile of the indent shows how the film and substrate are interacting. To compare to the topography of the metallic film on metallic substrates, a sample from the FIB cross section is shown in Figure 91. A gold film of 520 nm on annealed steel was indented to about double the film thickness at 1000 nm indent depth. When viewing the cross section, it is clear to see the difference between film (gray) and substrate (black), and they behave in a very unusual manner. The beam failed while cleaning the rest of the cut, resulting in the step that is seen ahead of the cross-section. It was expected that the indenter would break through the film and then engage the substrate, but the film is being pushed down with increasing indent depth. It is very curious that this happens in the compliant substrates, and reveals some interesting information about the interplay between film and

substrate. This phenomenon did not affect elastic properties, but perhaps there would be more pile-up if the material could not deform in this manner below the indenter tip. The input energy needs to be distributed, and in this case, it seems that the substrate is collapsing below the indenter tip.

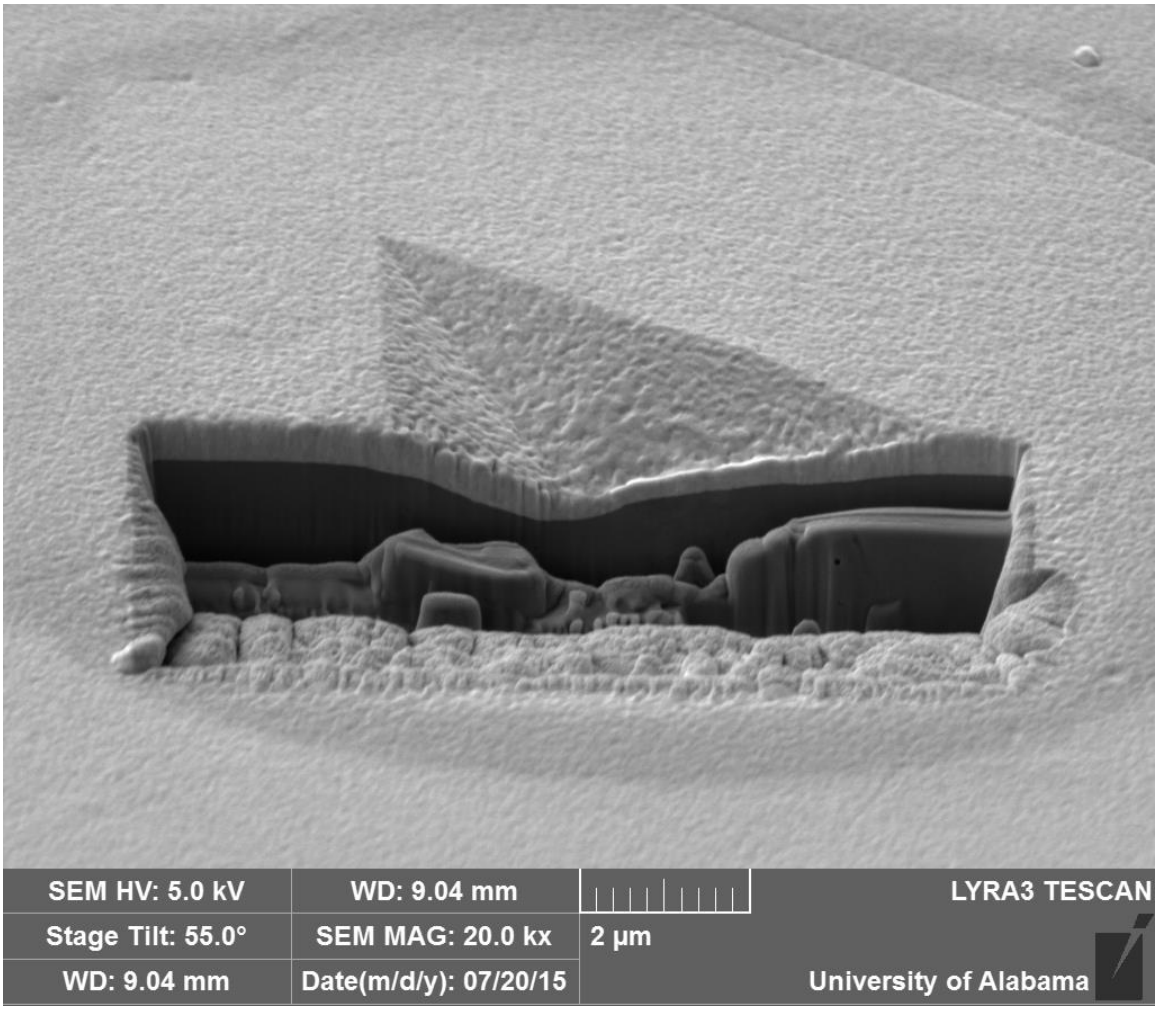

Figure 91. 1000nm indent on gold film of 480nm thickness with annealed steel substrate.

The same sample was prepared with a cross-section using FIB at a lower indent depth. A 400 nm indent depth into the 520 nm thick gold film on annealed steel is seen in Figure 92, next to the same image in Figure 91 for easy comparison. In this case, it is assumed that the indenter tip has not reached the substrate, and it is confirmed with the cross-sectional view. It is also clear to see the profile of the indent and how the substrate is collapsing and

deforming, decreasing the amount of pile-up that is formed in this material/substrate combination.

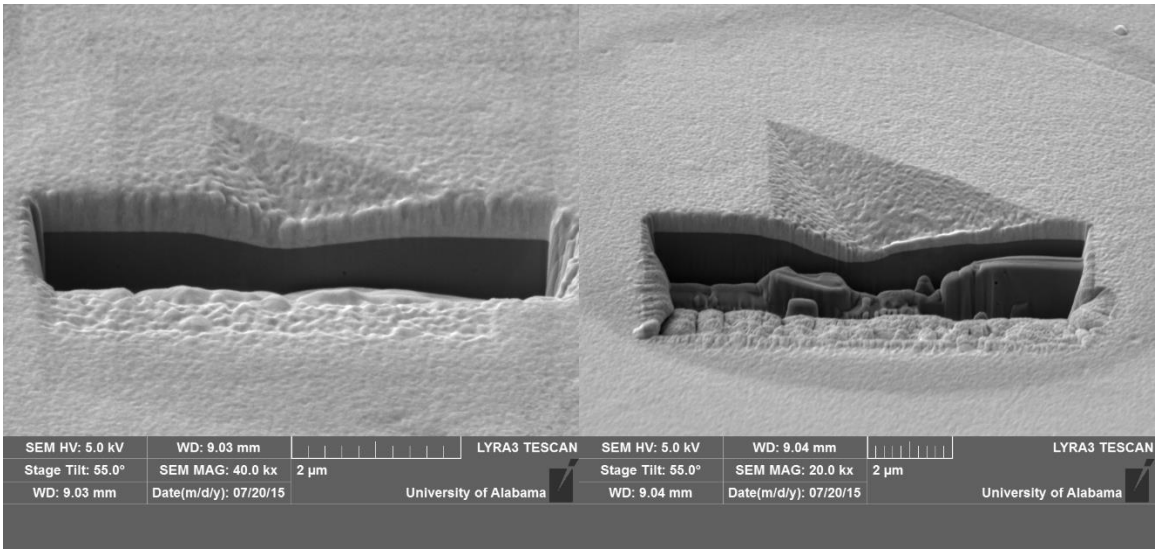

Figure 92. Annealed steel substrate with gold film of 480nm indented to 400nm (left) and 1000nm (right).

The samples were also created with a platinum film of about 520 nm film thickness, and a select few of these were also cut with FIB. It is interesting to compare these samples side-by-side to see the difference of the cross-section when the film is changed. For platinum, most of the samples exhibited sink-in, whereas the gold film has mostly pile-up. Aluminum substrates with gold or platinum are shown in Figure 93. When comparing these images, the top view is also shown to map out the differences in Figure 94. The Berkovich indent impression is the same, but there is sink-in to different extents in these samples. Having the ability to view the cross section helps to visualize the interplay between the film and substrate even further. Seen in the FIB images, the aluminum substrate wants to absorb the energy that is input during nanoindentation. This will affect the way the sample is viewed from the top, as well.

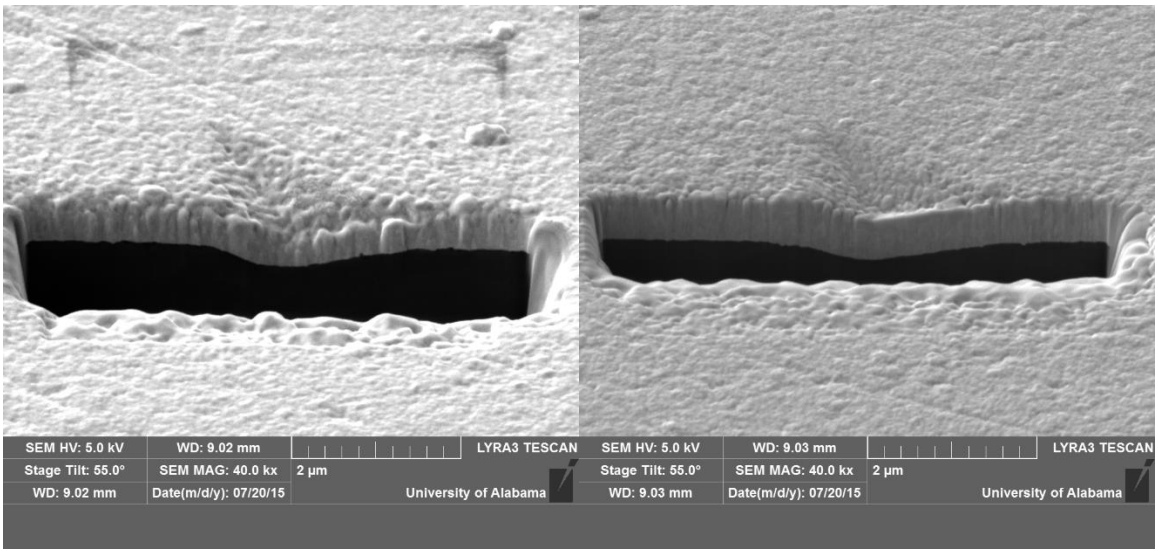

Figure 93. FIB cross-section of aluminum substrate with indents to 400nm with a gold film (left) and platinum film (right).

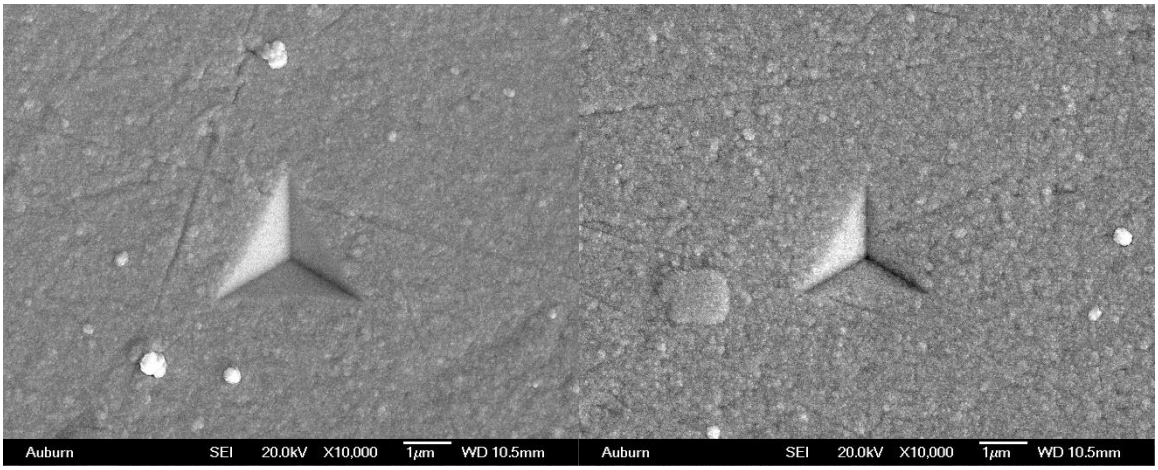

Figure 94. SEM top view of aluminum substrate with indents to 400nm with a gold film (left) and platinum film (right).

The next comparison using FIB is a cold rolled steel substrate with gold and platinum films. The cross section is seen in Figure 95 whereas the top view using SEM is seen in Figure 96. In the top view, it is absolutely clear that the pile-up is forming in the cold rolled to a greater extent that the platinum, which is slightly sinking in. The cross section confirms what is occurring in the substrate during the indentation process. The indent depth in both cases in 400 nm, and the films are both around 520 nm thick. The gold piles up, and barely

seems to affect the substrate. There is slight sink-in of the cold rolled steel substrate with a gold film. The platinum film, however, is engaging much more of the substrate plastically. The magnification is the same in both of these images; the cut was just made at a longer length for the platinum image. This is such a telling cross-section and it is exciting that these were chosen to be seen with FIB. With many more cuts, it will be possible to utilize this information quantitatively. For now, the qualitative difference is so exciting and reveals much about the interplay between film and substrate with varying plastic properties.

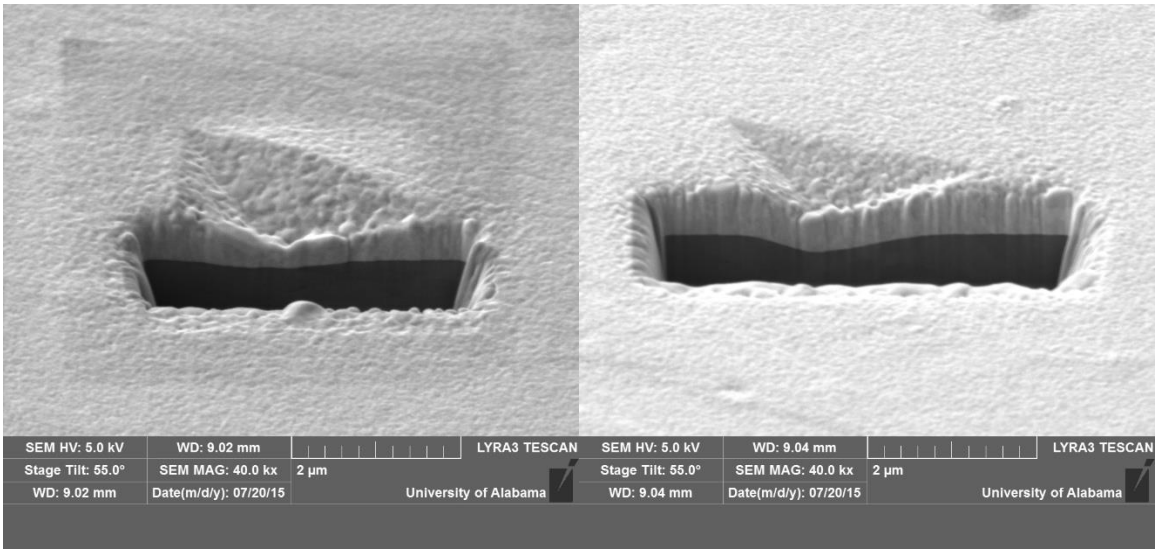

Figure 95. FIB cross section of gold on cold rolled steel (left) and platinum on cold rolled steel (right).

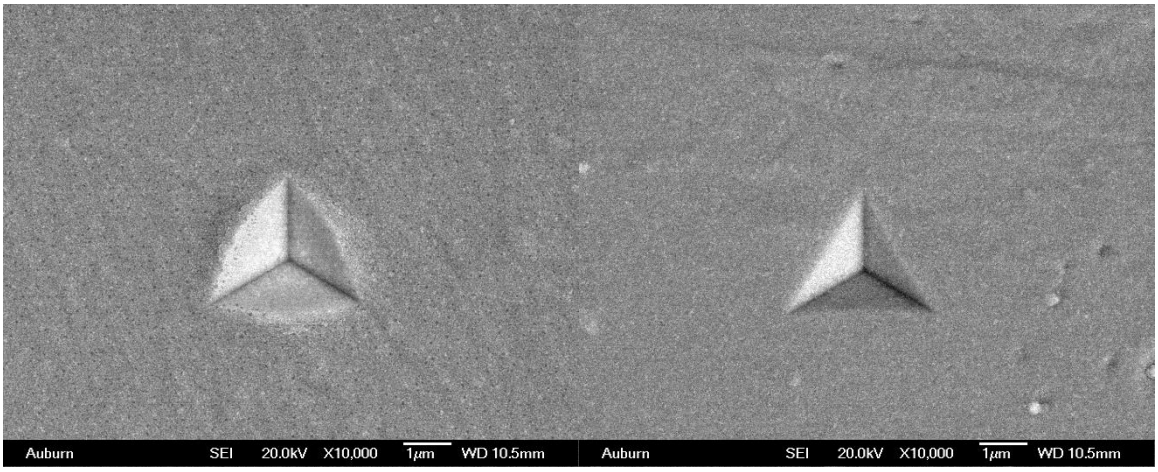

Figure 96. SEM top view of gold on cold rolled steel (left) and platinum on cold rolled steel (right).

For the previous work with gold on ceramic substrates, some FIB was also completed. In these cases, the film is punched through, and the cross-section shows the substrate does not significantly deform in the region of indentation. Figure 97 is a comparison of gold on silicon vs. gold on annealed steel. The indent depth is similar, 600 or 400 nm deep, and these cross sections show information about the substrate interaction. The silicon substrate does not appreciably deform, yet the annealed still does. Also, the silicon substrate is visible once the indent penetrates through to it, but in the metallic substrate, there is no point where the film is broken; instead it is pushed deeper towards the substrate.

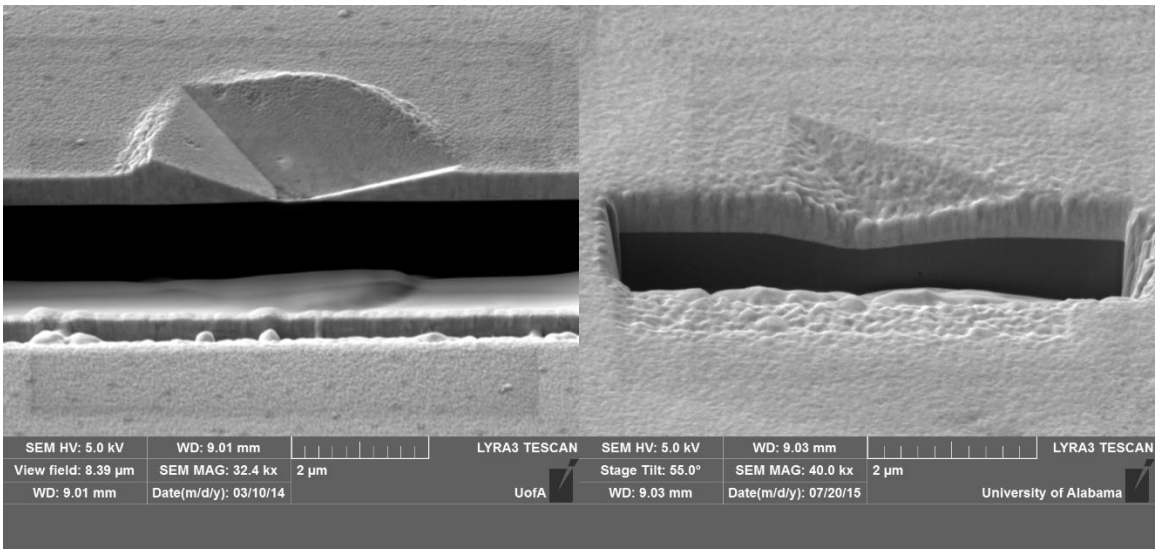

Figure 97. FIB cross-section of 480nm thick gold on silicon to 600nm (left) compared with 520nm gold on annealed steel to 400nm indent depth, (right).

To better exhibit how the FIB cuts through the sample, there is a top view post-FIB cut in Figure 98. This came from indent seen on the right of the figure, which is 480 nm gold indented to 1200 nm indent depth. The substrate is revealed, and this image is also interesting because evidence of CSM is left. Looking closely at the silicon substrate, there are lines that occur at every interval deeper into the sample. This is not visible in any of the metallic films or the metallic substrates that were tested.

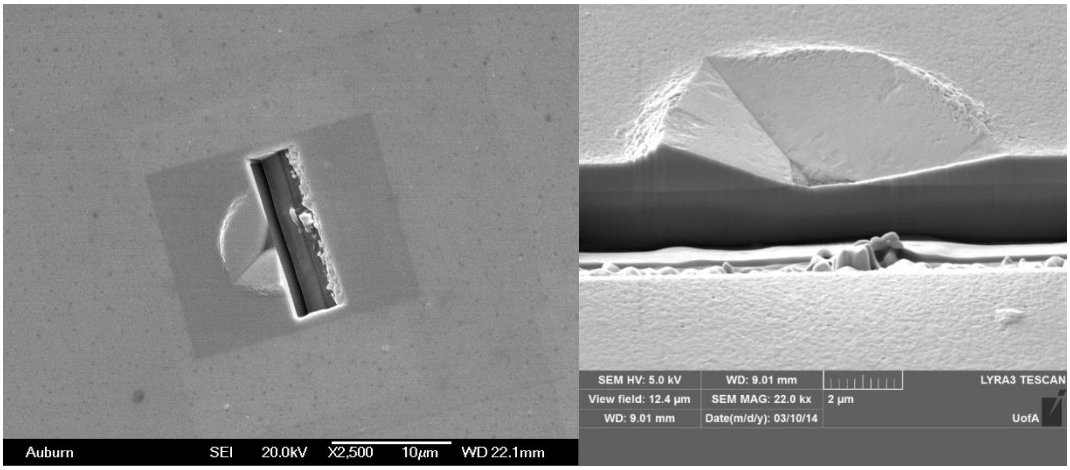

Figure 98. Top view of gold on silicon indent post-FIB cut (left) and cross-section (right), where the substrate is visible and there is no major deformation in the silicon substrate.

The FIB cuts from the silicon substrate with varying film criteria are seen in the next figures. As this was the initial time using this machine, the magnification was not consistent, so it is important to note the magnification before comparing any of the samples. First, there is the same film thickness, 777 nm, with varying indent depth, 300, 600, 900, and 1200. These are exhibited in Figure 99. Additionally, there is a progression of indents that utilize the same indent depth, 600nm, and compares different film thicknesses of 265, 480, 777, and 1283 nm in Figure 100. The two different progressions are interesting to compare to see the creation of pile-up and how it compares across film thicknesses. These images help to confirm the findings from Chapter 5.1 in this research and how the pile-up is independent of the film thickness and is only dependent on indent depth in these cases. Additionally, the profile of the pile-up changes with indent depth. In the thickest films, it seems to be more flat that the others. More work is necessary to measure these profiles, but it may result in much more information on pile-up formation than the projected area images.

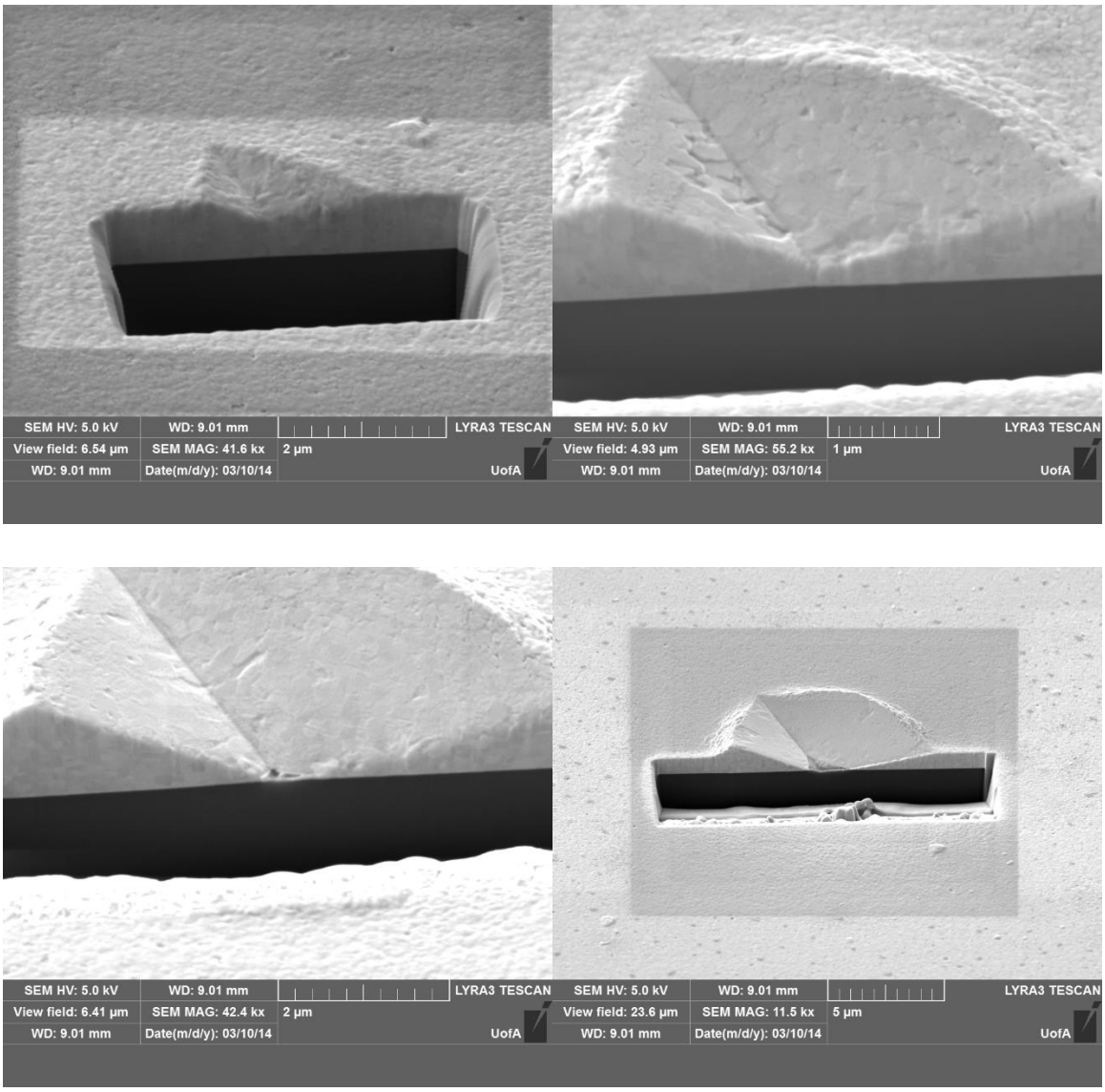

Figure 99. FIB cuts of all gold on silicon sample of 777nm thickness indented to 300, 600, 900, and 1200nm indent depth.

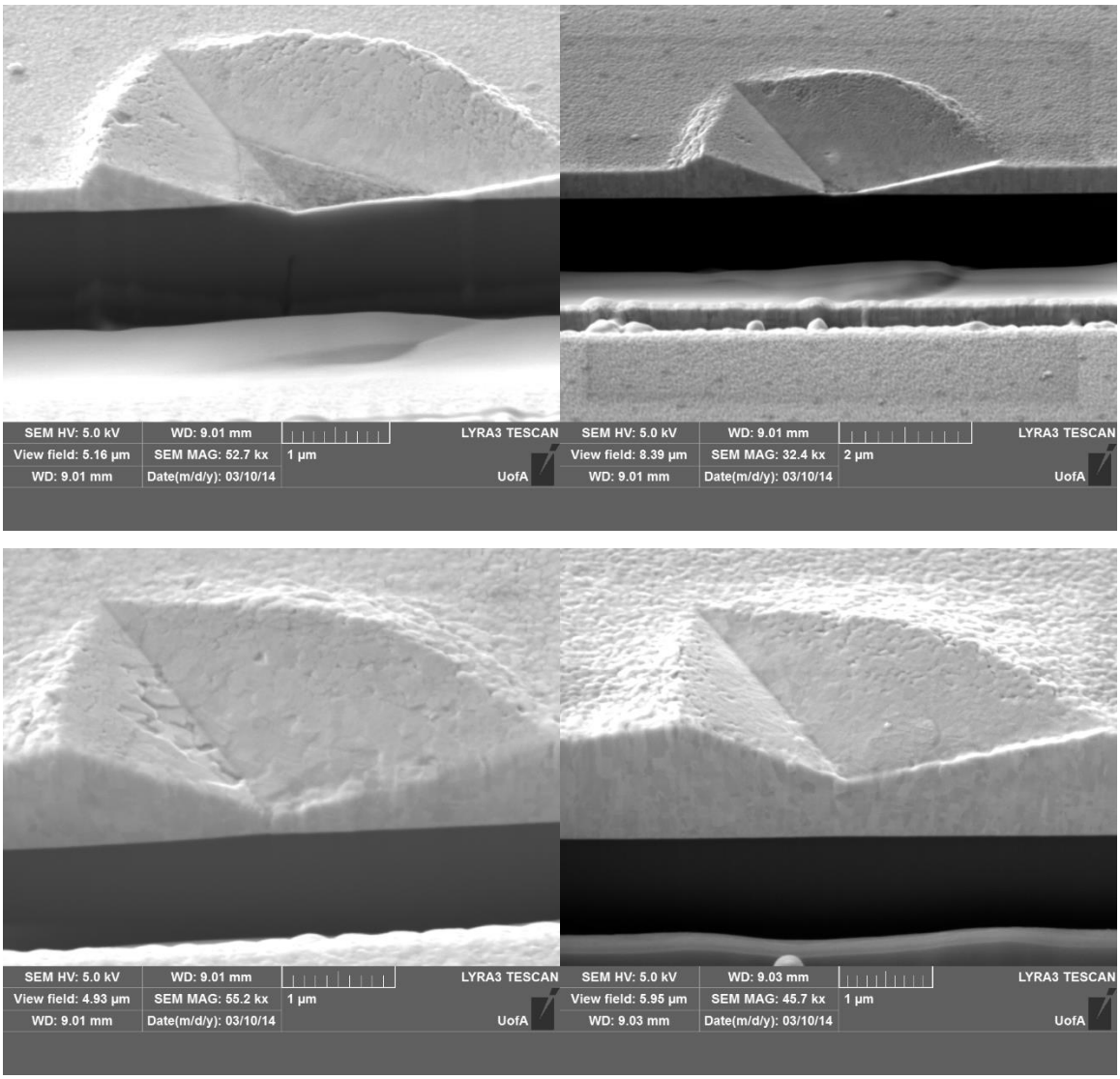

Figure 100. FIB cross-section images of same indent depth of 600nm indent four different film thicknesses: 265, 480, 777, and 1283nm.

6. Conclusions

In this work, many nuances of nanoindentation were studied. The results of these findings allow for an improved nanoindentation method of cases that involve the types of materials tested here, and beyond. Testing thin films on substrates has been dissected because it is the film properties that control material choices in applications such as microchips in electronics, which are vital every day.

First, it was found that pile-up was not affecting the Zhou-Prorok model. Instead of the model accounting for the pile-up, however, it was found that the changes in the area were not affecting the experimental data for elastic properties. Pile-up was found to be independent of film thickness and substrate modulus of the ceramic-like substrates. This striking finding shows that the elastic properties do not change with pile-up in these situations of a compliant film on a stiff substrate, and no additionally changes to the area measurements are necessary.

Next, as the stiff substrate moduli changes showed no different in the properties, plastic properties were examined. To modulate the substrate yield stress while keeping the elastic modulus constant, miniature tensile tests were completed to stretch the substrate past its initial yield stress and unload, essentially programming in a particular yield stress. With this progression, it was possible to modulate the substrate yield stress in series. After applying compliant films of gold and platinum, the pile-up measurements revealed there was a strong dependence on yield stress across materials. Although there was not a change dramatic enough in a single substrate with the change in yield stress, when comparing substrate materials, there was a clear trend of an increase in pile-up with an increase in substrate yield stress in both the gold and platinum data sets.

These findings have uncovered much information about the plastic properties of the film/substrate system and how they affect the extracted material properties from nanoindentation testing techniques. This research has made significant process in understanding the phenomena of pile-up and sink-in and how they relate to both the elastic and plastic properties during nanoindentation.

7. Future Work

There are many directions for this research to next lead. A more quantitative analysis of the cross-over point described in the pile-up vs yield stress plots will allow for confirmation of the film yield stress. Additionally, the yield stress of the film could be determined again from the membrane deflection tests with the same samples, as the ones used for comparison here had been created from separate tests.

Another direction in this work is to examine the hardness data from all of the tests completed. As there is a complete data set of gold and platinum on both ceramic and metallic substrates, there is much additional data that can be analyzed, but was outside the scope of this work. Also, the hardness may better correlate to the plastic properties, as only elastic modulus data had been compared previously.

With additional FIB cuts, much more information can be discovered, as well. Only a few cuts were able to be obtained through this work, and with the samples created, it would be easy to add more to quantitatively compare the cross-sectional indents. The most interesting idea that was discovered at the end of this research was the cross-section of a gold film on a metallic substrate past the film thickness. It is extremely curious that the indenter had not punched through the film, but instead, had pushed it along with the substrate. More cuts with a variety of samples could reveal information about the plasticity of the film and substrate, and what it may take to extract the changing mechanical properties of the film in this deformed area.

8. References

[1] L. Qian, M. Li, Z. Zhou, H. Yang, and X. Shi, "Comparison of nano-indentation hardness to microhardness," *Surface and Coatings Technology,* vol. 195, pp. 264-271, 2005.

[2] M. Gîrleanu, M. J. Pac, P. Louis, O. Ersen, J. Werckmann, C. Rousselot, and M. H. Tuilier, "Characterisation of nano-structured titanium and aluminium nitride coatings by indentation, transmission electron microscopy and electron energy loss spectroscopy," *Thin Solid Films,* vol. 519, pp. 6190-6195, 2011.

[3] N. A. Sakharova, M. C. Oliveira, J. M. Antunes, and J. V. Fernandes, "On the determination of the film hardness in hard film/substrate composites using depth-sensing indentation," *Ceramics International,* vol. 39, pp. 6251-6263, 2013.

[4] K. P. Sanosh, A. Balakrishnan, L. Francis, and T. N. Kim, "Vickers and Knoop Micro-hardness Behavior of Coarse-and Ultrafine-grained Titanium," *Journal of Materials Science & Technology,* vol. 26, pp. 904-907, 2010.

[5] S. R. Low, "Rockwell Hardness Measurement of Metallic Materials," *NIST Special Publication,* vol. 960-5, pp. 1-116, 2001.

[6] X. Li and B. Bhushan, "A review of nanoindentation continuous stiffness measurement technique and its applications," *Materials Characterization,* vol. 48, pp. 11-36, 2002.

[7] G. M. Pharr, W. C. Oliver, and F. R. Brotzen, "On the generality of the relationship among contact stiffness, contact area, and elastic modulus during indentation," *Journal of Materials Research,* vol. 7, pp. 613-617, 1991.

[8] A. C. Fischer-Cripps, "Critical review of analysis and interpretation of nanoindentation test data," *Surface and Coatings Technology,* vol. 200, pp. 4153-4165, 2006.

[9] M. F. Doerner and W. D. Nix, "A method for interpreting the data from depth-sensing indentation instruments," *Journal of Materials Research,* vol. 1, pp. 601-309, 1986.

[10] R. B. King, "Elastic Analysis of Some Punch Problems for a Layered Medium," *Int J Solids Struct,* vol. 23, pp. 1657-1664, 1987.

[11] H. Gao, C.-H. Chiu, and J. Lee, "Elastic contact versus indentation modeling of multi-layered materials," *Int. J. Solids Struct.*, vol. 29, p. 2471, 1992.

[12] J. Hay and B. Crawford, "Measuring substrate-independent modulus of thin films," *Journal of Materials Research,* vol. 26, pp. 727-738, 2011.

[13] Y.-T. Cheng and C.-M. Cheng, "Relationships between hardness, elastic modulus, and the work of indentation," *Applied Physics Letters,* vol. 73, pp. 614-616, 1998.

[14] S. Soare, S. J. Bull, A. G. O'Neil, N. Wright, A. Horsfall, and J. M. M. dos Santos, "Nanoindentation assessment of aluminium metallisation; the effect of creep and pile-up," *Surface and Coatings Technology,* vol. 177–178, pp. 497-503, 2004.

[15] D. Tranchida, S. Piccarolo, J. Loos, and A. Alexeev, "Mechanical Characterization of Polymers on a Nanometer Scale through Nanoindentation. A Study on Pile-up and Viscoelasticity," *Macromolecules,* vol. 40, pp. 1259-1267, 2007/02/01 2007.

[16] G. M. Pharr, "Measurement of mechanical properties by ultra-low load indentation," *Materials Science and Engineering: A,* vol. 253, pp. 151-159, 1998.

[17] S. V. Hainsworth and W. C. Soh, "The effect of the substrate on the mechanical properties of TiN coatings," *Surface and Coatings Technology,* vol. 163–164, pp. 515-520, 2003.

[18] I. N. Sneddon, "The relation between load and penetration in the axisymmetric Boussinesq problem for a punch of arbitrary profile," *International Journal of Engineering Science,* vol. 3, pp. 47-57, 1965.

[19] S. M. Han, R. Saha, and W. D. Nix, "Determining hardness of thin films in elastically mismatched film-on-substrate systems using nanoindentation," *Acta Materialia,* vol. 54, pp. 1571-1581, 2006.

[20] H. Buckle, "Progress in Micro-Indentation Hardness Testing," *Metallurgical Reviews,* vol. 4, pp. 49-100, 1959.

[21] B. Taljat and G. M. Pharr, "Development of pile-up during spherical indentation of elastic–plastic solids," *International Journal of Solids and Structures,* vol. 41, pp. 3891-3904, 2004.

[22] M. A. G. Maneiro and J. Rodríguez, "Pile-up effect on nanoindentation tests with spherical–conical tips," *Scripta Materialia,* vol. 52, pp. 593-598, 2005.

[23] J. Rodríguez and M. A. G. Maneiro, "A procedure to prevent pile up effects on the analysis of spherical indentation data in elastic–plastic materials," *Mechanics of Materials,* vol. 39, pp. 987-997, 2007.

[24] B. Zhou and B. Prorok, "A Discontinuous Elastic Interface Transfer Model of Thin Film Nanoindentation," *Experimental Mechanics,* vol. 50, pp. 793-801, 2010.

[25] B. Zhou and B. C. Prorok, "A new paradigm in thin film nanoindentation," *Journal of Materials Research,* vol. 25, pp. 1671-1678, 2010.

[26] X. Chen and J. J. Vlassak, "Numerical study of the measurement of thin film mechanical properties by means of nanoindentation," *Journal of Materials Research,* vol. 16, pp. 2974-2982, 2001.

[27] R. Saha and W. D. Nix, "Effects of the substrate on the determination of thin film mechanical properties by nanoindentation," *Acta Materialia,* vol. 50, pp. 23-38, 2002.

[28] R. Saha and W. D. Nix, "Soft films on hard substrates — nanoindentation of tungsten films on sapphire substrates," *Materials Science and Engineering: A,* vol. 319–321, pp. 898-901, 2001.

[29] K. W. McElhaney, J. J. Vlassak, and W. D. Nix, "Determination of indenter tip geometry and indentation contact area for depth-sensing indentation experiments," *J. Mater. Res.,* vol. 13, pp. 1300-1306, 1998.

[30] J. B. Frye, "Investigation of Pile-Up and Delamination of Au Thin Films on Various Substrates and the Behavior of the Films Described by a Discontinuous Elastic Strain Model," Masters, Materials Engineering, Auburn University, 2012.

[31] K. Kese and Z. C. Li, "Semi-ellipse method for accounting for the pile-up contact area during nanoindentation with the Berkovich indenter," *Scripta Materialia,* vol. 55, pp. 699-702, 2006.

[32] K. O. Kese, Z. C. Li, and B. Bergman, "Method to account for true contact area in soda-lime glass during nanoindentation with the Berkovich tip," *Materials Science and Engineering: A,* vol. 404, pp. 1-8, 2005.

[33] K. Kese and D. J. Rowcliffe, "Nanoindentation Method for Measuring Residual Stress in Brittle Materials," *Journal of the American Ceramic Society*, vol. 86, pp. 811-816, 2003.

[34] A. Bolshakov, W. C. Oliver, and G. M. Pharr, "Influences of stress on the measurement of mechanical properties using nanoindentation: Part II. Finite element simulations," *Journal of Materials Research*, vol. 11, pp. 760-768, 1996.

[35] W. C. Oliver and G. M. Pharr, "Measurement of hardness and elastic modulus by instrumented indentation: Advances in understanding and refinements to methodology," *J. Mater. Res.*, vol. 19, pp. 3-20, 2004.

[36] T. Y. Tsui and G. M. Pharr, "Substrate effects on nanoindentation mechanical property measurement of soft films on hard substrates," *Journal of Materials Research*, vol. 14, pp. 292-301, 1999.

[37] A. Bolshakov and G. M. Pharr, "Influences of pileup on the measurement of mechanical properties by load and depth sensing indentation techniques," *J. Mater. Res.*, vol. 13, pp. 1049-1058, 1998.

[38] Y. Wang, D. Raabe, C. Kulber, and F. Roters, "Orientation dependence of nanoindentation pile-up patterns and of nanoindentation microtextures in copper single crystals," *Acta Materialia*, vol. 52, pp. 2229-2238, 2004.

[39] W. D. Nix, "Elastic and plastic properties of thin films on substrates: nanoindentation techniques," *Materials Science and Engineering: A*, vol. 234–236, pp. 37-44, 1997.

[40] W. C. Oliver and G. M. Pharr, "An improved technique for determining hardness and elastic modulus using load and displacement sensing indentation experiments," *Journal of Materials Research*, vol. 7, pp. 1564-1583, 1992.

[41] A. M. Minor, E. T. Lilleodden, E. A. Stach, and J. J.W. Morris, "Direct observations of incipient plasticity during nanoindentation of Al," *J. Mater. Res.*, vol. 19, pp. 176-182, 2004.

[42] A. M. Minor, S. A. Syed Asif, Z. Shan, E. A. Stach, E. Cyrankowski, T. J. Wyrobek, and O. L. Warren, "A new view of the onset of plasticity during the nanoindentation of aluminium," *Nat Mater*, vol. 5, pp. 697-702, 2006.

[43] D. Lorenz, A. Zeckzer, U. Hilpert, P. Grau, H. Johansen, and H. S. Leipner, "Pop-in effect as homogeneous nucleation of dislocations during nanoindentation," *Physical Review B,* vol. 67, p. 172101, 2003.

[44] H. Bei, Z. P. Lu, and E. P. George, "Theoretical Strength and the Onset of Plasticity in Bulk Metallic Glasses Investigated by Nanoindentation with a Spherical Indenter," *Physical Review Letters,* vol. 93, p. 125504, 2004.

[45] H. Bei, E. P. George, J. L. Hay, and G. M. Pharr, "Influence of Indenter Tip Geometry on Elastic Deformation during Nanoindentation," *Physical Review Letters,* vol. 95, p. 045501, 2005.

[46] H. S. Leipner, D. Lorenz, A. Zeckzer, H. Lei, and P. Grau, "Nanoindentation pop-in effect in semiconductors," *Physica B: Condensed Matter,* vol. 308–310, pp. 446-449, 2001.

[47] W. A. Soer, K. E. Aifantis, and J. T. M. De Hosson, "Incipient plasticity during nanoindentation at grain boundaries in body-centered cubic metals," *Acta Materialia,* vol. 53, pp. 4665-4676, 2005.

[48] J. Li, K. J. Van Vliet, T. Zhu, S. Yip, and S. Suresh, "Atomistic mechanisms governing elastic limit and incipient plasticity in crystals," *Nature,* vol. 418, pp. 307-310, 2002.

[49] J. Jin, S. A. Shevlin, and Z. X. Guo, "Multiscale simulation of onset plasticity during nanoindentation of Al (0 0 1) surface," *Acta Materialia,* vol. 56, pp. 4358-4368, 2008.

[50] Y. Lee, J. Y. Park, S. Y. Kim, S. Jun, and S. Im, "Atomistic simulations of incipient plasticity under Al(1 1 1) nanoindentation," *Mechanics of Materials,* vol. 37, pp. 1035-1048, 2005.

[51] H. D. Espinosa, B. C. Prorok, and B. Peng, "Plasticity size effects in free-standing submicron polycrystalline FCC films subjected to pure tension," *Journal of the Mechanics and Physics of Solids,* vol. 52, pp. 667-689, 2004.

[52] C. Liang, S. Morshed, and B. C. Prorok, "Measuring the thin film elastic modulus with a magnetostrictive sensor," *Applied Physics Letters,* vol. 90, 2007.

[53] H. D. Espinosa, B. C. Prorok, and M. Fischer, "A methodology for determining mechanical properties of freestanding thin films and MEMS materials," *Journal of the Mechanics and Physics of Solids,* vol. 51, pp. 47-67, 2003.

[54] H. D. Espinosa and B. C. Prorok, "Size effects on the mechanical behavior of gold thin films," *Journal of Materials Science,* vol. 38, pp. 4125-4128, 2003.

[55] B. C. Prorok and H. D. Espinosa, "Effects of nanometer-thick passivation layers on the mechanical response of thin gold films," *Journal of Nanoscience and Nanotechnology,* vol. 2, pp. 427-433, 2002.

[56] J. William D. Callister and D. G. Rethwisch, *Fundamentals of Materials Science and Engineering: An Integrated Approach* vol. 3: John Wiley & Sons, 2008.

[57] P. Boch, J. C. Glandus, J. Jarrige, J. P. Lecompte, and J. Mexmain, "Sintering, oxidation and mechanical properties of hot pressed aluminum nitride," *Ceram. Int.,* vol. 8, 1982.

[58] R. R. Gupta and M. D. Lechner, *Landolt-Bonstein-Group III Condensed Matter*. New York: Springer, 2005.

[59] C. A. Schneider, W. S. Rasband, and K. W. Eliceiri, "NIH Image to ImageJ: 25 years of image analysis," *Nature Methods,* vol. 9, pp. 671-675, 2012.

[60] M. Sullivan and B. C. Prorok, "Evaluating indent pile-up with metallic films on ceramic-like substrates," *Journal of Materials Research,* vol. 30, pp. 2046-2054, 2015.

[61] M. Sullivan and B. C. Prorok, "Newly Discovered Pile Up Effects During Nanoindentation," in *The Society for Experimental Mechanics*, Greenville, SC, 2014.

[62] L. Wang, C. Liang, and B. C. Prorok, "A comparison of testing methods in assessing the elastic properties of sputter-deposited gold films," *Thin Solid Films,* vol. 515, p. 7911, 2007.

[63] L. Wang and B. C. Prorok, "Characterization of the strain rate dependent behavior of nanocrystalline gold films," *J. Mater. Res.*, vol. 23, pp. 55-65, 2008.

[64] G. M. Pharr, J. H. Strader, and W. C. Oliver, "Critical issues in making small-depth mechanical property measurements by nanoindentation with continuous

stiffness measurement," *Journal of Materials Research*, vol. 24, pp. 653-666, 2009.

[65] L. Wang and B. C. Prorok, "The Influence of Deposition Technique on the Strain Rate Dependence Behavior of Nanocrystalline Gold Films," in *Proceedings of the 2009 SEM Annual Conference and Exposition on Experimental and Applied Mechanics*, Session 35 ed. Albuquerque, NM, 2009.

[66] K. Schwieker, "Substrate Effect, Pile-Up and Sink-In Factors during Thin Film Nanoindentation," Masters, Materials Engineering, Auburn University, 2011.